WARWICK
THE UNIVERSITY OF WARWICK

A Thesis Submitted for the Degree of PhD at the University of Warwick

Permanent WRAP URL:
http://wrap.warwick.ac.uk/79952

Copyright and reuse:
This thesis is made available online and is protected by original copyright.
Please scroll down to view the document itself.
Please refer to the repository record for this item for information to help you to cite it.
Our policy information is available from the repository home page.

For more information, please contact the WRAP Team at: wrap@warwick.ac.uk

warwick.ac.uk/lib-publications

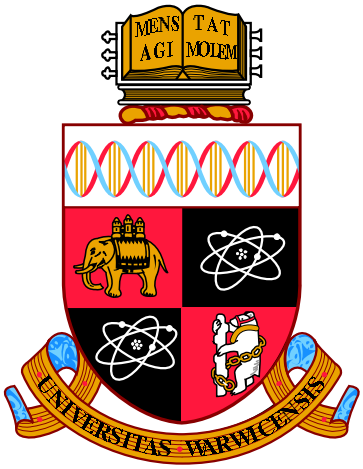

Mechanical inhibition of microtubule depolymerisation by kinesin

by

Daniel R. Peet

Supervisors: Robert A. Cross and Nigel J. Burroughs

Thesis

Submitted to the University of Warwick

for the degree of

Doctor of Philosophy

Systems Biology

September 2015

Contents

List of Tables

List of Figures

Acknowledgments

I would like to thank my supervisors Rob Cross and Nigel Burroughs for their ongoing support and invaluable advice throughout the duration of this project. It has been a pleasure working with them and all the other talented, friendly and like-minded people at the Centre for Mechanochemical Cell Biology.

Special mentions go to Rob for having boundless ideas for experiments, pushing me when I needed it and hosting great dinner parties for the lab; Doug Drummond for giving such detailed explanations, knowing something about everything and having a gadget to go with it (I'll never forget the time he measured the wind speed inside the lab to make an official complaint about the air pressure!); Naomi McIntyre for always being lively and cheerful in the lab; Nick Carter for encouraging me to use the 3D printer and, along with Douglas Martin, for getting me started using the Warwick Open-Source Microscope (WOSM).

I must thank my family and friends, especially my parents and my brother for supporting me all along the way including my journey here. I would like to mention my friends both at the University and elsewhere for keeping me upbeat, especially when experiments were not working. In particular, Annie Hughes and Jessica Bonham for donating Frank the dragon who now lives on top of the microscope enclosure (data quality has certainly improved since he arrived – a coincidence?); Richard Westbrook and Mark Walsh for also hosting amazing dinner parties, games nights and getting stuck in the mud with me on obstacle course races; everyone on the Warwick medics mixed hockey team for being a great crowd to let off steam with each week. Most of all, I would like to thank Toni McHugh for sharing these experiences with me and being so caring and supportive. Her company has made this time so enjoyable.

Finally, I would like to thank the Biotechnology and Biological Sciences Research Council (BBSRC) for funding this project.

Declarations

This thesis is submitted to the University of Warwick in support of my application for the degree of Doctor of Philosophy. It has been composed by myself and has not been submitted in any previous application for any degree.

Parts of this thesis have been published by the author:

- Structural remodelling of dynamic microtubules by kinesin (submitted to Nature Nanotechnology).

Abstract

Kinesin-driven transport of molecular cargo along microtubules is central to the self-organisation of eukaryotic cells. We investigated the effect of kinesin-1 on microtubule stability using *in vitro* techniques. We found that kinesin-1, which was previously reported to have no influence on microtubule dynamics, to reduce shrinkage rates by approximately two orders of magnitude if maintained in a nucleotide-free or ATP-bound state. No effect was observed in the presence of high ADP concentrations, indicating that the microtubule-stabilising ability of kinesin-1 is constrained to a subset of the kinetic states of its ATPase cycle. By decorating just one side of the microtubule lattice with kinesin, we were able to gain additional insights into the mechanics of microtubules. By stabilising just 2-3 protofilaments with kinesin, the structural integrity of most of the microtubule could be maintained. Curiously, in such circumstances the microtubule would split at its ends. We further showed that microtubule curvature induced by hydrodynamic flow is trapped or even increased by nucleotide-free kinesin. We propose a mechanism whereby kinesin-1 drives the conformation of polymerised GDP-tubulin into a slightly elongated and shrinkage-resistant conformation. This is essentially the converse mechanism of that reported for the kinesin-13, MCAK, which supports tubulin in a curved conformation that is incompatible with the microtubule lattice.

Abbreviations

ADP	Adenosine diphosphate
AFM	Atomic force microscopy
AMPPNP	Adenosine 5'-(β,γ-imido)triphosphate (slowly-hydrolysable ATP analogue)
ATP	Adenosine triphosphate
DIC	DIfferential-interference contrast (light microscopy technique)
EM	Electron microscopy
GDP	Guanosine diphosphate
GMPCPP	Guanosine-5'-[(α,β)-methyleno]triphosphate (slowly-hydrolysable GTP analogue)
GTP	Guanosine triphosphate
GTPγS	Guanosine 5'-O-[gamma-thio]triphosphate (slowly-hydrolysable GTP analogue thought to mimic GDP·P_i)
MAP	Microtubule-associated protein
MD	Molecular dynamics
MT	Microtubule
P_i	Inorganic phosphate
PF	Protofilament
PTM	Post-translational modification
SEM	Standard error of the mean
+TIP	Plus-end-tracking microtubule-associated protein

-TIP	Minus-end-targeting microtubule-associated protein
TIRF	Total internal reflection fluorescence (illumination technique for light microscopy)

1

Introduction

1.1 The cytoskeleton

Cells constantly reshape and rearrange throughout the cell cycle. They are able to undergo dramatic morphological changes as they move and divide. These changes are primarily driven by the internal scaffolding of the cell, collectively known as the cytoskeleton. The cytoskeleton is comprised of dynamic polymers that perpetually grow and shrink to remodel the inside of the cell.

Microtubules (MTs), filaments assembled from the protein tubulin, are a key component of the cytoskeleton. They provide vital mechanical forces that drive and support remodelling processes such as cell division [1]. The characteristic behaviour of MTs is to repeatedly cycle between modes of growth and shrinkage, a process known as dynamic instability [2]. The growing and shrinking processes allow MTs to generate intracellular forces [3]. For example, depolymerisation of MTs attached to kinetochores drives the segregation of chromosomes during mitosis [4]. Forces associated with these processes can feed back upon MT dynamics. For instance, Kinetochore-bound MTs generate tension as they depolymerise but MTs become increasingly stabilised by tension [5]. Tension-mediated stabilisation occurs at other sites of MT attachment such as the cell cortex [6]. Compression of MT tips can also influence dynamics [3].

1.2 MT structure and dynamics

1.2.1 MT structure

The structure of MTs is most naturally described as an arrangement of protofilaments (PFs), linear chains of $\alpha\beta$-tubulin heterodimers. PFs run along the axis of MTs, binding laterally to form a hollow tube (Figure 1.1A). MTs most commonly consist of 13 PFs both *in vivo* [8] and *in vitro* [9]. However, MT configurations are highly sensitive to assembly conditions *in vitro*. PF numbers differ when MTs are assembled in the presence of different solvents [10], slowly hydrolysable nucleotides [11], MT-stabilising drugs [12] and MAPs [13, 14]. Furthermore, the number of PFs can change along the length of a single MT due to defects in the lattice [15]. Within each PF, tubulin heterodimers are arranged head-to-tail. The intrinsic polarity of the tubulin heterodimer (which consists of an α and a β monomer) is therefore reflected in the macromolecular structure of the MT itself [16]. The α monomers are exposed at the 'minus end' of the MT and the β monomers at the 'plus end'.

The most common arrangement of PFs is known as the B-lattice. In this configuration, inter-PF contacts assume the form of α-α and β-β interactions (Figure 1.1B). These contacts stagger 13 PFs by 0.9 nm in a left-handed helix, resulting in a symmetry-breaking seam where a shift of 4.9 nm must be accommodated [14]. This 4.9 nm axial stagger between neighbours defines the A-lattice, in which lateral interfaces occur between α and β monomers (Figure 1.1B). MTs of this form are referred to as 13_3 MTs, meaning there are 13 PFs and the lateral contacts form a (left-handed) helix with a pitch of 3 monomers. *In vitro*, the number of PFs ranges from 10 to 17 and helical pitches range from 2 to 4. Many of the less favourable conformations that differ from the 13_3 arrangement require PFs to skew relative to the MT axis [17, 18].

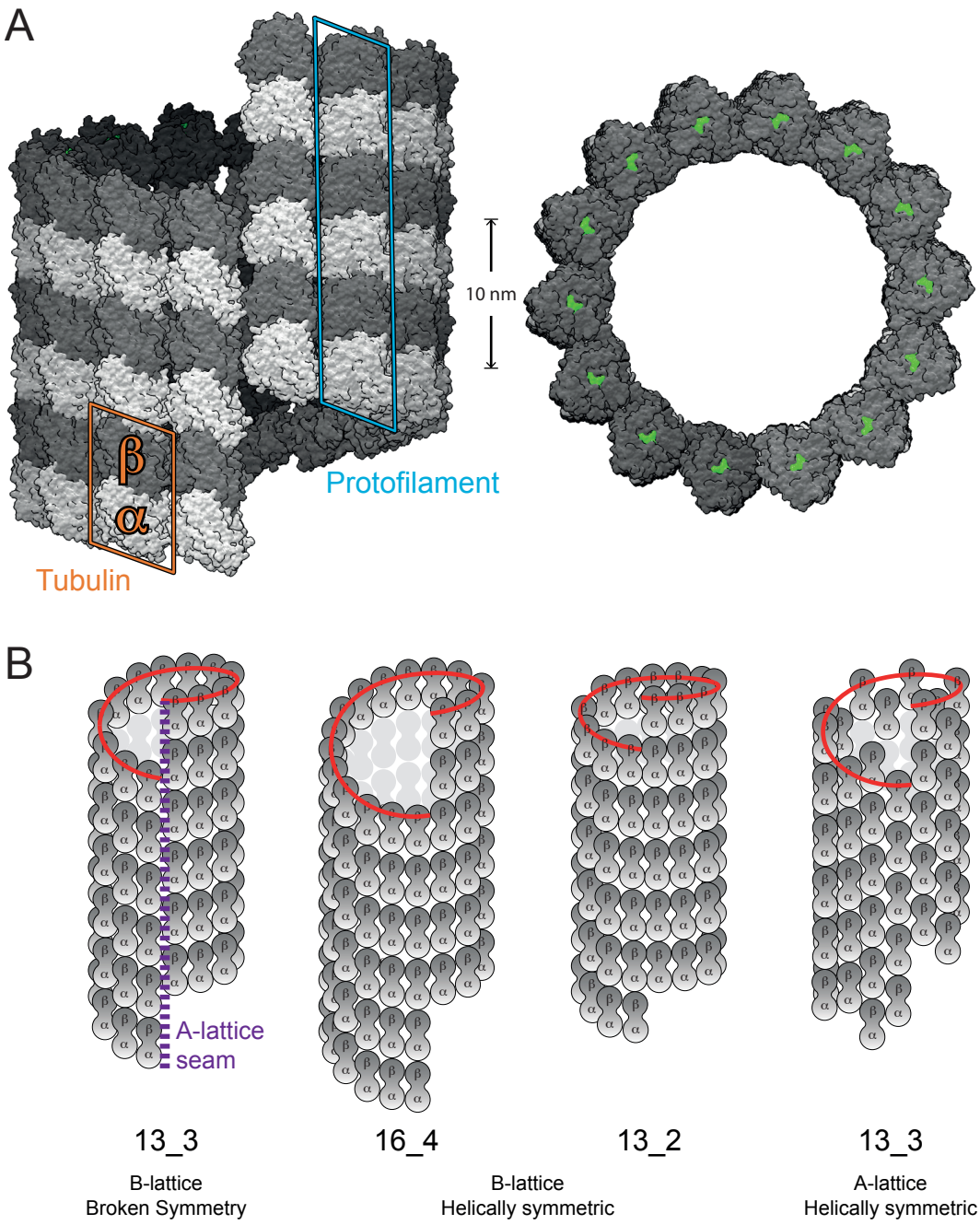

Figure 1.1: MT anatomy. **A.** The structure of a 14_3 (B-lattice) MT. *Left*: $\alpha\beta$-tubulin subunits bind head-to-tail to form PFs, which make up the MT wall. The plus-end of the MT is where the β-subunits are endmost (towards the top), whereas α-subunits are exposed at the minus end. *Right*: The nucleotide-binding pocket of β-tubulin is exposed at the MT plus-end (shown). GDP is shown in green. The image was generated by aligning multiple copies of a 3×3 tile of taxol-GDP-MT structure (3J6F). **B.** A selection of MT lattice configurations. The most common MT lattice configuration (13_3) is shown on the left, whereby lateral contacts are all α-α and β-β interactions (B-lattice), except at a single symmetry-breaking seam. At the seam, lateral contacts are all between α and β subunits (A-lattice). It is possible for MTs to form entirely A-lattice configurations, as shown by the diagram on the far right. This image was adapted from [7], kindly provided by Robert Cross.

1.2.2 The A-lattice seam

The most common MT lattice arrangement (13_3) involves a single symmetry-breaking A-lattice seam, which begs the question "Why has an asymmetrical structure been evolutionarily selected for?". MTs primarily consist of the B-lattice, so an intuitive assumption would be that these contacts are more favourable, with bonds at the seam forming more slowly [19]. Conflicting results have been reported for the relative strengths of the A- and B-lattices [20, 21]. However, recent experimental data and molecular dynamics simulations [22] are in agreement that the A-lattice is less stable [23]. A logical prediction is therefore that the MT seam may serve as a hotspot for the regulation of MT catastrophe. Indeed, MTs that are cold-shocked into depolymerisation tend to unzip into open sheets along a single cold-labile seam [24].

1.2.3 Dynamic instability

Perpetual switching between slow growth and rapid shrinkage is known as *dynamic instability*, which constitutes the predominant dynamic behaviour of MTs [2]. MT growth occurs through the addition of $\alpha\beta$-tubulin at the MT tip (Figure 1.2). Polymerisation kinetics are regulated by a guanosine nucleotide that is located at the periphery of the β-subunit (Figure 1.1A). Guanosine triphosphate (GTP) promotes assembly, whereas guanosine diphosphate (GDP) favours disassembly except under extreme experimental conditions [25, 26]. A second nucleotide-binding pocket resides at the intradimer interface. However, it is permanently occupied by a molecule of GTP that cannot exchange due to steric confinement [27, 28].

GTP-tubulin is typically incorporated into the lattice one dimer at a time [29], consistent with the observation that oligomers of more than two dimers rarely form in solution [30]. Tubulin is incorporated in a head-to-tail fashion, such that only α-subunits are exposed at one end (the 'minus-end') and only β-subunits at the other (the 'plus-end'). The contacts within each PF join the α- and β-subunits of consecutive dimers. GTP hydrolysis is accelerated by this interaction, leaving the majority of

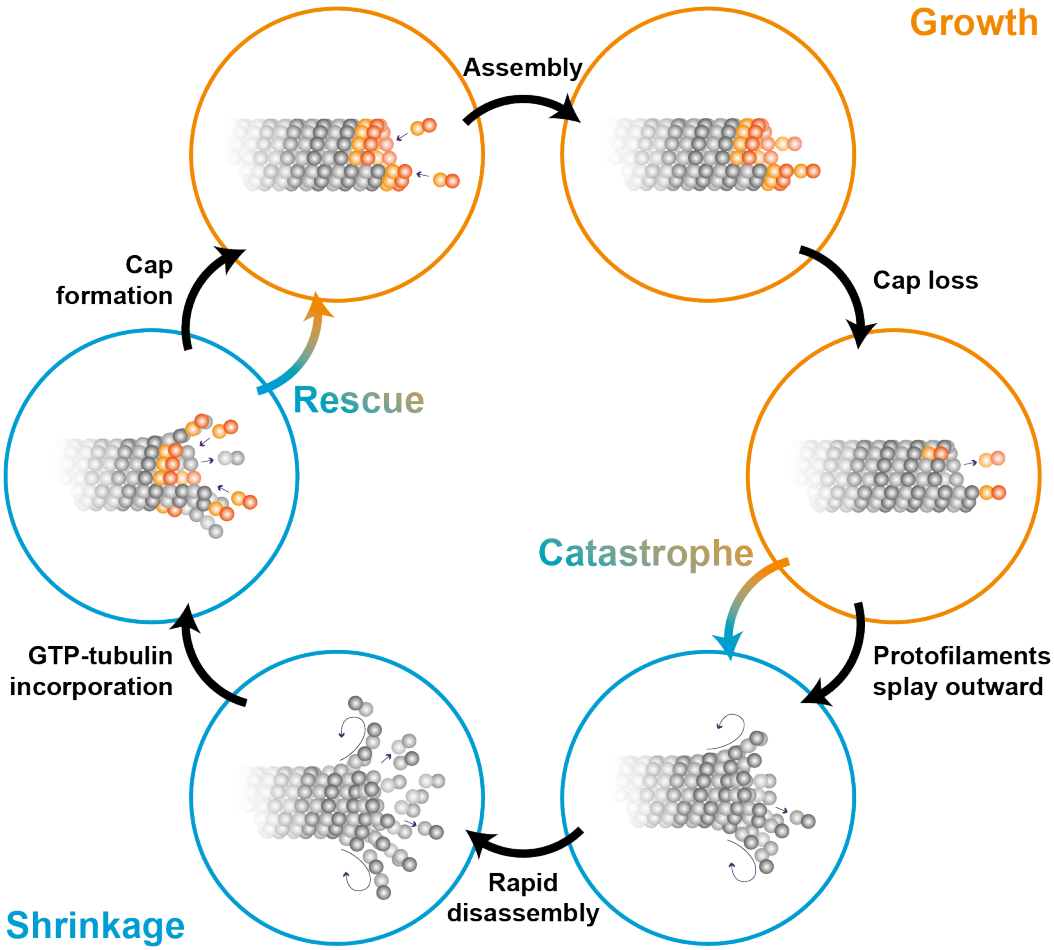

Figure 1.2: Dynamic instability of MTs. MTs grow through the addition of GTP-tubulin at their tips. Over time the GTP hydrolyses to GDP, resulting in a largely GDP-bound MT with a 'GTP cap'. Unlike GTP-tubulin, GDP-tubulin favours shrinkage over growth. When the GTP cap is lost, either by hydrolysis or dissociation of tubulin, the unstable GDP-tubulin core of the MT becomes exposed. At this point a *catastrophe* occurs – the GDP-tubulin PFs are no longer constrained and splay outward, actively unzipping the MT into a phase of rapid depolymerisation. If the MT tip becomes stabilised and reacquires a GTP cap, a *rescue* occurs and growth resumes, concluding the cycle of dynamic instability.

polymerised tubulin in a GDP-bound state [31]. A 'GTP cap' remains at the growing MT tip that protects against disassembly.

If the GTP cap is lost by hydrolysis or dissociation of GTP-tubulin, or if a significant crack forms between PFs, the unstable GDP-core of the MT lattice becomes exposed [32]. PFs peel outward from the tip, actively unzipping the MT into a phase of rapid depolymerisation. Splayed PFs, commonly referred to as 'rams-horns', are a hallmark of depolymerising MTs and are easily observed using electron microscopy (EM) [24, 33–36]. A MT may transition back from shrinkage to growth if the tip becomes stabilised and GTP cap reforms. Transitions from growth the shrinkage and vice versa are known as *catastrophes* and *rescues*, respectively.

A remarkable property of MTs is that no MAPs are required in order to achieve dynamic instability; it is an intrinsic property of tubulin [37]. Indeed, this forms the basis for reconstituting MT dynamics *in vitro*. Above a critical concentration of tubulin, MTs can be grown from nucleation templates such as axonemes. Net growth does not occur below this concentration. Dynamics can only be observed for a narrow range of tubulin concentrations. If the tubulin concentration is too high then MTs nucleate spontaneously in solution. The flux of tubulin across a population of MTs converges to a steady state over time; total polymer mass and the free tubulin concentration equilibrate [38]. Each end of the MT shows different dynamical behaviour. The plus-end typically shows faster growth, undergoes catastrophe more frequently and has a lower tendency for rescue [39].

1.3 Complexities of MT dynamics

The GTP-cap model explains the large-scale behaviour of dynamic instability. However, many of the molecular mechanisms underlying this process are still unclear; namely the geometry of growing MT tips, the effect of nucleotides on tubulin, the mechanism of GTP hydrolysis and the precise requirements for a MT tip to remain stable. We discuss these factors in the following sections.

1.3.1 Tip composition: geometry and nucleotide distribution

Growing MT tips have been observed by negative staining electron microscopy (EM). Initially, tip structures of growing MTs were reported as open sheets of PFs [24, 40, 41]. Subsequent studies using cryo-EM to image the tips argued both for [19] and against this view [35]. In the latter case, a blunt tip with short protrusions of individual PFs was the preferred description but the interpretation of these data is not trivial; the data could be argued to depict either geometry (highlighted previously in [32]). Computational modelling predicts that open sheets are highly unstable and potential precursors to MT catastrophe [42]. The degree of sheet closure has been suggested to modulate tip stability, whereby total closure is a structural mechanism for triggering a catastrophe due to an increasing strain on lateral contacts [43]. This suggestion is however inconsistent with the observation that the degree of tapering at MT tips positively correlates with the catastrophe frequency [44].

Not only is the geometry of the tip contentious, but also the quantity of GTP residing within the MT. Many estimates for the size of the GTP cap have been made. It has been suggested that it may simply consist of a monolayer of GTP-tubulin [45, 46]. MTs capped with GMPCPP-tubulin (a slowly hydrolysable GTP analogue) remain in a highly stable state until the cap is lost by dissociation, demonstrating the feasibility of a minimal cap [47]. On the other hand, *in vitro* estimates have reported a cap with as many as 200 GTP-tubulin subunits [48]. Some evidence suggests that an even larger cap size is possible and that it fluctuates substantially [49]. The first estimates of the cap size *in vivo* were determined by using the MT plus-end tracking protein (+TIP) EB1 as an indicator of GTP-tubulin content, giving a figure of approximately 750 subunits [50].

1.3.2 Nucleotide effects

Broadly speaking, two models have been proposed for why GTP-tubulin polymerises more readily than GDP-tubulin [51]. These are the 'allosteric' and 'lattice' models. The allosteric model proposes that GDP-tubulin is intrinsically curved and therefore incompatible with the MT lattice, whereas GTP tubulin is straight and assembly-competent.

This view was inspired by the presence of 'rams-horns' that can be observed at depolymerising MT tips *in vitro* [35, 36], suggesting that GDP-tubulin has an innate tendency to bend. Early crystal structures of GDP-tubulin were found to adopt a curved conformation, further supporting the allosteric model [52]. Tubulin was complexed with the stathmin-like domain of RB3 protein to obtain this structure. The same complex was later solved for GTP-tubulin [53], which was also found to be curved. This cast doubt on the allosteric model. GTP-tubulin has since been crystallised with a wide range of ligands, each of which shows a high degree of curvature [54].

The alternative lattice model proposes that both nucleotide states of tubulin are naturally curved in solution but GTP-tubulin is easily straightened upon incorporation to the MT lattice. Molecular dynamics (MD) simulations have contributed much towards investigating the opposing models. For instance, laterally unbound PFs have been predicted to adopt a curved configuration in either nucleotide state [55], in agreement with the lattice model. MD simulations further suggest that lateral lattice contacts are enhanced for GTP-tubulin, particularly at the β-β interfaces [22, 56, 57]. The α-subunits of polymerised tubulin are also thought to be affected [58]. Empirical data further supports the lattice model, as GDP-tubulin can be incorporated into growing MT tips so long as it is accompanied by GTP-tubulin [59].

Experimental data from a hydrogen/deuterium exchange mass spectrometry study favours a mixed model whereby either form of tubulin may be incorporated, but GDP-tubulin is more flexible and pays a higher entropic cost when incorporated into the lattice [60]. Furthermore, polymerised tubulin has been shown to compact upon hydrolysing GTP, demonstrating that nucleotide-dependent allosteric effects occur

within the MT lattice [61, 62]. To conclude, the lattice model explains the majority of the published data on MT assembly but nucleotide-dependent allosteric effects also occur.

GTP has also been proposed to have a secondary mechanism to ease tubulation during MT assembly [63, 64]. GMPCPP-stabilised sheets (or 'ribbons') have been reported to form under unique experimental conditions, specifically at low temperatures ($< 15\,^{\circ}\mathrm{C}$) [65]. Upon heating to $37\,^{\circ}\mathrm{C}$, the sheets were observed by EM to roll up into tubes. The ribbons showed alternating lateral contacts, both favouring and opposing inter-PF curvatures that would be expected for a MT lattice. It was thus speculated that GTP-tubulin is able to form secondary lateral contacts. Indentation of MTs using atomic-force microscopy (AFM) supported this claim, showing nonlinear responses to compressive forces [66]. Recently, the published structure of helically symmetric 15 PF GMPCPP-MTs has confirmed the presence of such interactions [67].

1.3.3 GTP HYDROLYSIS

The spatial distribution of GTP-tubulin in the lattice is a product of both tip geometry and the rate of hydrolysis. The mechanism of hydrolysis dictates how deep in the lattice GTP-tubulin may occur and whether or not it is interspersed with GDP-tubulin. Three modes of hydrolysis are prevalent in the literature; coupled, vectorial and random (reviewed in [68]). Coupled hydrolysis is where the addition of a dimer instantly hydrolyses the previously terminal GTP-tubulin, resulting in a minimal cap. This assumption is inferred from structural data that shows tubulin dimers to act as their own GTPases; α monomers catalyse the hydrolysis of GTP via longitudinal contacts with β monomers [31]. Vectorial is a mode of graduated hydrolysis that is restricted to the GDP/GTP-tubulin interface. Finally, random hydrolysis is said to occur stochastically anywhere in the lattice. Individually, these three modes are insufficient to account for all experimental results, at least when applied to a 2D lattice model [68]. Random-vectorial [69, 70] and random-coupled [32, 42, 68, 71] hydrolysis have been shown to explain a large amount of current empirical data.

The vast majority of free energy from the hydrolysis reaction is stored in the MT lattice [72]. Consequently, if the cap is hydrolysed, GDP-PFs are released from their GTP-dependent shackles, allowing them to splay radially. Theoretically, this motion could generate forces of ~ 5 pN per PF, allowing MTs to be molecular motors 10 times as strong as kinesin-1 [73]. If GDP-tubulin is incorporated into the MT during polymerisation, the rate of depolymerisation is correspondingly decreased [59]. Not only is this in agreement with the principle of hydrolysis providing the energy required to generate substantial forces, but it also provides firm evidence for the existence of structural plasticity in the lattice. For a review of structural plasticity in MTs, see [74]. Clearly, the influences of nucleotide state on MT dynamics are complex.

1.3.4 MT STABILITY

MT dynamics cannot be fully explained by a simplistic GTP-cap model. For example, unusual behaviour is revealed if a MT lattice is laterally severed through its cross-section. The newly exposed plus-end tends to disassemble, as expected, whereas the stability of the minus end remains unaffected [75, 76]. In addition, some evidence suggests that GTP-tubulin, or at least tubulin adopting a 'GTP-like' conformation, may reside deep inside the lattice [49].

It has been reported that MT growth durations (or catastrophe frequencies) do not obey first order reaction kinetics, suggesting that hydrolysis alone is insufficient to explain catastrophe [77]. Instead, MTs are more susceptible to catastrophe as they have been growing for longer, giving rise to the notion of 'MT ageing' [78]. One possible explanation for this is a potential accumulation of lattice defects during growth [68]. Another is based on evidence that MT tips become more tapered with age, which is proposed to decrease their stability [44]. It is thus possible that MT dynamics emerges from several different contributing mechanisms.

1.4 Regulators of MT dynamics

MT dynamics are affected by many factors. In the following subsections, we discuss the predominant influencers of dynamic instability.

1.4.1 MT associated proteins

MT dynamics differ significantly *in vitro* from those measured *in vivo*. At physiological tubulin concentrations, polymerisation is drastically slower [79], catastrophes and rescues are less frequent, and MT tips are rarely seen to pause for extended periods of time [39]. A fundamental reason for these discrepancies is that MT dynamics are tightly regulated by a diverse collection of MAPs *in vivo* [80]. MAPs are known to have diverse functions spanning MT polymerases, catastrophe and rescue factors, nucleation factors, MT severing proteins and MT cross-linkers [81]. Many MAPs exploit the distinct binding sites that emerge from the polarity of MTs, leading to the classification of plus-end-tracking proteins (+TIPs) and minus-end-targeting proteins (-TIPs) [82–85].

A key family of +TIPs are the end-binding (EB) proteins, which track MT plus-ends exclusively during polymerisation [86]. They bind to the lattice of MTs grown in the presence of slowly-hydrolysable GTP analogues (GTPγS or GMPCPP), demonstrating sensitivity to nucleotide-related tubulin conformations [87–89]. Hence, the surrounding structure of the GTP cap may be reflected in the distribution of EB proteins at MT tips. Conflicting results have been reported for the effect of EB proteins on MT dynamics but the most commonly reported effects are to increase growth rates and to promote catastrophes [7, 43, 90, 91]. Several reports suggest that EB proteins help to 'zip' PFs together during MT growth by promoting lateral bond formation at MT tips, which could explain the heightened growth rate [43, 90, 91]. Indeed, EB1 must regulate inter-PF contacts because they constrain MT assembly to 13-PF configurations [14, 43, 62, 87]. Recently, it has been shown that EB promotes two distinct conformational changes in lattice-bound tubulin [91]. High-resolution

structural data suggests that these changes have a catalytic effect on GTP hydrolysis [62], providing an explanation for the accompanied increase in catastrophe frequency.

Although EB proteins have the ability to track growing MT ends autonomously *in vitro*, it has recently been shown that CLASP proteins are required to retain this functionality *in vivo* [92]. Moreover, the *in vitro* tip-specificity of EBs is amplified by CLASPs. Intriguingly, these results are independent of a direct interaction between the two proteins. This implies that CLASPs interfere with EB-MT binding kinetics by modifying the MT lattice, most likely by promoting GTP hydrolysis or the associated transitions [92].

XMAP215 is a +TIP MT polymerase that accelerates MT growth by up to ten-fold [93, 94]. Unlike EB proteins, XMAP215 retains its tip-tracking ability during MT depolymerisation [94]. Although EB proteins increase XMAP215 recruitment to the lattice [95], the proteins are spatially separated as they regulate MT dynamics [90, 91]. EB proteins in fact localise close to, but not at the very end of, MT tips. Despite being separated, the combined polymerase activity of EB and XMAP215 outweighs their individual contributions [90]. The synergy presented by this simple system can drive MT polymerisation to those rates observed *in vivo*, approaching the theoretical limit [90, 96]. Therefore, like CLASPs, XMAP215 appears to communicate with EBs via conformational changes in the MT lattice.

The largest energy barrier to be overcome in MT dynamics is in nucleation [97]. Naturally, the process of nucleation is tightly regulated by MAPs. The canonical MT nucleation factor, which nucleates MTs both from centrosomes and anchor points on the sides of preformed MTs, is the gamma tubulin ring complex (γTuRC) [98, 99]. The γTuRC contains several MAPs and γ-tubulin (a monomeric tubulin species) [100]. It forms a helical structure that matches the chirality of a 13_3 MT lattice, topped with γ-tubulin to produce a template for MT growth [101, 102]. However, *in vitro* MT dynamics suggest that nucleation from a rigid template is inefficient in the absence of additional MAPs (such as EBs and XMAP215) [103], suggesting that MT tip conformations mature to aid the incorporation of subsequent tubulin dimers.

It is apparent that MAPs can change MT dynamics via allosteric interactions

with tubulin. Thus, the combination of changes induced by GTP-hydrolysis and MAPs could lead to a 'patchwork' of tubulin conformations in the MT lattice [104]. It has also been suggested that tubulin conformations at the MT tip may be affected via MAPs indirectly, through transduction of external tensile forces [5].

MAPs affect the conformation of tubulin, but the conformation of tubulin can affect its affinity for MAPs. For example, both CLASPs and XMAP215 contain TOG domains, which have greater binding affinities for unpolymerised tubulin, which is thought to be curved, than for MTs [105]. Similarly, doublecortin has been shown to bind preferentially to curved PFs and less well to 'straight' conformations of the MT lattice [106]. Conversely, the Ndc80 complex binds selectively to the MT lattice, such that interactions are destabilised upon PF curling [107]. Interestingly, the Ska complex has a flexible structure and multiple binding modes that allows it to bind to a range of tubulin curvatures without preference [108].

1.4.2 Kinesin motor proteins

Kinesins are a diverse family of molecular motors that use the energy from ATP hydrolysis to perform mechanical work. The kinesin superfamily is unified by a highly conserved 'motor' domain [109]. The motor domain is a globular structure that has a nucleotide-binding pocket and a MT-binding domain on opposing sides 1.4. Despite the evolutionary conservation of the motor domain, kinesins have remarkably diverse functions [110].

Fourteen subgroups of the kinesin superfamily have been identified by phylogenetic analysis [109, 111]. The associated nomenclature for each subgroup is 'kinesin-n', where n denotes the group number. Kinesin-(1-12)s have a motor domain situated at the N-terminus. They convert chemical energy from ATP hydrolysis into mechanical energy, which they use to literally 'walk' along MTs towards plus-ends. This mechanism is used *in vivo* to facilitate intracellular transport [112, 113]. Conversely, kinesin-13s have a motor domain in the centre of their structures. Unlike other subgroups, kinesin-13s are not capable of walking along MTs. Instead, they diffuse along the MT lattice

until they reach an end, whereby they promote a curved conformation of tubulin that induces MT catastrophes [114, 115]. Kinesin-14s have a motor domain situated at the C-terminus. Like kinesin-(1-12)s, they walk along MTs. However, they walk towards MT minus-ends rather than plus-ends. It must be noted that this categorisation bares little resemblance on the functional diversity of kinesins [116].

Besides the motor domain, which is also known as the 'head', kinesins typically have long fibrous regions, which comprise a 'tail'. Tails have been identified to have roles in kinesin oligomerisation [117], as well as providing specific binding sites for cargo and adaptor proteins (which may also facilitate cargo binding, e.g. [112]). The cargos that kinesins transport include tubulin, vesicles, organelles and also MTs (resulting in a sliding motion). In the absence of attached cargo, kinesin tails interfere with the motor domains by preventing them from binding to MTs, presumably as an autoinhibitory mechanism to mitigate futile ATP hydrolysis [118].

The degree of oligomerisation varies between kinesin species. The canonical kinesin (kinesin-1) takes the form of a homodimer [117]. However, monomeric and tetrameric assemblies are common for other kinesin subgroups. Some kinesins even form complexes with members from other subgroups [119]. Tetrameric kinesins have been shown to walk along two MTs simultaneously [120]. This naturally cross-links MTs to form a bundle and, if arranged in an anti-parallel fashion, subsequently slides MTs apart.

Several kinesins have been shown to effect MT dynamics [119]. They do this through a variety of different mechanisms. For example, kinesin-13s are distinct from other kinesin family members in that they don't walk along the MT. Instead, they rely either on transportation by other kinesins to reach their destination [121], or they bind to the MT lattice and enter a diffusive mode [114]. Their functionality is limited to MT tips, where they bind to the end tubulin dimers in the MT lattice. A well-studied kinesin-13, MCAK, has been shown to promote a curved conformation of tubulin [115], breaking lateral lattice bonds as it does so. This action is thought to induce MT catastrophe by breaking the GTP cap.

Kinesin-13s are not the only kinesins to exhibit depolymerase activity. The

kinesin-8 Kip3 has been characterised as a MT-length-dependent depolymerase [122]. Its depolymerase activity has been shown to be distinct to kinesin-13s [78]. Unlike kinesin-13s, kip3 walks to the end the MT, where it pauses for a long time before detaching. If another Kip3 reaches the MT at the same time, it 'bumps' the first one off, taking one or two tubulin dimers as it goes [122].

Kinesins have also been reported to positively influence MT stability. For instance, CENP-E [123] and Kif17 [124] have been reported to stabilise MTs, as have the tails of several kinesins [124, 125]. Recently, both Kip2 [126] and Eg5 [127] have been shown to function as MT polymerases.

1.5 Kinesin-1

Kinesin-1 is commonly adopted as the model species for studying the how kinesins walk along MTs. In the following subsections we give a broad description of what is known about this process.

1.5.1 The kinesin stepping cycle

Kinetic mechanism of kinesin motility

For a review of the kinetics of the kinesin stepping cycle, see [128]. Briefly, the cycle progresses as follows. Kinesin-1 has ADP tightly bound to its motor domains in solution. Exchanging for ATP and undergoing hydrolysis thereafter is very slow in the absence of MTs. In an ADP-bound state the kinesin has a low affinity for the MT lattice. One head of kinesin-1 binds to the MT. Upon binding to the lattice, ADP is released from this head. The nucleotide-free state of kinesin binds tightly to the MT. Whilst the first (MT-bound) head is in a nucleotide-free state the conformation of the dimer is such that the second head is unable to bind.

ATP binds to the first head and generates a 'power stroke', moving the second kinesin head in close proximity with the MT lattice (Figure 1.3). The second head is

then able to bind to the next tubulin dimer in the PF (releasing a molecule of ADP in the process) whilst the ATP in the first head undergoes hydrolysis. The second head (now in front of the first head) enters the tightly-bound nucleotide-free state whilst the first (rear) head contains ADP and phosphate. Finally, the rear head releases phosphate, resulting in a weakly-bound ADP state that subsequently detaches from the lattice. This concludes the ATPase cycle of kinesin-1, as the motor is one tubulin dimer closer to the tip of the MT but with the other head bound.

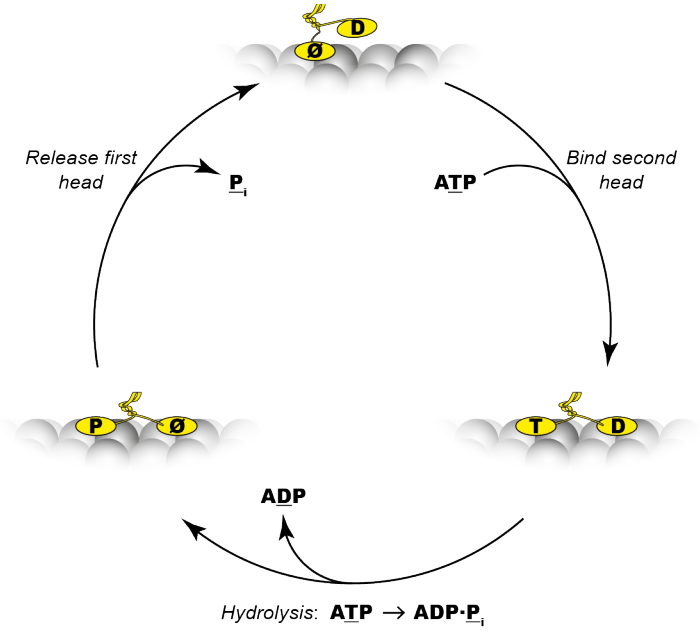

Figure 1.3: Kinesin-1 ATPase cycle. Kinesin binds to the MT lattice with one head in a no-nucleotide state (*top*). This (first) head is able to bind ATP, which promotes binding of the second head (*right*). The second head releasee ADP as it binds, whilst ATP in the first head undergoes hydrolysis (*left*). The γ-phosphate (P_i; product of hydrolysis) is released, allowing the now ADP-bound head to detach from the lattice. This concludes the ATPase cycle, as the kinesin returns to the 'starting' position, only one binding-site closer to the MT plus-end and with the other head bound.

In this way a kinesin will step along a single PF in the MT lattice [129–131]. It hydrolyses one molecule of ATP per step it takes, which are approximately 8 nm in length [132], corresponding to the length of a single tubulin dimer. Kinesin-1 motility follows a hand-over-hand mechanism, alternating which head binds to consecutive tubulins along a PF [133]. ATP hydrolysis is tightly coupled to the specific interactions between kinesins and MTs. The basal rate of kinesin-stimulated ATP hydrolysis is very low. Unpolymerised tubulin accelerates the turnover but the effects are marginal

compared to those induced by MTs [134].

Structural basis for kinesin stepping

Kinesin motor domains have highly conserved structures, which may be described as a composition of 3 layers. The first layer, which contains the MT-binding surface, is a cluster of α-helices. The second and third layers consist of an 8-stranded β-sheet and a second cluster of α-helices, respectively (Figure 1.4). The nucleotide-binding pocket is located distal to the MT-binding surface. Three highly conserved sequences have been identified to interact with the nucleotide, the functionality of which are mirrored in G proteins and myosins [135]. The first domain is the p-loop, located optimally to sense the presence or absence of a γ-phosphate on bound nucleotides. The other domains are the so-called 'switch' regions. Switch I is found in loop 9 of the kinesin structure, whereas switch II is comprised of the α-helix cluster (and connecting loops) on the MT-binding face (Figure 1.4).

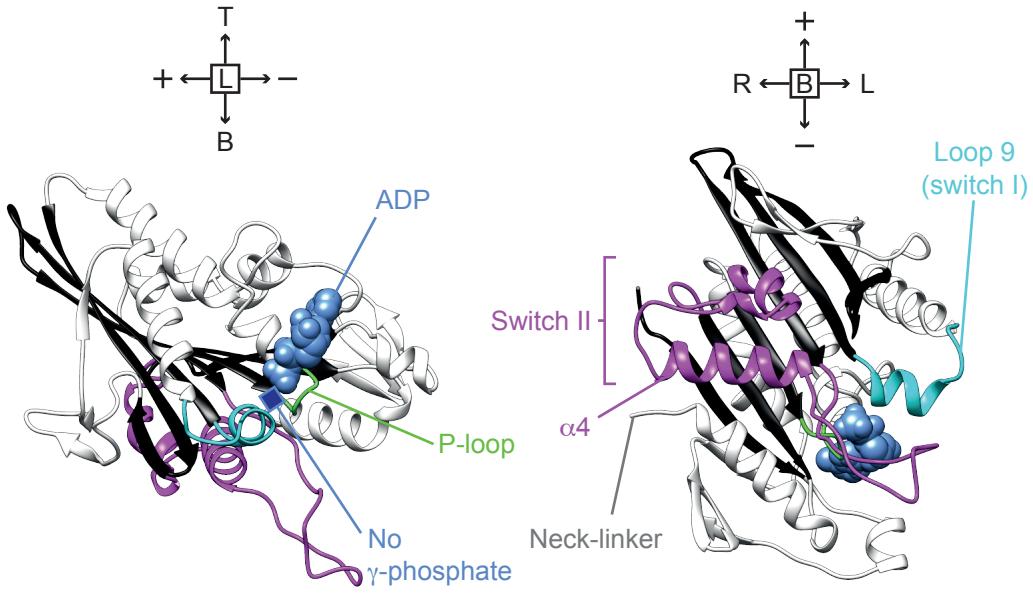

Figure 1.4: Crystal structure of an ADP-bound kinesin-1 motor domain. Two orientations of the same structure (1BG2 [136]) are shown, denoted by the arrows at the top of the figure. B – bottom (MT-binding surface), T – top, ± – the polarity adopted upon binding to a MT, L/R – left/right assuming a 'birds-eye view' with the MT plus-end at the top of the page. The central β-sheet is shown in black, the switch regions are colour-coded and the location of γ-phosphate in the case of ATP is highlighted.

Due to the association between the switch regions and bound nucleotides, one might expect conformational changes to occur upon nucleotide exchange. However, a comparison of kinesin crystal structures revealed that there is little or no correlation between the nucleotide state and the conformation of the switches [137].

Kinesin-stimulated ATP hydrolysis is over thirty times faster in the presence of MTs than in solution [138]. This demonstrates that kinesins are sensitive to bound nucleotides and that the ATPase cycle is tightly regulated by interactions with MTs. Recently published crystal structures of kinesin-tubulin complexes shed light on this mechanism (Figure 1.5) [139, 140]: When bound to ADP, the N-terminal end of the α4 helix and loop 11 are highly flexible [136]. In fact, high-resolution EM reconstructions of MT-kinesin complexes have shown this region to be flexible even upon binding to the MT, prior to ADP release [141]. Upon binding to tubulin and releasing ADP, much of loop 11 is incorporated into helix α4, extending it by 2.5 turns. This remodelling serves two purposes; it negates the steric clash between loop 11 and α-tubulin and establishes bonds between the switches that seem to be maintained until a post-hydrolysis state is reached [142].

Subsequent binding of ATP sees that large conformational changes occur. Subdomains rotate in a manner that closes the nucleotide-binding pocket (Figure 1.5, [142]). Simultaneously, the neck-linker docks in a groove that arises along the side of the motor domain. Docking of the neck-linker is thought to be an essential force producing stage of the stepping cycle [143]. Closure of the nucleotide-binding pocket stimulates ATP hydrolysis. The γ-phosphate is released following hydrolysis, which returns the motor domain to an ADP-bound state. As discussed, this has a low affinity for the MT lattice and so detaches.

1.5.2 Inhibition of MT shrinkage by kinesin-1

Reports are conflicting as to whether kinesin-1 directly affects MT dynamics [113, 144]. Indirect effects have been shown to occur, as kinesin-1 transports cargo to MT tips that modify their dynamics [112, 113]. Kinesin-1 has been reported to have no affect on

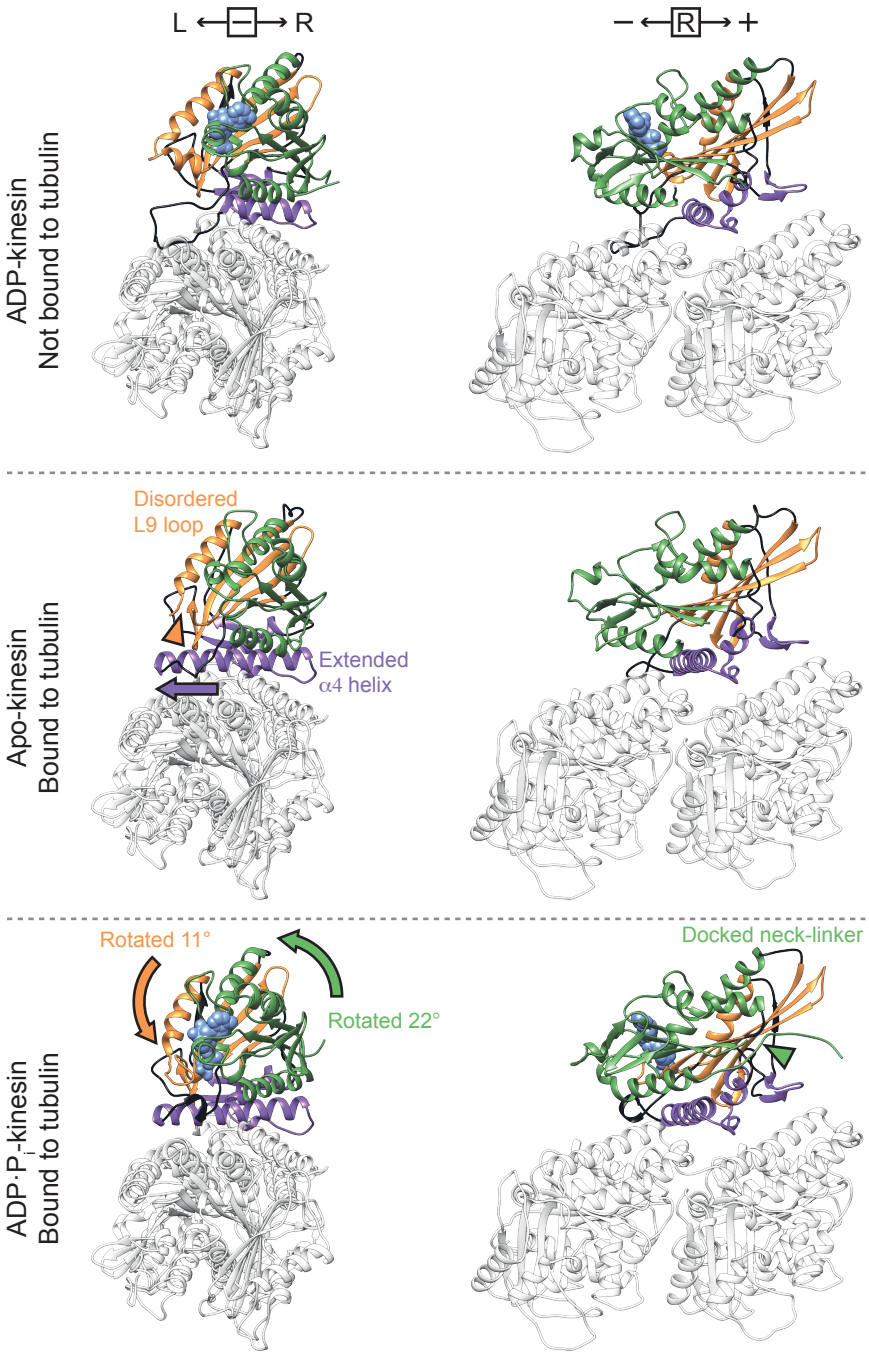

Figure 1.5: Conformational states of the kinesin-1 ATPase cycle. *Top*: A crystal structure of an ADP-bound kinesin-1 motor domain. Tubulin is shown for completeness of the illustration only; it is not part of the crystal structure. The structure shown is the same as in Figure 1.4 (1BG2). The α4 helix is short. Loop 11 is extended, frequently found to be disordered in ADP-kinesin structures; the conformation shown has steric clashes with tubulin. *Middle*: Upon binding to tubulin, kinesin naturally adopts a nucleotide-free state (structure 4LNU). Helix α4 adopts an extended conformation. Loop 9/switch II is disordered in this structure. *Bottom*: The upper domains of the kinesin are seen to rotate upon binding ATP (structure 4HNA), closing the nucleotide-binding pocket. These rearrangements allow the neck-linker to dock along the right-hand-side. The neck-linker is not shown in the other crystal structures because it is intrinsically disordered when undocked. Orientation markers follow the same notation as in Figure 1.4. Kinesin subdomains are coloured according to [140].

MT dynamics *in vitro* [145]. However, Katsuki et al. demonstrated that GDP-MTs can be stabilised by binding them to a kinesin-coated surface in the absence of nucleotides [23].

We refer to the experimental arrangement that was used as a kinesin-clamp. MTs are bound to a layer of kinesins that are tethered to a cover-slip, similar to a conventional gliding-motility assay. The factors that distinguish a kinesin-clamp from a motility assay are that the MTs are dynamic (rather than stabilised), and nucleotides and unpolymerised tubulin are washed from the flow chamber.

Depletion of GTP-tubulin triggers MT catastrophes and rapid depolymerisation typically follows [48]. However, MTs depolymerise very slowly in the absence of GTP-tubulin in a kinesin-clamp. This phenomenon cannot be explained by the literature published to date.

Many of the complexities underlying MT and kinesin dynamics are not present in a kinesin-clamp assay. In the absence of nucleotides, kinesins bind tightly to the MT lattice and do not step. MT polymerisation is negligible due to the lack of GTP-tubulin in solution. Furthermore, GTP-cap theory suggests that depolymerising MTs consist exclusively of GDP-tubulin. Therefore, in a kinesin-clamp assay mechanical factors are isolated from chemical complexities.

Splaying of PFs is thought to have a great effect on MT shrinkage rates [32]. Due to the loss of lateral contacts upon PF bending, the dissociation of tubulin is no longer limited to one dimer at a time; oligomeric loss is equally likely (Figure 1.6A). Increasing the on-rate of tubulin to PF tips is not an effective way to enhance MT stability for this reason. The main challenge for inhibiting MT shrinkage is therefore about preventing dissociation. To do this effectively, lateral contacts must be maintained. There are several ways how this could be achieved, which we discuss in the context of a kinesin-clamp.

Firstly, the coverslip could serve as a brace which prevents PFs from curling outward. Given plentiful attachment sites, the rigidity of the substrate could be imposed upon PFs, ensuring that a linear geometry is maintained (Figure 1.6C). Indeed, fluorescently-labelled MTs bound to a glass cover-slip by anti-fluorophore

antibodies exhibit increased stability [23]. This suggests that the geometry of a clamp assay presents a mechanism for MT stabilisation. Such a mechanism would have implications for the dynamics of MTs in bundles, where instead of a coverslip, another MT could be used as a brace.

Other possible mechanisms include cross-linking between tubulin dimers in the MT lattice (Figure 1.6B,D). Lateral cross-linking (between PFs) could promote stability. If inter-PF bonds are reinforced, the tendency for PFs to splay outward at the MT tip may be reduced. Similarly, longitudinal cross-linking (within PFs) could decrease dissociation or prevent curling at the inter-dimer interface.

Two distinct possibilities remain. Firstly, if the tether length is sufficient to reach around the MT, stability may be conferred by steric constraints. PFs will be unable to splay outward if the whole MT structure is tied to the substrate (Figure 1.6F). A final mechanism would arise if the binding of kinesin-1 induces conformational changes in the MT lattice (Figure 1.6E). Stabilisation of MTs by kinesins that are not bound to a substrate has very recently been reported for GTP-tubulin (but not GDP-tubulin) [146]. If kinesins could stabilise the tracks that they walk upon, they could provide a mechanism to ensure that cargo reaches its destination prior to MT disassembly *in vivo*.

We hypothesised that, based on the reports in the literature discussed above, the kinesin-clamp phenomenon is most likely to arise by the 'rigid substrate' mechanism (Figure 1.6C).

1.6 Outline

In this project we aimed to clarify the mechanism of MT shrinkage inhibition in a kinesin-clamp assay, and how the effect might be regulated.

Firstly, we present our methods (Chapter 2). We then discuss the optimisation of a kinesin-clamp assay for the characterisation of novel tip structures that we found to emerge at shrinking MT tips (Chapter 3). We performed quantitative analysis on data obtained from the optimised assay. Models were fitted to intensity profiles extracted from

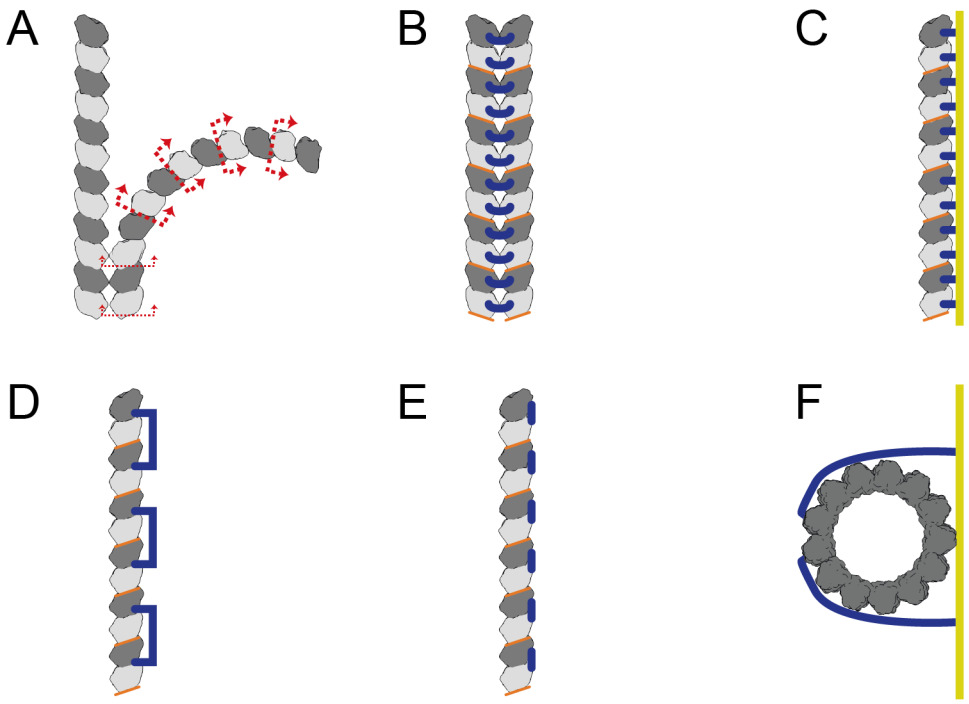

Figure 1.6: Possible mechanisms for the inhibition of MT depolymerisation. **A.** Normal MT depolymerisation. In the absence of lateral contacts, PFs are equally likely to break at any point along their length. **B.** Tubulins are laterally cross-linked. **C.** PFs are unable to bend because they are tethered to a rigid substrate (e.g. a coverslip or another MT). **D.** Tubulins are cross-linked longitudinally. **E.** Protein (e.g. kinesin) allosterically modifies tubulin to enhance lattice contacts. **F.** Long tethers reach around the MT, sterically hindering PF splaying. Orange lines are included to highlight inter-dimer interfaces.

the image data, which gave deeper insights to the underlying mechanisms (Chapter 4). The potential for kinesin-regulated MT dynamics in solution was investigated along with the influence of nucleotides on MT depolymerisation (Chapter 5). In Chapter 6 we propose models to explain our data and discuss the implications for the regulation of MT dynamics *in vivo*.

2

Materials and methods

2.1 List of reagents

Reagents used during the course of this PhD are listed below. Unless stated otherwise (in parentheses), reagents were obtained from Sigma-Aldrich Co. LLC. Square brackets identify product numbers.

ADP	Adenosine 5'-diphosphate sodium salt [A2754]
Alexa Fluor-488 dye	(Fisher Scientific) Alexa Fluor-488 carboxylic acid, succinimidyl ester mixed isomers [10266262]
AMPPNP	Adenosine 5'-(β,γ-imido)triphosphate lithium salt [A2647]
ATP	Adenosine 5'-triphosphate [A2383]
Anti-His antibodies	(Qiagen) Anti-5×Histidine IgG1 antibody [34660], (Thermo Scientific) Anti-6×Histidine IgG2b antibody [MA121315], (Invitrogen) Anti-6×Histidine IgG1 antibody [372900]. All are monoclonal from mouse.
Biotinylated tubulin	(Cytoskeleton Inc.) [T333P]
α-casein	[C6780]
Catalase	[C40]
Cover glasses	(Menzel-gläser) Number 1,5. Both 22 mm × 22 mm [MNJ-400-030Y] and 22 mm × 50 mm [12362128] were used depending upon the application.
Dimethyldichlorosilane	[40136-1ML-F]
D-glucose	[7528]
GFP-His	(Millipore) 6×Histidine-tagged green fluorescent protein (GFP) [14-392]

Glucose oxidase	[G-7016]
GMPCPP	(Jena Bioscience) Guanosine-5'-[(α,β)-methyleno]triphosphate, Sodium salt [NU-405S]
GTP	Guanosine 5'-triphosphate sodium salt hydrate [G8877]
$MgSO_4$	Magnesium sulphate [M3409]
Microscope slides	(Menzel-gläser) 1.0 mm × 1.2 mm thickness, 76 mm × 26 mm [BS7011/2].
Neutracon® detergent	(Decon Laboratories Ltd) [10253710].
NeutrAvidin	(Thermo Fisher Scientific)
PELCO® optical lens tissue	(Ted Pella Inc.) [806-1]
PIPES, free acid	(Melford Laboratories Ltd.) Piperazine-N,N'-bis-(2-ethanesulfonic acid) [B2004]
PLL-PEG-biotin	[SuSoS AG] Poly-L-Lysine (20 kDa) grafted with poly(ethylene glycol) (2 kDa) and poly(ethylene glycol)-biotin(50% functionalised) (3.4 kDa). Diluted to a stock concentration of 2 mg ml^{-1} in PBS buffer, pH 7.4.
Trichloroethylene	[251402]
Tween®20	[P6585]
X-rhodamine labelled tubulin	(Cytoskeleton Inc.) [TL334M-A]

2.2 Frequently used solutions & practices

Some solutions and techniques are common to all of the experiments, which we describe in this section.

2.2.1 Buffers

We use K-PEM as the standard buffer in each of our experiments. All dilutions of reagents were made using K-PEM unless stated otherwise. We use the following recipe: 100 mM PIPES, 2 mM EGTA, 1 mM $MgSO_4$, pH 6.9. The pH is adjusted using KOH (we do not use NaOH because it accelerates the hydrolysis of GMPCPP).

Phosphate-buffered saline (PBS) is used for storage and subsequent dilutions of PLL-PEG-BTN.

2.2.2 Oxygen-scavenger system

We use the GOC (glucose, glucose oxidase, catalase) system to reduce photodamage in our experiment, following the handling guidelines in the Mitchison protocols online (http://mitchison.med.harvard.edu/protocols.html). Glucose, glucose oxidase and catalase were stored at 100× concentration in K-PEM; 450 mg ml^{-1}, 20 mg ml^{-1} and 3.5 mg ml^{-1}, respectively. A 10× oxygen scavenger solution was made by mixing the stocks to 10% (v/v), supplementing the solution to a final concentration of 5% (v/v) β-Mercaptoethanol.

2.2.3 Handling of reagents

We found each of the following to improve conditions in our assays.

- Tubulin was kept in liquid nitrogen until minutes before use, at which point it was thawed rapidly.
- Every reagent was centrifuged prior to imaging with dark-field illumination to improve image quality. This means centrifuging components of the oxygen-scavenger system separately.
- Ends of the flow chamber were kept moist. We achieved this by 3D-printing specimen racks to fit inside empty pipette tip boxes. Damp tissues could then be placed inside the box underneath the sample to maintain humidity.
- Many of our experiments required solutions to be flowed through a sample chamber while mounted on the microscope stage. In such experiments it is difficult to avoid stage drift. Our typical procedure for minimising stage drift is to enclose the microscope in a custom-made housing with regulated temperature. However, the casing had to be opened in order to perform the flow-throughs. Maintaining the room temperature close to the enclosure temperature improved conditions.

2.3 Protein purification and labelling

K340 was purified as in [147] and T93N as in [144]. Purified kinesin was available throughout the duration of this project, as purified previously by Maria Alonso. Tubulin was purified as described in [23]. Purification was done with the help of Douglas Drummond and Naomi McIntyre.

Alexa Fluor-488 labelling of tubulin was achieved by following the protocol described in [148]. However, we used K-PEM buffer for the polymerisation steps rather than MES buffer.

2.4 Coverslip treatment

A critical step in ensuring the success of a microscopy-based assay is the treatment of the coverslips. It is important that the surface has the right chemical properties to attract or repel proteins as desired. Proteins can be immobilised either through specific chemical interactions or, more commonly, through non-specific adsorption.

2.4.1 Ultrasonic glass-cleaning (for a hydrophilic surface)

Cleaning is the simplest method for treating glass. The method described below uses an ultrasonic bath to remove the majority of particles from the glass surface, followed by plasma cleaning to remove small organic contaminants. The resulting surface is highly hydrophilic Figure 2.1A.

300 ml of ultra-pure water (18.2 MΩ cm resistivity) was heated to just below boiling point on a hotplate, before adding 9 ml of Neutracon detergent. Cover-slips held in metal or polytetrafluoroethylene (PTFE) racks (Molecular Probes, C14784) were immersed in the solution and transferred to a 600 W ultrasonic bath (Ultrawave Ltd). The solution was sonicated at 60 °C for 30 min. The racks were rinsed in 300 ml

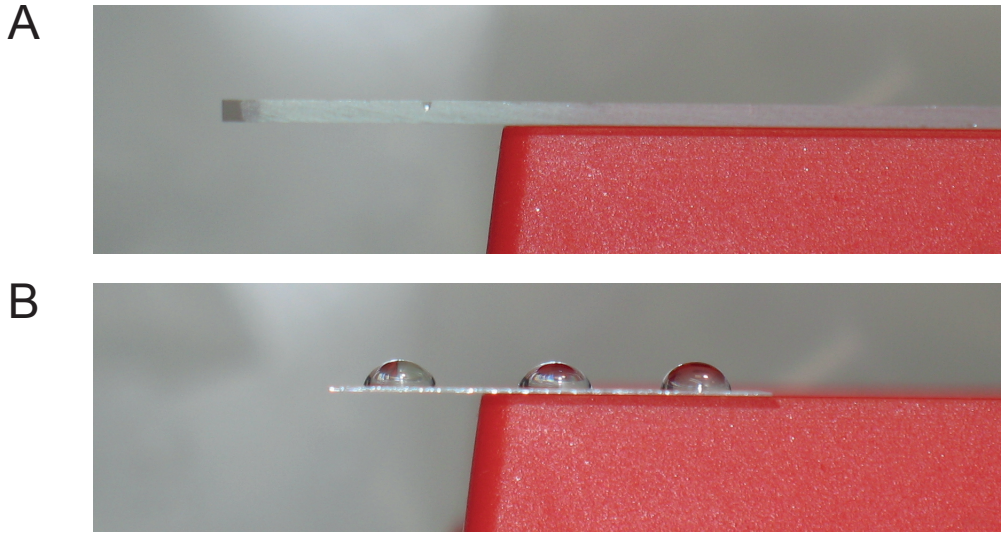

Figure 2.1: Glass treatment. 10 µl of ultra-pure water was pipetted onto glass. The hydrophobicity of the glass can be determined by measuring the contact angle of each water droplet. **A.** Hydrophilic slide. The glass was cleaned using detergent and extensive washing interspersed with rounds of sonication in an ultrasonic bath. The contact angle is too shallow for the water droplet to be seen, indicating a highly hydrophilic surface. **B.** Hydrophobic cover-slip. The glass was silanised with dimethyldichlorosilane. Three droplets can be clearly seen. The average contact angle of the three droplets is ~78° (measured by hand).

of ultra-pure water 10 times. A 6 min sonication followed by 3 rinses was repeated 3 times. A final round of cleaning consisted of a 5 min sonication followed by a single rinse, repeated 8 times. Racks were immersed in ethanol before drying the coverslips in a cover-slip spinner (Technical Video Ltd).

Clean cover-slips were wrapped in PELCO optical lens tissue, boxed and stored in a desiccator for up to two weeks. Immediately prior to using, cover-slips were plasma-cleaned for 5 min.

2.4.2 Silanisation (for a hydrophobic surface)

Due to the hydrophilic nature of clean glass, chemical modifications are necessary when a hydrophobic surface is desired. This is commonly achieved by reacting a silane with the hydroxyl groups exposed on clean glass . Silanes bind covalently to the glass, forming a monolayer with with a specified hydrophobicity. The following silanisation protocol involves the use of strong acid, so coverslips were housed in PTFE (rather than metal) racks.

Cover-slips were racked in a solution containing 150 ml of methanol (MeOH) and 150 ml of hydrochloric acid (HCl). The solution was sonicated in an ultrasonic bath for 30 min at room temperature. The racks were rinsed in 300 ml of ultra-pure water followed by 5 min of sonication, repeated 4 times. Racks were transferred to a beaker containing 200 mM potassium hydroxide (KOH) for a further sonication of 60 min. Five iterations of rinses in ultra-pure water with 5 min of sonication followed. Cover-slips were dried in a spin-drier and incubated in dry racks at 100 °C for 30 min. Dry cover-slips were plasma-cleaned for 5 min before beginning the silanisation process.

Dimethyldichlorosilane (DDS) was added to 250 ml of trichloroethylene (TCE) to a final concentration of 0.05 % (v/v) in a histology dish and mixed well with a PTFE stirrer. Racks were immediately submerged in the solution. The dish was closed with a lid and the cover-slips were left to incubate for 1 h. silanised cover-slips were rinsed in 300 ml of MeOH. Subsequently, they were sonicated for 5 min and rinsed in 300 ml of MeOH 6 times. Finally, cover-slips were spun-dry and wrapped in PELCO optical lens tissue for storage. Glass treated using this protocol would remain clean and hydrophobic for many weeks.

2.5 Flow chambers

Flow chambers were assembled using double-sided Scotch® tape (3M, 70070778074). Tape was cut into 2 strips (~30 mm in length) and firmly secured 2 mm apart on a clean glass slide. A suitably-treated cover-slip (see Section 2.4) was stuck to the other side of the tape to form a channel. Regions of tape that extended beyond the cover-slip were removed using a scalpel. The perimeter of the cover-slip, excluding the ends of the channel, was secured further using nail polish (Revlon).

Solutions were drawn through the chamber by capillary action. Droplets of solution were added to one end of the channel, while Whatman® filter paper (Sigma-Aldrich, WHA1001090) was used to draw fluid from the other end. Flow chamber volumes were consistently found to be ~5.5 µl.

2.6 Microscopy

2.6.1 Overview of common techniques

Currently, the most popular techniques for imaging cytoskeletal proteins involve the use of fluorescent probes. Synthetic dyes, fluorescent nucleotides or fluorescent fusion proteins are excited by a particular wavelength of light and emit at a longer wavelength. Only proteins that have been specifically labelled are illuminated. A downside of using fluorescent probes is that they only emit a finite number of photons before they become permanently extinguished, an endpoint known as photobleaching. As a consequence, there is a limit on the amount of images that can be captured. A second concern is that using invasive probes can potentially modify protein behaviour. The most frequently used fluorescence-oriented technique used for imaging MT dynamics is total internal reflection fluorescence (TIRF) microscopy.

Non-invasive methods have been successfully used to image MTs. An early characterisation of MT dynamic instability was done using differential interference contrast (DIC) microscopy [39]. A drawback of DIC microscopy is that it generates polarised images, potentially complicating subsequent analyses. Dark-field illumination is another non-invasive technique used to study MTs [37]. Dark-field microscopy is highly sensitive to *all* objects in a sample, so small contaminations such as dust particles can render samples unusable. By the same token, micro-scale objects such as MTs can be seen with exceptional contrast in clean solutions.

Many other types of microscopy are used to study the cytoskeleton. Those described here are among the most common techniques used for looking at MT and motor dynamics *in vitro*.

2.6.2 Dark-field & epifluorescence microscopy

Images were captured by an EM-CCD camera (iXon^{EM}+DU-897E, Andor) fitted to a Nikon E800 microscope with a Plan Fluor 100× 0.5–1.3 NA variable iris objective

and intermediate 1.25× magnification (1 pixel = 128 nm). A custom-built enclosure with an air heater (Air-Therm ATX, World Precision Instruments) was used to keep samples at 25 °C. Dark-field illumination was achieved using a 100 W mercury lamp connected to the microscope via a fibre optic light scrambler (Technical video), cold mirror, 500–568 nm band-pass filter (Nikon) and a dark-field condenser (Nikon). A stabilised mercury lamp (X-cite exacte, Lumen Dynamics) provided illumination for epifluorescence, connected to the microscope with a light pipe. Motorised filter wheels (Ludl Electronic Products) housed the fluorescence excitation and emission filters: 485/20 and 536/40 for Alexa-488 and 586/20 and 628/32 for X-rhodamine (Chroma). Combined dark-field and fluorescence imaging was achieved using an FF505/606-Di01-25x36 dichroic mirror (Semrock) and electronic shutters to switch between illumination modes. The shutters, filter wheels and camera were controlled using Metamorph software (Molecular Devices).

2.7 Antibody immobilisation

Summary

Proteins may appear to have reduced functionality when bound non-specifically to a coverslip . This may be due to undesired interactions with the surface or unfavourable orientations . Methods commonly used to circumvent this problem involve a 'protein sandwich' arrangement. Secondary proteins are bound to the surface nonspecifically, which link to the protein of interest at a point distal to the functionally important domain. A common strategy is to bind a biotinylated blocking agent (e.g. bovine serum albumin (BSA)) to the surface, followed by multivalent biotin-binding protein such as Streptavidin . This leaves a surface that binds exclusively to biotin-tagged proteins. Similarly, antibodies can be bound to the surface, which specifically bind a label of choice. Proteins are commonly tagged at a functionally redundant site for purification purposes, lending wide applicability to the antibody-based method. These methods only work if the first layer of the 'sandwich' is suitably secure. A protocol was

developed to assess how glass treatment and blocking agents influence binding efficacy in the antibody-based arrangement.

Method

A flow chamber was filled with $0.2\,\mathrm{mg\,ml^{-1}}$ of anti-His antibodies and left to incubate for 10 min. 20 µl of 35 µM His-tagged green-fluorescent protein (GFP) was flowed through the chamber and left for a further 10 min, before washing with 20 µl of K-PEM buffer. Casein was tested as a blocking agent at each stage of the process, added to a concentration of $0.5\,\mathrm{mg\,ml^{-1}}$. The extent of specific long-term binding was quantified by epifluorescence microscopy. Twenty spatially distinct regions were imaged for each flow chamber and pixel intensities were averaged for each field of view.

2.8 Gliding-motility assay

Summary

The gliding motility assay is a basic experiment used to characterise the velocity of motor proteins walking along MTs. Motors are attached to a coverslip before being exposed to stabilised MTs and ATP. The motors use ATP to step along the MTs, which are consequently pushed across the surface.

Preparation of GMPCPP-stabilised MTs

Tubulin (12 µM) was incubated on ice with 0.5 mM GMPCPP (slowly-hydrolysable analogue of GTP) for 15 min to promote nucleotide exchange. MTs were then polymerised by incubating the solution at 37 °C for 1 h in a water bath. Following polymerisation, the solution (80 µl) was centrifuged for 10 min at 45 krpm in a TLA-100 rotor (Beckman Coulter) to pellet the MTs. Unpolymerised tubulin was aspirated using a pipette. MTs were resuspended in 80 µl of warm K-PEM buffer, making a 200X MT solution for

motility assays.

Method

A flow chamber was assembled using a clean hydrophobic coverslip. 10 µl of 0.2 mg ml^{-1} anti-His antibodies were flowed through the chamber and incubated for 10 min. The surface was passivated with 10 µl of 0.5 mg ml^{-1} α-casein in K-PEM for 10 min. 30 µl of wash buffer (0.2 mg ml^{-1} of α-casein, 5 mM of dithiothreitol (DTT) in K-PEM). 10 µl of His-tagged rat kinesin (k430-His) was flowed through at a concentration of 12 µM with 0.2 mg ml^{-1} of α-casein and left for 10 min. The chamber was washed again, then 10 µl of MTs were added for 5 min before rinsing again (20 µl of wash buffer). Finally, 10 µl of motility buffer (1 mM ATP, 10 nM DTT, 1 mM $MgCl_2$ in K-PEM) was flowed through the chamber before sealing the channel with nail polish. MTs were imaged using dark-field microscopy.

2.9 MT dynamics

MT dynamics can be reconstituted *in vitro* by polymerising tubulin from nucleation templates such as axonemes or stabilised MT 'seeds'. MAPs and motors can then be added to see how they influence the parameters of dynamic instability. Polymerisation buffers commonly used for MT dynamics have 80–100 mM PIPES, 1–5 mM $MgCl_2$, 1–2 mM EGTA and 1–5 mM GTP. MT dynamics and mechanics are sensitive to these components, in particular the concentration of $MgCl_2$. In our experiments, 1 mM GTP and K-PEM buffer (100 mM PIPES, 1 mM EGTA, 1 mM $MgCl_2$, pH 6.9) were used, comparable to the characterisation of dynamic instability by Walker et al. [39].

Several approaches were tested for passivating the surface (to reduce non-specific binding) and specifically attaching seeds to the glass. The most effective arrangement for both criteria used a biotin-avidin-biotin sandwich. Poly-L-lysine-poly(ethylene glycol)-biotin (PLL-PEG-biotin), formed the first layer, followed by NeutrAvidin and biotinylated MT seeds. Proteins are repelled by PEG side-chains of the PLL-PEG-biotin

and NeutrAvidin is engineered to minimise non-specific binding. Non-specific binding was very low using this system and the seeds remained fixed to the surface even when high concentrations of blocking agent were added.

2.9.1 Reconstituted MT dynamics

Preparation of GMPCPP-stabilised MT seeds

A seed-polymerisation buffer was made by mixing tubulin (1:1:8 ratio of Alexa Fluor-488:biotin:unlabelled tubulin) with GTP in K-PEM to final concentrations of 26 µM and 1 mM, respectively. The solution was incubated on ice for 15 min to promote nucleotide exchange before snap-freezing 5 µl aliquots in liquid nitrogen. To make MT seeds, an aliquot of seed-polymerisation buffer was incubated at 37 °C for 25 min. The solution was diluted in 95 µl of 37 °C K-PEM before centrifuging for 5 min at 25 °C either in a TLA-100 rotor at 90 krpm or an A-110 airfuge rotor at 25 psi. Seeds were resuspended in 100 µl of warm K-PEM to make a 20X solution for MT dynamics assays.

Method

A flow chamber was assembled using a clean hydrophilic coverslip. The flow chamber was filled with PLL-PEG-biotin diluted to 0.2 mg ml^{-1} in PBS buffer (pH 7.4) and left for 10 min or longer. Extensive washing was carried out (100 µl of K-PEM) to remove any unbound PLL-PEG-biotin after. 20 µl of 1 mg ml^{-1} NeutrAvidin was flowed through the chamber and incubated for 5 min, followed by 20 µl of K-PEM. A 1X MT seed solution in K-PEM was flowed through to a volume of 20 µl. Unbound seeds were washed out with 20 µl of K-PEM. Finally, 15 µl of a MT dynamics solution was flowed through, comprised of tubulin (10–20 µM), 1X oxygen-scavenger system, 1 mM GTP, 1 mg ml^{-1} BSA and 1 % Tween20 (v/v) in K-PEM. The flow chamber was incubated at 25 °C for at least 20 min before imaging to give MT dynamics time to equilibrate.

Images were captured using dark-field microscopy for dynamic MTs and epifluorescence for the seeds.

2.9.2 Tubulin depletion

A tubulin depletion assay was developed to investigate the effects of kinesin on the dissociation of tubulin from MT tips. The complication of GTP-tubulin association is removed by isothermal dilution, which naturally induces catastrophes [48].

MTs were initially grown as in the dynamics assay described above (using 15 µM tubulin). MT dynamics in an unsealed flow chamber were imaged at an appropriate frame rate. 30 µl of dilution buffer (dynamics solution minus GTP-tubulin) was flowed through the chamber to initiate MT depolymerisation. Monomeric kinesin (K340-His) was included in the dilution buffer to assess the effect of kinesin on tubulin dissociation. Nucleotides (ADP or AMPPNP) were added at saturating concentrations (1 mM) to isolate kinesins in particular phases of the ATPase cycle. Examinations of the no-nucleotide state were most frequently carried out using a mutant kinesin (K340T93N-His).

2.10 Kinesin-clamp

The kinesin-clamp assay was described in Chapter 1. Optimisation of the protocol is given in Chapter 3. Here, we describe the preparation of dual-colour fluorescence controls used in the optimised version of these experiments. 30% Alexa Fluor-488 labelled tubulin diluted to 25 µM in the presence of 1 mM GMPCPP was incubated on ice for 20 min to promote nucleotide exchange, before snap-freezing in 5 µl aliquots. X-rhodamine labelled tubulin stocks were prepared similarly.

An Alexa Fluor-488 labelled stock solution was diluted 5-fold with warm K-PEM and incubated for 1 h at 37 °C. MTs were centrifuged for 10 min in an airfuge and resuspended in a 5-fold dilution of the X-rhodamine labelled stock supplemented with β-mercaptoethanol to 0.5% (v/v). Seeds were kept in a sealed tube and away from

light sources to prevent photodamage. The solution was left at room temperature overnight to allow MT segments to anneal. This resulted in a 50× solution for use in the optimised kinesin-clamp assay.

2.11 Image analysis

Image analysis was performed using Matlab. Stage drift was apparent in some of our data, particularly in long movies. We therefore corrected for stage drift in all of our movies using an efficient registration algorithm [149]. We exploited the static MT seeds in our data for this purpose. All images of seeds were aligned to the image of seeds at time $t = 0$. Once the transformations had been found for the images of seeds, they were applied to the corresponding time points for dynamic MTs also.

Flat-field correction was applied to our fluorescence data to counter the effects of uneven illumination. We imaged a dilution series of free Alexa Fluor-488 dye in solution, each of which serve as a uniform sample. We fitted a straight line to a plot of dye concentration vs. fluorescence signal for each pixel. The intercept was found to be non-zero (and much greater than a measured dark signal) for all pixels, having approximately the same values as a blank sample (buffer but no dye). This demonstrates that there was some background signal. To correct for the uneven illumination, we subtracted pixel intensities measured for a blank sample and then divided by the slope of the best fit lines.

Shrinkage rates of MTs were measured by kymograph analysis. A straight line was drawn manually to identify the location of a MT. Pixel intensities were averaged over a cross-sectional range of ±5 pixels (640 nm) to produce a line scan that is representative of the total fluorescence per unit length of the MT. This was repeated for all time points in a movie. Line scans are then displayed sequentially to produce a kymograph. MT tips were then traced manually and their average shrinkage rates calculated accordingly. Time and length calibrations were automated by extracting the image metadata. Shrinkage rates were converted to dimer $\mathrm{PF}^{-1}\,\mathrm{s}^{-1}$ by assuming each tubulin dimer is 8 nm long.

3

Optimisation of a kinesin-clamp assay

Defining the mechanisms of kinesin-regulated MT dynamics is important for building a comprehensive understanding of the cytoskeleton. However, conflicting results have been reported for the effect of kinesin-1 on MTs (see Chapter 1). From the work of Katuski et al., it is clear that kinesin-1 has the ability to inhibit MT depolymerisation [23].

In their 'kinesin-clamp' assay, dynamic MTs are bound to a kinesin-coated surface before removing nucleotides and tubulin from solution. The lack of GTP-tubulin in solution means that subunit loss, but not addition, can occur at MT tips. Consequently, the GTP-cap dissociates early in the experiment, resulting in a single-nucleotide-state (GDP) MT. Additionally, the absence of nucleotides means that the kinesins bind but don't walk along the MT. As such, nucleotide-related chemical effects are removed, thus isolating the mechanical factors of kinesin and MT dynamics.

The reduction of kinesin-MT interactions to a mechanical problem provides a strong basis for investigating possible regulatory mechanisms. We developed a kinesin-clamp assay to investigate the mechanisms of kinesin-induced MT stabilisation. By perturbing the system, we aimed to discover how kinesin-1 is able to inhibit MT depolymerisation and how the effect might be regulated.

3.1 Optimising the foundations of a kinesin-clamp assay

The foundations of a kinesin-clamp are the same as those used for a conventional gliding-motility assay (i.e. a bed of kinesins bound to a glass coverslip). However, a gliding-motility assay is a much simpler system because it involves non-dynamic MTs. We exploited this simplification in order to optimise imaging conditions and to ensure that the foundations of the experiment are robust. Anti-His antibodies were bound nonspecifically to the glass surface and used to immobilise the kinesin. Kinesin therefore binds in the desired orientation, with the 6×His-tag closest to, and the MT-binding site furthest from, the coverslip. This maximises the density of functionally oriented kinesins for binding to MTs.

3.1.1 Dark-field imaging conditions

We adopted dark-field illumination for imaging motility assays. Using this technique, MTs can be observed without the use of fluorescent probes that could potentially interfere with MT-kinesin interactions or the structural integrity of the MT [150, 151]. Furthermore, it permits many images of a sample to be taken because photobleaching does not occur.

The main problem with dark-field illumination is that nanoscale particles in solution generate a large signal. Small protein aggregates can substantially diminish the signal-to-noise ratio and larger contaminations render a sample unusable. Indeed, MTs were difficult to see in our early gliding-motility assays (Figure 3.1A).

Gliding-motility assays were produced by flowing antibodies ($0.2\,\mathrm{mg\,ml^{-1}}$) into a flow chamber, sequentially followed by α-casein ($0.5\,\mathrm{mg\,ml^{-1}}$) to passivate the surface, buffer, kinesin ($12\,\mu\mathrm{M}$), buffer, GMPCPP-stabilised MTs and finally a motility buffer containing $1\,\mathrm{mM}$ ATP. Initially, MTs showed a poor signal-to-noise ratio and many aggregates appeared to be bound to the surface (Figure 3.1A).

By imaging each component of the experiment separately, we identified several problems. The aggregates on the glass were largely attributed to the anti-His antibodies,

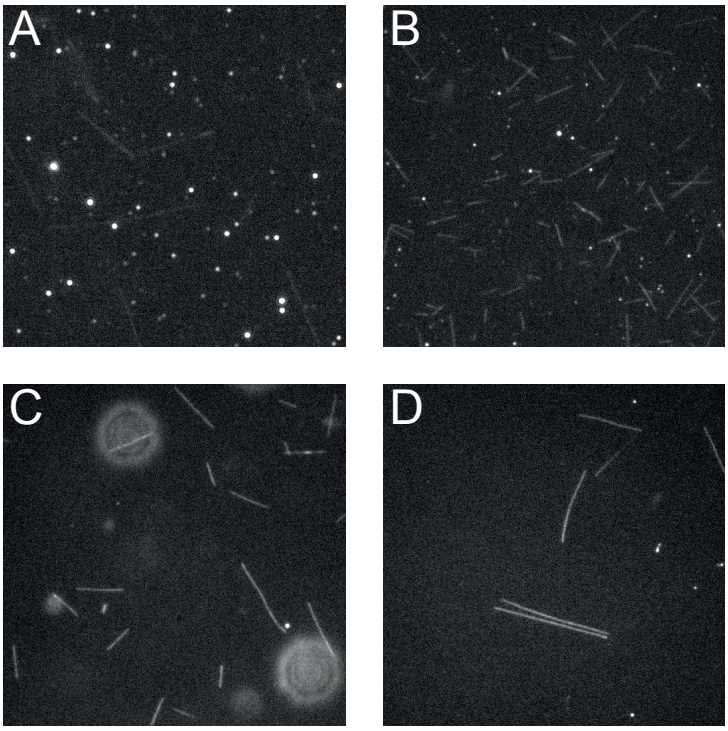

Figure 3.1: Progression of dark-field imaging conditions for a gliding-motility assay. **A.** First observations of MTs showed a poor signal-to-noise ratio and many aggregates obscured the field-of-view. **B.** Image quality was improved by using different antibodies (Thermo Scientific [MA121315]) and clarifying by centrifugation. **C.** Casein was stored at $1\,\mathrm{mg\,ml^{-1}}$ rather than $10\,\mathrm{mg\,ml^{-1}}$. All components (antibodies, casein, kinesin) were clarified by centrifugation, producing in a strong signal. A few aggregates remained in solution (large concentric rings). **D.** Casein was omitted from the motility buffer, which reduced the number of aggregates in solution.

although the kinesin solution contributed slightly. Fresh antibodies were tested under different storage conditions (before and after snap-freezing in liquid nitrogen) and after centrifugation to clarify the solution. However, aggregates remained in all cases. Major improvements were observed when using different antibodies (Thermo Scientific [MA121315] rather than Qiagen [34660]), which were clarified further by centrifugation (Figure 3.1B).

Aggregates in solution were attributed to α-casein. Storage at $1\,\mathrm{mg\,ml^{-1}}$ rather than $10\,\mathrm{mg\,ml^{-1}}$ followed by centrifugation improved the signal-to-noise ratio significantly. The kinesin solution was also clarified by centrifugation, which produced a clean image (Figure 3.1C). Some aggregates still remained in the α-casein solution and the extent of aggregation was seen to increase over time. This complication was overcome simply by omitting α-casein from the motility buffer (Figure 3.1D). Casein is important for achieving optimal kinesin functionality in a gliding-motility

assay. However, omitting casein from the motility buffer has minimal impact if it is supplemented to all prior solutions that are flowed through the chamber [152].

3.1.2 Specific immobilisation of histidine-tagged proteins on a glass surface

MTs in the gliding-motility assay could occasionally be seen to pivot rather than move linearly, indicating a low density of kinesin on the surface. Such conditions are clearly undesirable for studying the effect of kinesins on MT dynamics. We designed a simple assay for assessing the effectiveness of the antibody-coated surface.

Anti-His antibodies were bound to glass cover-slips before passivating the surface with α-casein, as in the motility assay. His-tagged green-fluorescent protein was then added as a probe in place of the kinesin. The density of His-tag-binding sites was then assessed by epifluorescence microscopy after washing the flow chamber with buffer. Results are shown in Figure 3.2A. A fluorescent signal was present after washing the flow chamber with 20 µl of buffer. However, the signal diminished to background levels when the volume was increased to 100 µl, indicating that the antibodies bound to the glass weakly (or not at all). Indeed, omitting the antibodies showed little difference. When the surface was not passivated with casein, there was a marked increase in the amount of GFP that remained bound. A similar response could be seen when both antibodies and casein were not included. Casein clearly passivated the surface well and prevented non-specific binding of GFP to the cover-slip. However, the results suggest that the antibodies were not functioning as intended.

The glass-cleaning protocol involves a cycle of plasma-cleaning. We checked whether this weakens antibody-glass interactions but the results proved negative (Figure 3.2B). We then tested cover-slips with a chemically modified (dimethyldichlorosilane-treated) surface. Dimethyldichlorosilane (DDS) is widely used to render cover-slips with a hydrophobic surface [153]. When antibodies were not included the fluorescence we recorded did not exceed background levels. In contrast, a high signal was retained even after extensive washing when all components were included. Therefore, antibodies bind

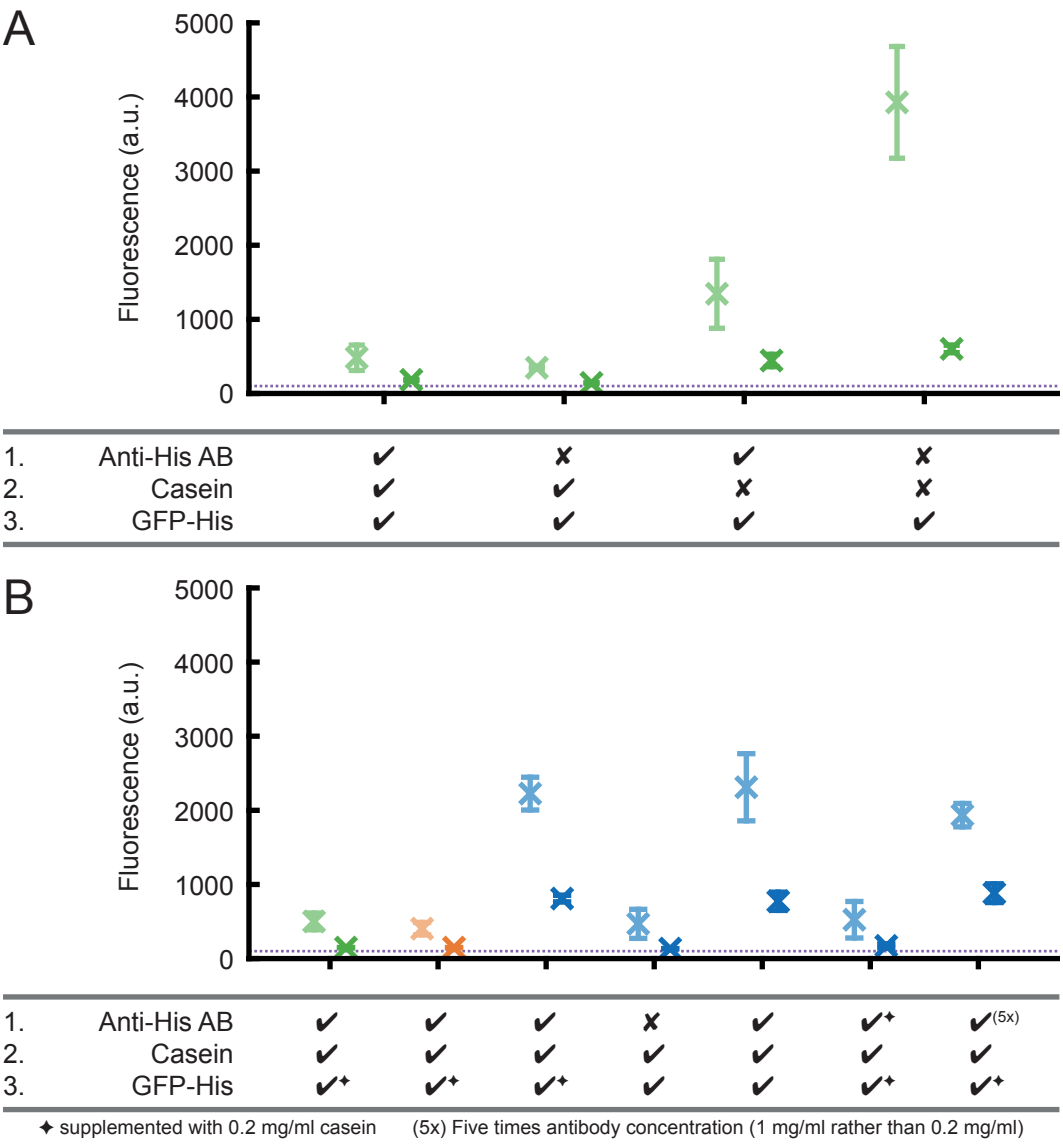

	Cover-slip treatment		
Wash volume	Hydrophilic (plasma cleaned)	Hydrophilic (not plasma cleaned)	Hydrophobic
20 µl	✘	✘	✘
100 µl	✘	✘	✘

Figure 3.2: Optimisation of specific protein immobilisation on glass. Components were flowed into a flow chamber (in the order given, #1-3), followed by extensive washing. The extent of specific GFP-His immobilisation was assessed by epifluorescence microscopy after $20\,\mu l$ and $100\,\mu l$ of washing. Images were captured for each condition at 20 random locations within each flow chamber and median fluorescence intensities for each image were calculated. Error bars are mean ± standard deviation. **A.** Clean (hydrophilic) glass was tested for specific antibody immobilisation. Antibodies did not increase the binding of GFP-His. **B.** Binding to DDS-treated (hydrophobic) glass was compared to hydrophilic glass. Casein successfully passivated the surface to prevent non-specific binding of GFP-His. Antibodies bound to hydrophobic glass and demonstrated high levels of specific GFP-His immobilisation. Hydrophobic glass clearly outperforms hydrophilic glass (whether the glass is plasma-cleaned or not). The dotted line marks the signal background, measured by imaging a sample with no GFP present.

effectively to DDS-treated glass, while nonspecific binding is readily prevented by passivating the surface with casein. Supplementing the GFP with casein (to $0.2\,\mathrm{mg\,ml^{-1}}$) showed no effect but supplementing the antibodies with casein returned the signal to background levels. This indicates that casein can outcompete the antibodies for binding to the glass if they are incubated at the same time. It is therefore important that antibodies are allowed to bind to the glass before any blocking agents are added to the flow chamber. No improvement was seen by increasing the antibody concentration above $0.2\,\mathrm{mg\,ml^{-1}}$.

3.1.3 Development of a basic kinesin-clamp assay

We developed a basic kinesin-clamp assay once a robust kinesin surface had been established (Figure 3.3). MTs were nucleated from GMPCPP-stabilised MT seeds, which we found to be crucial for method optimisation. Seeds were bound to the kinesin surface before dynamic MT extensions were grown by adding 1 mM of GTP and 16 µM of tubulin. Dynamic MTs could be observed before GTP-tubulin was depleted. Following tubulin depletion, MT shrinkage rates could be measured to see whether depolymerisation was inhibited.

An alternative approach to using seeds is to nucleate MTs by using high tubulin concentrations. However, the density of MTs is so great at these concentrations that individual MTs cannot be distinguished by 2D micrographs until after the tubulin is depleted. MTs that are not immobilised on a kinesin-coated surface depolymerise at $130\,\mathrm{nm\,s^{-1}}$ at 25 °C (see Chapter 5). Hence, if the kinesin density is low or if the MTs do not bind to the surface effectively for any other reason, all of the MTs can fully disassemble in the time it takes to focus a microscope.

Tubulin that was used to assemble seeds was labelled with Alexa Fluor-488 (1:10 labelling stoichiometry) and imaged using epifluorescence, while dynamic MT extensions were again imaged using dark-field illumination. Seeds were seen to glide over the surface prior to the tubulin depletion step, demonstrating the ability of kinesin to generate motility using the energy from GTP hydrolysis. The polarity of

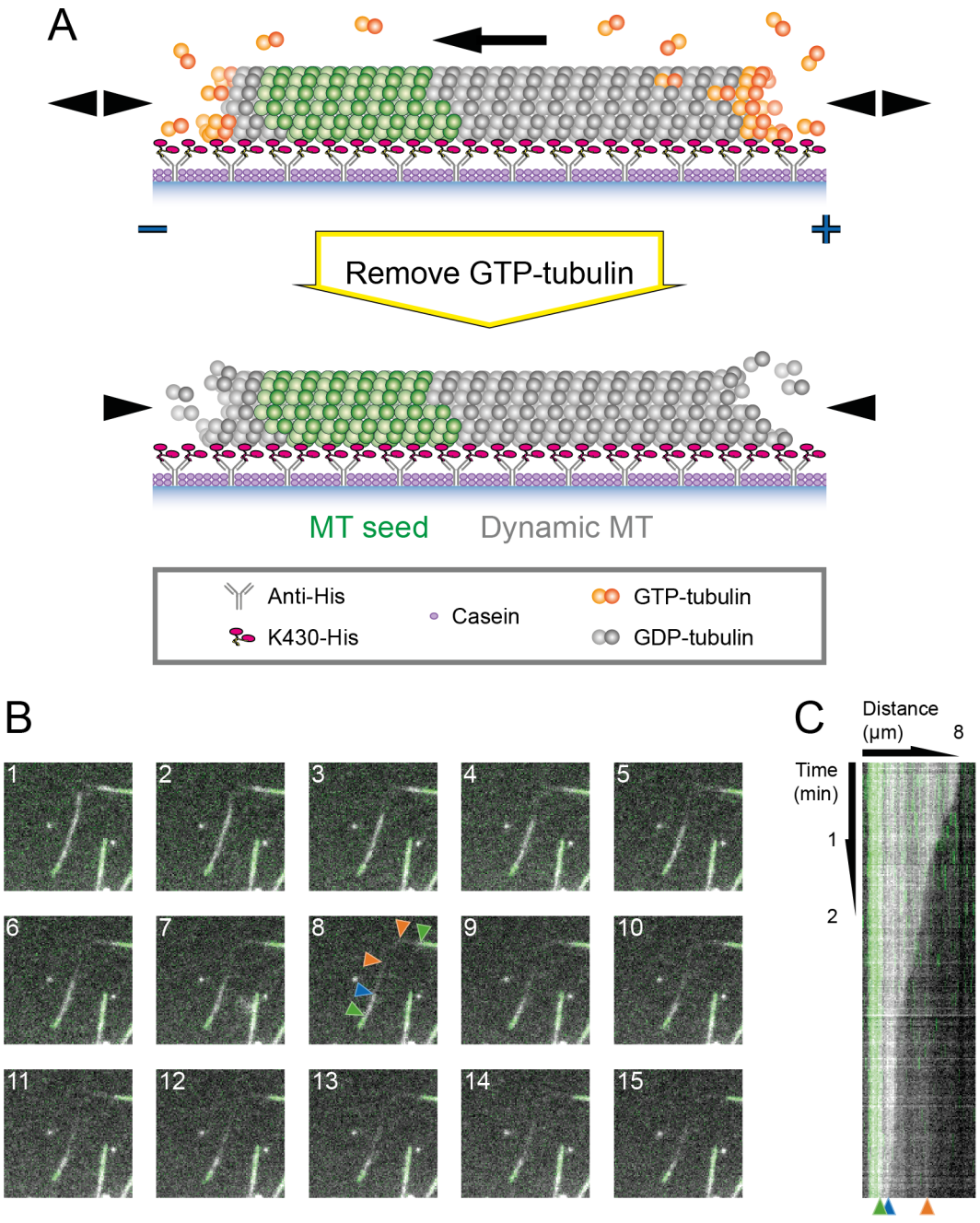

Figure 3.3: A kinesin-clamp assay for MTs grown from seeds. **A.** Kinesin-clamp schematic. Dynamic MTs (shown in grey) are grown from fluorescently labelled (Alexa Fluor-488) MT seeds (shown in green). In the presence of GTP and tubulin, MTs undergo dynamic instability and kinesins (K430-His) step in the direction of the MT plus-end. MTs are consequently pushed across the surface in the direction of their minus-end. Removal of GTP-tubulin by buffer exchange prevents MTs from growing and kinesins from stepping. MT growth proceeds at a greatly inhibited rate. **B.** Image sequence showing shrinking MTs in a kinesin clamp (frames are $21\,\mathrm{s}$ apart). Faint trails emerge in the wake of shrinking MT tips, highlighted in Frame 8. Triangles mark the ends of seeds (green), dynamic MTs (blue) and trails (orange). **C.** Kymograph corresponding to the central MT in (B). Features are highlighted by triangles at the bottom of the image, using the same colour-coding as in (B).

MTs can be identified from this motion because the directionality of kinesin-1 is well known. Kinesin-1 walks to MT plus-ends, so gliding MTs always translocate with their minus-ends leading.

We found 20 µM to be the optimal tubulin concentration for maximising the length of MTs. Using higher concentrations increased MT lengths but spontaneous nucleation occurred. MTs were incubated at 25 °C (imaging temperature) for 20 min to allow MT dynamics to equilibrate. MTs were then imaged while tubulin was depleted by flowing buffer through the flow chamber. We found that when GTP-tubulin was depleted, MT depolymerisation occurred at $\sim 0.3\,\mathrm{dimer\,PF^{-1}\,s^{-1}}$ (assuming tubulin dimers to be 8 nm in length). Results could only be obtained for MT plus-ends because minus-ends were too short to measure accurately.

Katsuki et al. previously showed that MT shrinkage rates could be increased by supplementing a kinesin-clamp with 1 µM ATP [23], which we confirmed. As kinesins use ATP to generate motility they cycle through multiple nucleotide states, each of which has a different affinity for the MT lattice. Supplementing a kinesin-clamp with ATP causes the kinesins to cycle through multiple nucleotide states. The ATPase cycle includes weak-binding states (e.g. the ADP-bound state). Adding ATP to a kinesin-clamp therefore reduces the density of tightly bound kinesins. As the kinesins step in the presence of ATP they naturally propel MTs along the surface but velocities are so slow at a concentration of 1 µM that they are immeasurable on the timescale of these experiments.

A striking feature of these experiments is that we occasionally observed unusual structures emerging at MT tips upon depolymerisation in the absence of nucleotides. Faint 'trails' were seen in the wake of shrinking MTs (Figure 3.3B). Unfortunately, trails were difficult to observe under dark-field illumination, indicating that they are very slender structures.

3.2 Refinement of the kinesin-clamp assay for the characterisation of trails

It was unclear what the MT 'trails' seen in the dark-field images could be. We considered the following possibilities. Firstly, kinesins could bind tightly to the MT lattice and retain individual tubulin dimers as they dissociate from the MT tip during shrinkage. Alternatively, trails could be subsets of intact PFs that are not released from the surface. In either case, if trails represent long-term kinesin-tubulin interactions then comparing the density of tubulin in the trails to the density in MTs would provide a measure for how much of the MT lattice directly interacts with the kinesin surface. A final possibility that must be carefully addressed is that MTs form bundles in kinesin-clamp assays; kinesin-1 has indeed been shown to bundle MTs *in vitro* [154]. If two MTs become cross-linked then they would produce a trail-like image unless they are of the same length and their tips are perfectly aligned.

3.2.1 Preliminary investigation of MT trails

We refined the kinesin-clamp assay in order to gain a better understanding of MT trails. Several adjustments were made to improve imaging conditions. Although imaging MTs using dark-field illumination provides a high signal-to-noise ratio. However, this is not true for the trails we observe. Dark-field illumination produces a nonlinear signal, so it is difficult to assess how much material comprises a trail in relation to a MT. A linear signal can be obtained using fluorescence microscopy. Hence, the main alteration we made to better understand the trails was a switch from dark-field to epifluorescence illumination for imaging the dynamic MTs.

Typically, epifluorescence is unsuitable for illuminating dynamic MTs because the full depth of the sample is illuminated. Any fluorescently-labelled tubulin in solution thereby generates a high background signal. However, we found it possible to attain a high signal-to-noise ratio because tubulin is washed out of the flow chamber during the

kinesin-clamp assay. Under these conditions, greater tubulin labelling stoichiometries result in higher signal-to-noise ratios. We limited the labelling ratio to 3:10 (dye molecules:tubulin dimers) to reduce the risk of interfering with interactions between proteins. Dynamic MTs were assembled from tubulin labelled with Alexa Fluor-488, whereas seeds were assembled from X-rhodamine-labelled tubulin (3.4A).

A second adjustment we made was the method of polymerising MTs. Although growing MTs in the flow chamber provided useful for the initial optimisation, it was no longer necessary. We found that growing MTs from seeds in solution before adding them to the chamber reduced the background signal. This simply illustrates that high concentrations of tubulin (16 µM) will outcompete α-casein for binding sites on the glass if left for extensive periods of time (> 20 min).

Trails could be seen very clearly when fluorescent MTs were used (3.4B). Remarkably, trails were seen to shrink endwise. This implies that they have a filamentous structure. Trails are clearly not tubulin dimers that independently remain bound to the kinesin following MT depolymerisation.

A benefit of using dual-colour fluorescence imaging is that MT seeds leave a negative trace in the channel used for imaging dynamic MTs (and vice versa). See Figure 3.4B; evidently, the dynamic MT and its trail are neatly aligned at the intersection with the seed. This provides evidence suggesting that trails are not an artefact of MT bundling, rather they are substructures extending from single MT tips.

3.2.2 Shrinkage rates of MTs in a refined clamp assay

Impact of ADP on MT depolymerisation

We found that fluorescent MTs in the absence of nucleotides shrank at 0.4 dimer PF^{-1} s^{-1} in the refined kinesin-clamp, similar to the unlabelled MTs in the basic (dark-field) version of the assay (Figure 3.5). The fluorescent labelling of MTs therefore has little or no effect on the MT stability in these experiments. We could measure the shrinkage rates of trails in the refined clamp assay, as the signal-to-noise ratio was much increased.

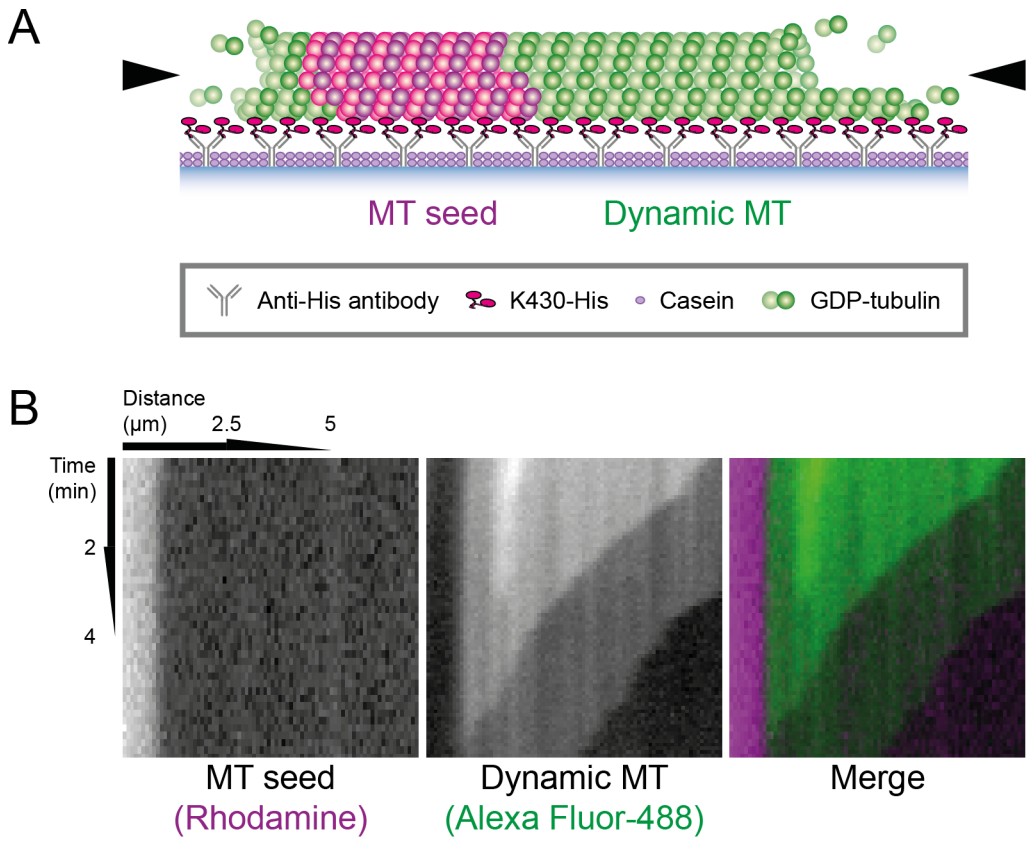

Figure 3.4: Observation of trails in a fluorescent kinesin-clamp. **A.** Schematic of a fluorescent kinesin-clamp. Dynamic MTs (Alexa Fluor-488-labelled, shown in green) were grown from stabilised seeds (X-Rhodamine-labelled, shown in magenta). MTs were bound to a kinesin- (K430-His-) coated surface and starved of GTP-tubulin. Slow depolymerisation followed. Trails were regularly left behind as MTs shrank (see (B)). Trails are proposed to subsets of PFs that interact with the kinesin surface, depicted as extensions at the tip of the MT. **B.** A kymograph that clearly shows a trail left in the wake of a depolymerising MT. Trails shrink endwise, indicative of a filamentous structure. The central image demonstrates that the MT and the trail are aligned at the intersection with the seed, ruling out the possibility of the pattern formation being due to MT bundling.

Surprisingly, trails depolymerised at very similar rates to complete MTs.

The ADP-bound state is the stage of the kinesin ATPase cycle that naturally allows a motor domain to detach from the MT lattice during processive movement 1.3. ADP therefore makes an ideal candidate for modulating the affinity of kinesins for MTs in a clamp assay. ADP does not promote kinesin motility, which simplifies data analysis. Moreover, MTs have been proposed to undergo molecular wear during kinesin-driven locomotion, which would complicate the interpretation of results [155]. We supplemented a kinesin-clamp with low concentrations of ADP (200 µM). Shrinkage rates then increased, as expected. This preliminary evidence suggests that it could be possible to fine-tune MT shrinkage rates by titrating ADP concentrations (investigated

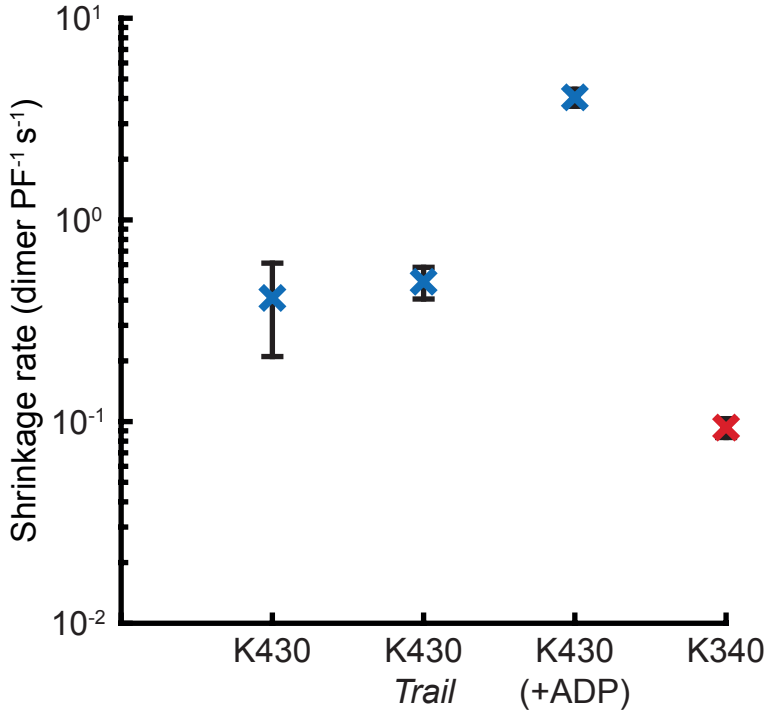

Figure 3.5: Preliminary measurements from kinesin-clamp variants. Shrinkage rates were measured for MTs in solution (upon depletion of GTP-tubulin) and MTs in a kinesin-clamp. Clamps were assembled using dimeric kinesin (K430-His) and perturbed by adding 200 µM ADP, or they were assembled using monomeric kinesin (K340-His). Values shown are mean ± SEM, which are summarised in Table 3.1.

further in Section 3.4).

The clamp-release procedure not only provides important insights for the underlying mechanisms of MT stabilisation but it also improves the signal-to-noise ratio. We found that allowing the clamp to release by adding 200 µM ADP (for ≤30 s) and once again washing out the nucleotides would reduce the background fluorescence significantly. This is presumably due to kinesins binding tightly to tubulin dimers in the absence of nucleotides, which are released upon addition of ADP. Washing through with nucleotide-free buffer was less effective in reducing the background signal.

Table 3.1: Preliminary kinesin-clamp measurements corresponding to Figure 3.5. Values shown are mean ± SEM (n).

Kinesin construct	Added ADP (µM)	MT/trail	Shrinkage rate (dimer $PF^{-1}\,s^{-1}$)
K430	0	MT	0.41 ± 0.20 (6)
K430	0	Trail	0.49 ± 0.09 (9)
K430	200	MT	4.05 ± 0.39 (5)
K340	0	MT	0.09 ± 0.01 (7)

Effects of kinesin dimerisation

The data presented to this point has involved the use of dimeric kinesin (K430-His). Dimeric kinesin binds to MTs with both motor domains as it takes a step. Hence, tubulin dimers in the MT lattice are transiently cross-linked by motile kinesin, which could provide a mechanism for MT stabilisation. Second-head binding occurs when the first (already bound) head binds a molecule of ATP (Figure 1.3). It is therefore unlikely that kinesin would cross-link tubulin dimers when no nucleotides are present. Nonetheless, we could not rule this out as a possibility. Regardless of the number of heads bound, it is plausible that dimeric kinesin has stabilising capabilities that monomeric kinesin does not.

We repeated the kinesin-clamp assay with a monomeric construct of kinesin (K340-His) to see whether inhibition of MT shrinkage is an intrinsic property of the motor domain. Remarkably, shrinkage rates were reduced by over two orders of magnitude (Figure 3.5). Although these shrinkage rates are much slower than those reported for K430-His, it must be noted that we also observed a much greater density of MTs on the surface. This is indicative of a higher density of (accessible) motor domains on the surface, so it not possible to draw comparisons between the effectiveness of the two constructs from the data presented. However, the mechanism of MT stabilisation is clearly independent of kinesin dimerisation. All experiments described hereafter use the kinesin motor domain rather than dimeric kinesin. This simplifies the interpretation of results.

3.3 Optimisation of a kinesin-clamp for quantitative fluorescence microscopy

In Section 3.2.1, we demonstrated that trails are filamentous and are unlikely to correspond to MTs overlaying in bundles (revisited later in Section 3.3.3). The only feasible explanation for filamentous substructures extending from MT tips is that

they are subsets of PFs. An upper bound for the number of PFs that interact with the kinesin-coated surface can be estimated from the geometry of a kinesin-clamp (Figure 3.6). At most 5 PFs can be bound if the antibodies on the glass coverslip are oriented optimally. The antibody-kinesin linkers are only able to reach 5 PFs if the antibodies directly beneath the MT lay flat, minimising the distance between the MT and the glass. An $\alpha\beta$-tubulin dimer has a footprint of $\sim 4\,\text{nm} \times 8\,\text{nm}$. The antigen-binding heads of each antibody are approximately the same size but the remainder of the protein occupies an additional $\sim 6\,\text{nm} \times 8\,\text{nm}$. Therefore, if the MT is lying close enough to the glass that the kinesins can reach 5 PFs, they cannot bind to every tubulin dimer along the MT axis due to steric limitations. It is more likely that the antibodies are immobilised in a range of orientations, spacing the MT further from the surface. Alternatively, if all antibodies lay flat against the glass, the kinesin motor domains could not reach 5 PFs. Either case leads us to consider the upper bound of 5 PFs to be an overestimate. We conclude that MTs can be split along their axis by binding kinesins to fewer than 5 PFs on one side of the lattice.

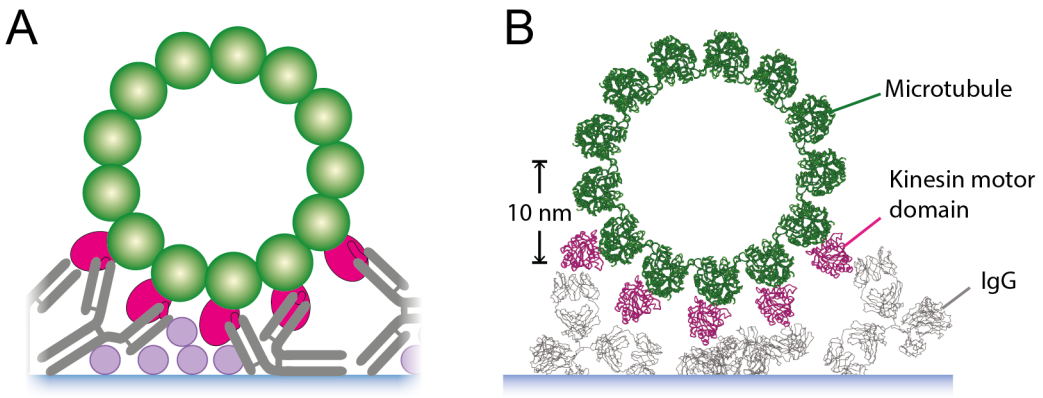

Figure 3.6: Cross-sectional views of a kinesin-clamp. **A.** Schematic showing the approximate geometry of a clamp assay, viewing the MT from the plus-end. Only a subset of PFs can interact with the kinesin-antibody surface due to geometric limitations. Assuming that the diagram is approximately to scale, the number is unlikely to exceed 5 PFs. **B.** Reference of scale. Protein Data Bank structures are shown for a kinesin-1-decorated MT in the absence of nucleotides [141] (PDB 4UXT) and a mouse IgG1 antibody [156] (PDB 1IGY). The image of the kinesin-decorated MT was generated by docking the structure into the corresponding electron density map (EM 2769) using UCSF Chimera. The relative sizes of these proteins suggests that the schematic in (A) is approximately to scale.

We carried out a final round of experimental optimisation with the aim of titrating MT shrinkage rates over a wide range of ADP concentrations. The optimisation steps

are described in the following sections. A comparison of the key differences between the kinesin-clamp variants is given in Table 3.2.

3.3.1 Surface optimisation

We addressed the possibility that kinesin might detach from the glass surface and reattach to PFs that were previously undecorated. If this were happening it would complicate the interpretation of results. We minimised the potential for this effect by reducing the kinesin concentration we used from 16 µM to 75 nM. Unbound kinesin was subsequently removed by extensive washing of the flow chamber (50 µl of buffer). Kinesin-clamps assembled this way retained the ability to significantly inhibit MT depolymerisation.

3.3.2 Improvements regarding MT assembly

The second issue that we addressed was that MTs in the clamp were typically too short (< 10 µm) to accurately measure shrinkage rates when high concentrations of ADP were added. Such measurements are important for assessing the extent that MT shrinkage rates can be fine-tuned. The short lengths of MTs was unsurprising for two reasons. Firstly, due to the cyclic nature of dynamic instability only a subpopulation of MTs are close to reaching their maximum lengths at any given time. The second reason for short MTs is due to the use of ADP to improve the signal-to-noise ratio. Whilst the quality of the data is improved, the quantity is compromised due to the temporary increase in MT depolymerisation.

We found the optimal procedure that resolved this issue to be nucleating the dynamic MTs spontaneously by incubating high concentrations of tubulin (50 µM) at 37 °C. MTs grown this way reached maximum lengths exceeding the width of the microscope field of view (65.5 µm). Immediately prior to flowing MTs into the flow chamber, they were isothermally diluted in buffer to 2.5 µM and mixed by pipetting the full volume (20 µl) twice. A fine (gel-loading) pipette tip was used for mixing,

Table 3.2: Comparison of the kinesin-clamp protocols. Numbers indicate the order in which components are flowed into the flow chamber. Volumes, concentrations and incubation times are given. Finer details (such as the composition of the buffer used for washing stages) are provided in Chapter 2.

	Kinesin-clamp protocol		
	Basic	**Refined**	**Fully-optimised**
1. Anti-His antibodies	1 flow-chamber volume (5.5 µl) at 0.1 mg ml^{-1}		
Incubate	10 min		
2. α-casein	20 µl at 0.5 mg ml^{-1}		
Incubate	5 min		
3. Kinesin	20 µl at 16 µM	20 µl at 16 µM	20 µl at 75 nM
Incubate	10 min	10 min	10 min
4. Wash	20 µl	20 µl	50 µl
5. Seeds★	Single-colour	✗	Dual-colour
Incubate	3 min	-	0 min
6. Wash	20 µl	✗	20 µl
7. Tubulin	20 µl at 20 µM	20 µl at 20 µM†	20 µl at 2.5 µM‡
Incubate	20 min	5 min	0 min
8. ADP	✗	20 µl at 200 µM	✗
Incubate	-	30 s	-
9. Wash	30 µl	30 µl	50 µl
10. Nucleotide	20 µl at 1 µM	30 µl at 200 µM	30 µl at various
	(ATP)	(ADP)	(ADP)
11. Taxol, ATP	✗	✗	30 µl at 10 µM, 200 µM resp.

★See Chapter 2 for details on seed preparation.

†Tubulin was incubated with 85 nM seeds for 45 min at 37 °C.

‡1 µl of 50 µM tubulin was incubated for 45 min at 37 °C before isothermal dilution to 5%.

which sheared MTs to approximately 20 µm to 30 µm. It is critical that this process is completed quickly because rapid depolymerisation is initiated upon dilution.

As MT dynamics equilibrate, the concentration of unpolymerised tubulin converges to a steady-state concentration that is independent of the initial concentration [39]. Under the assembly conditions we use, the steady state concentration of tubulin is approximately 7.5 µM. Therefore, the fraction of tubulin that remains unpolymerised can be reduced by using high initial concentrations. For example, the transition we made from using 16 µM to 50 µM reduces the fraction of unpolymerised tubulin from 47% to 15%. Thus, the signal-to-noise ratio (noise generated by free tubulin binding to the surface) can be increased this way. Following a 5% dilution of the latter sample, unpolymerised tubulin concentrations are 7.5 µM and 375 nM, respectively (assuming negligible depolymerisation in the time frame). We found that the improved protocol did not require an ADP-release stage in order to 'clean up' the image. Presumably this is an indication that fewer tubulin dimers are binding to the kinesin-coated surface (and thereby increasing the background signal) due to the reduced concentration of tubulin in solution.

MTs were flowed through the chamber as rapidly as possible and extensive washing (50 µl of buffer) immediately followed. This was essential to the effectiveness of the assay. It was critical that the number of MT overlaps were minimised for subsequent fluorescence quantification. By flowing through rapidly, we were able to align MTs in a parallel arrangement (Figure 3.8). Immediate washing was then important for two reasons. Firstly, late-binding MTs would align with the others if the flow was maintained. Secondly, MTs would rapidly disassemble until the GTP is thoroughly depleted.

3.3.3 Fluorescence controls

As discussed previously, one of the difficulties with nucleating MTs without the use of seeds is that it becomes difficult to distinguish between individual MTs, trails and MT bundles. We solved this problem by controlling for fluorescence levels. MT seeds were

produced using the same stock of fluorescently labelled (Alexa Fluor-488) tubulin that were used to polymerise the dynamic MTs. GMPCPP-stabilised extensions were grown from the seeds using differently X-rhodamine labelled tubulin and allowed to anneal. This way, stabilised and fluorescently barcoded MTs were formed that could be easily distinguished from dynamic MTs (Figure 3.7 and Figure 3.8A).

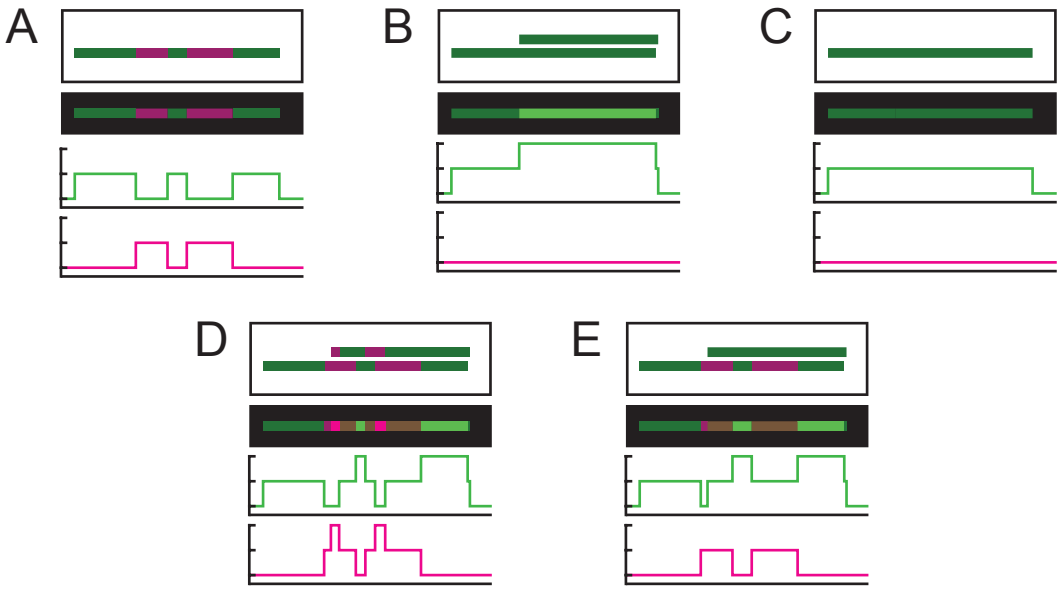

Figure 3.7: Fluorescence controls. The two-colour segmented microtubules allow for unambiguous identification of single MTs and MT bundles. Controls consist of stabilised MTs with a binary labelling pattern. Each subpanel shows, from the top down, (1) the number of MTs; (2) the appearance when MTs are overlaid; (3) the corresponding signal in the green channel; (4) the signal in the magenta channel. **A.** An isolated fluorescence control, allowing the intensity of a single MT to be determined. The channels show complementary binary signals. **B.** A bundle of two dynamic MTs, showing twice the intensity of the stripy seed in (**A**). **C.** A single dynamic MT. **D.** Overlapping seeds show irregular signals in each channel. **E.** Similarly, the two channels are not complementary if dynamic MTs bundle with fluorescence controls.

Seeds that are spatially separated from other MTs show complementary binary signals in the two imaging channels (Figure 3.7A and Figure 3.8B). The green (Alexa Fluor-488 labelled) segments of the fluorescence controls mark the intensity of an individual MT. Therefore, dynamic MTs are unambiguously identified as individual MTs or MT bundles by comparing fluorescence levels with those of the controls (Figure 3.7B-C). Fluorescence controls are clearly only meaningful if they are spatially separated from other controls or dynamic MTs. The barcoded labelling reveals instances where controls bundle, allowing them to be discarded from the analysis (Figure 3.7D-E).

Using this technique we were able to differentiate between trails,with a weaker

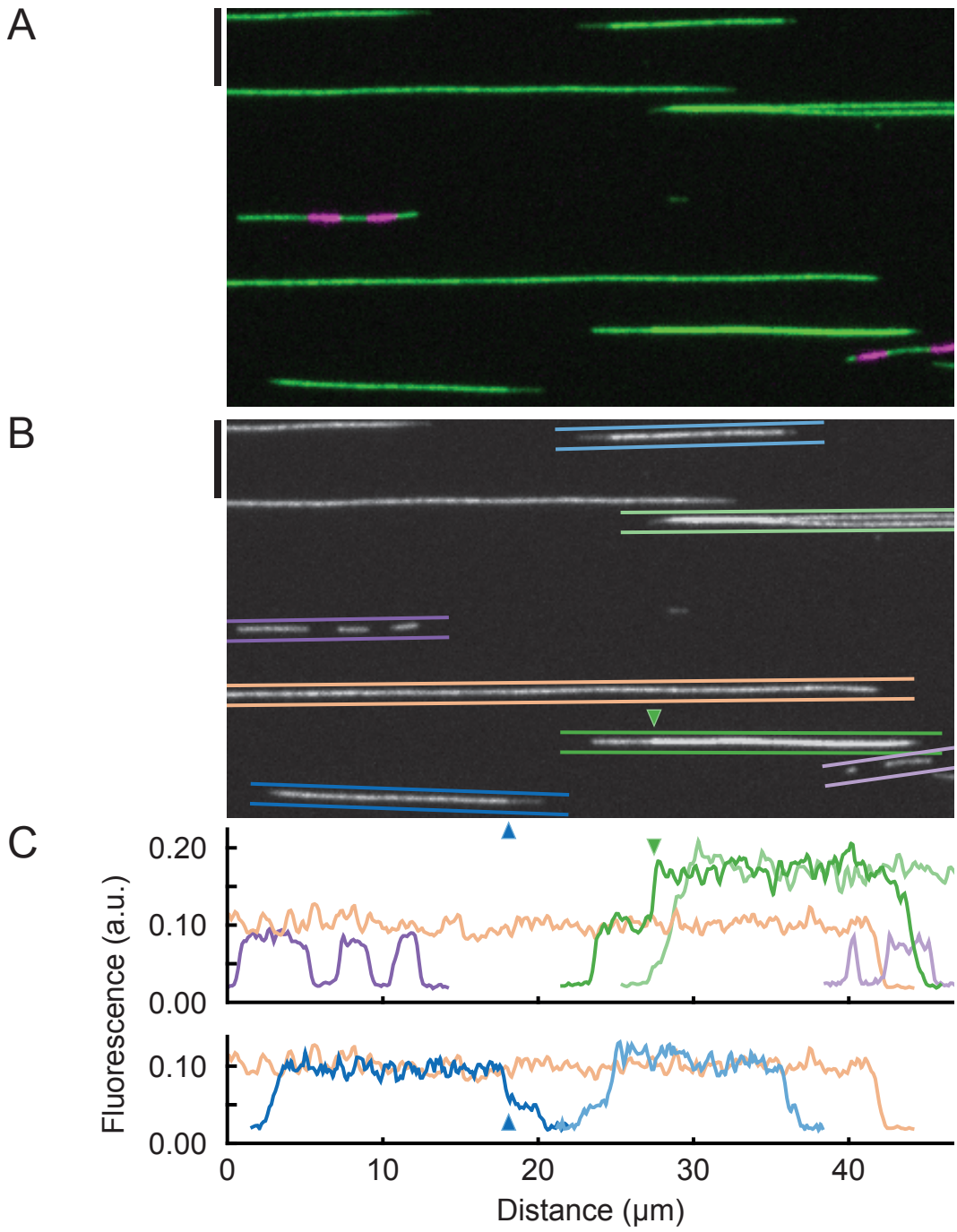

Figure 3.8: Intensity profiles of MTs in a kinesin-clamp. **A.** Two-colour image of MTs in a kinesin-clamp (no ADP present). GMPCPP-stabilised MTs are clearly identified by their alternating colours. Scalebar is $5\,\mu\mathrm{m}$. **B.** Regions used for linescans shown in (C). Linescans were calculated by averaging cross-sections of ±5 pixels ($\pm 0.64\,\mu\mathrm{m}$), as marked by parallel lines. Regions are colour-coded: MT with no trail (orange), seeds (purple), bundles (green), MTs with trails (blue). Blue and green triangles mark transitions from individual MTs to trails and bundles, respectively. **C.** Colour-coded intensity profiles corresponding to the regions shown in (B). Fluorescence intensity is plotted against the x-coordinates from the image in (B) to enable direct visual comparison. Profiles are separated by type to improve clarity.

signal than individual MTs, and bundles with greater intensities (Figure 3.8C). MT intensity profiles found to be greater than 1.75 times the intensity of the fluorescence controls were classified as MT bundles and discarded from all analyses described hereafter. The approach used for quantifying fluorescence intensities is discussed later in Chapter 4.

3.3.4 Inferring MT polarity

It was not possible to extract shrinkage rates of MT minus-ends in previous versions of the kinesin-clamp assay due to MT length limitations. We were able to measure shrinkage rates for both ends of the MT using the optimised protocol (growing MTs without using seeds to aid nucleation). Identifying the polarity of freely-nucleated MTs is however nontrivial, so further adaptations needed to be made.

Once the kinesin-clamp assay had been fully optimised, it consisted of three distinct stages (Figure 3.9). In the first stage, MTs are bound to the kinesin surface in the absence of nucleotides. ADP is added to catalyse shrinkage in the second stage. The third and final stage enables the MT polarity to be identified. Before the majority of MTs disassembled completely, we added 10 µM taxol (a MT-stabilising drug) to prevent further depolymerisation. 200 µM ATP was simultaneously added to promote kinesin-driven MT gliding. As mentioned previously, the polarity of the MT can be inferred from these motions. Kinesin-1 is a plus-end-directed motor so the leading MT tip is always the minus-end.

3.4 MT shrinkage in an optimised kinesin-clamp

3.4.1 Characterisation of trail behaviour

Trails were observed for the majority of MTs in the initial (no nucleotide) stage of the optimised kinesin-clamp assay. Curiously, trails were present at over three times as many minus-ends as plus-ends (Figure 3.10A). We counted trails at 75% of minus-ends

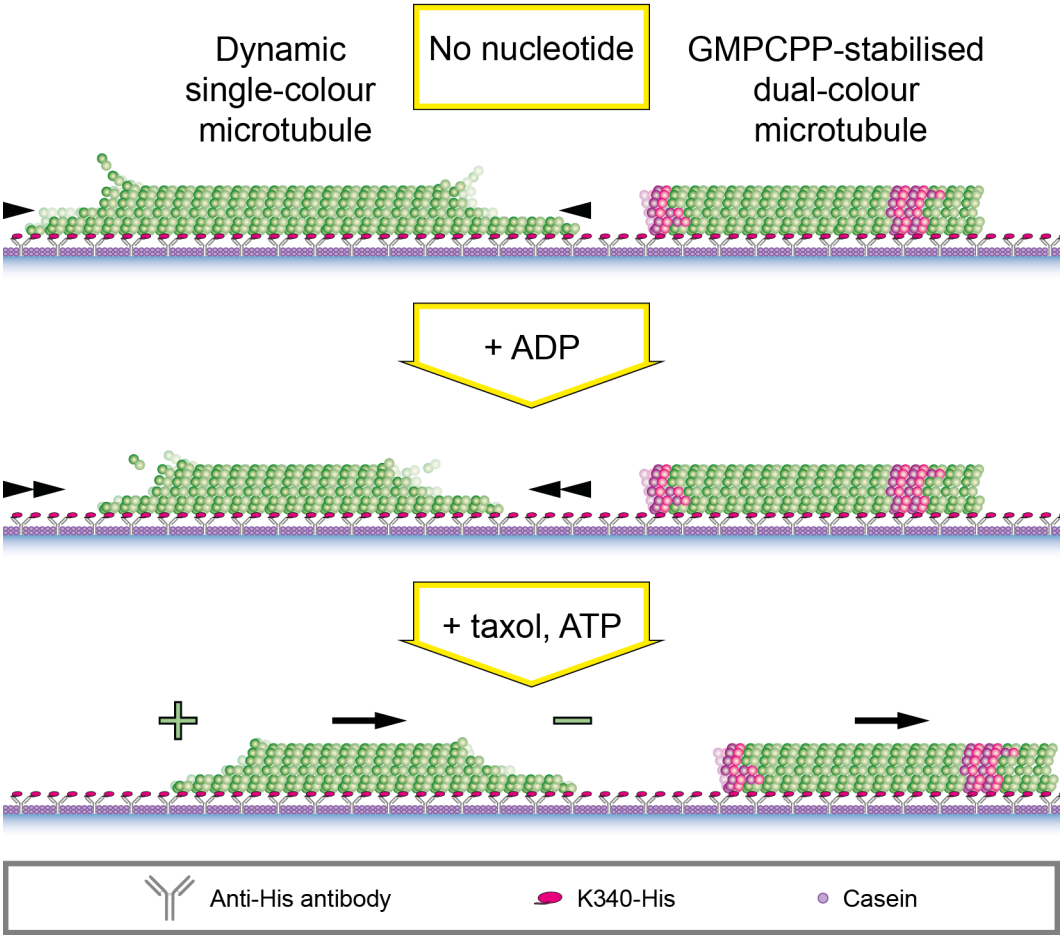

Figure 3.9: Optimised kinesin-clamp assay. Dynamic single-colour (Alexa Fluor 488) MTs and GMPCPP-stabilised dual-colour (Alexa Fluor 488, X-rhodamine) MTs are immobilised in a kinesin-clamp with no nucleotides present. Upon the addition of ADP, kinesins enter a low-affinity binding state. This reduces the density of kinesins in a strong binding state and MT shrinkage rates therefore increase. The polarity of MTs can be assessed by tracking their motion in the presence of ATP; kinesin-1 walks to the plus end, pushing MTs in the direction of the minus end. Taxol is supplemented simultaneously to inhibit further depolymerisation.

compared to only 23% at plus-ends (assessed by eye from the raw data but where MTs > 1.75 times brighter than the fluorescence controls have been discarded). The proportion of trails that form during ADP-induced shrinkage follows a similar ratio, independent of the ADP concentration (Figure 3.10B).

We observed a wide range of dynamic behaviours of MTs in the kinesin-clamp. Trails present in the no nucleotide phase of the experiment showed no observable shrinkage over timescales on the order of minutes (Figure 3.11A). Trails were observed to shorten upon addition of ADP. In some cases, trails would become undetectably short during this burst of shrinkage (Figure 3.11B). In others, trails would clearly be

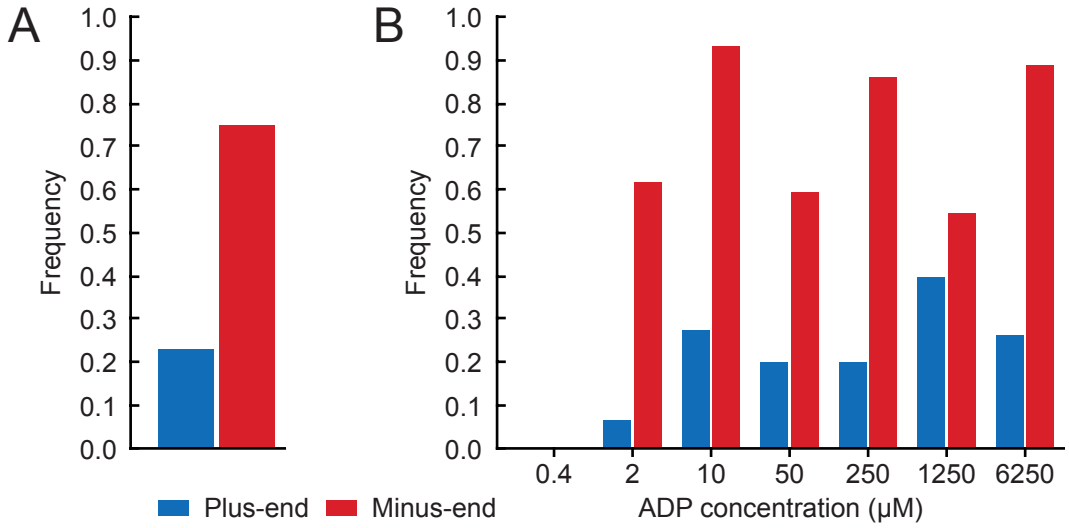

Figure 3.10: Distribution of trails. **A.** Frequency of trail sightings at plus- and minus-ends in the first (no added nucleotide) stage of the optimised kinesin-clamp assay. **B.** Frequency of trail formation upon the addition of ADP. The number of trails that formed a trail during the ADP-induced shrinkage phase were counted. Trail formation was defined as the emergence of trails on portions of the MT that were not present in the no added nucleotide stage of the experiment. For example, the kymograph in Figure 3.11A was scored as forming a trail in the presence of $50\,\mu\text{M}$ ADP. *n*-values are given in Table 3.3.

Table 3.3: Frequency of trails observed at MT plus- and minus-ends.

ADP concentration (μM)	Count (trails observed)/(total counted)	
	Plus-end	Minus-end
0	21/91	78/104
0.4	0/6	0/6
2	1/15	8/13
10	3/11	14/15
50	4/20	16/27
250	3/15	12/14
1250	2/5	6/11
6250	5/19	16/18

present throughout the duration (Figure 3.11A).

Trail lengths underwent substantial fluctuations. Trails that shrank to the point of being undetectable were seen to re-emerge even in the presence of high ADP concentrations (Figure 3.11B). The emergence or lengthening of trails frequently coincided with a burst of rapid MT shrinkage. Over time, trails would often be seen to shorten again. Consequently, the average shrinkage rate of trails and MTs were very similar. This was observed not only for trails with large length fluctuations, but also for MTs that retained long trails throughout the duration of the experiment (Figure 3.11A).

It must be noted that kinesins have been reported to denature when retained in a no-nucleotide state for extensive lengths of time [157]. Denaturation is however mitigated when kinesins bind to MTs [158]. The fact that kinesin-clamps are able to both release upon addition of ADP and generate smooth motility upon addition of ATP provides assurance that trail formation is not an artefact caused by kinesin denaturation.

Although most MTs in the kinesin-clamp displayed trails, we observed some instances of MTs with no trails (Figure 3.12A). At the opposite end of the spectrum, a few rare cases saw trails forming not only at MT ends but also from the middle of the lattice (Figure 3.12B). MTs would split deep within their lattice and shrinkage would follow in both directions. Trails formed this way were also seen to split over time, before shrinking endwise in the same way as 'regular' trails.

3.4.2 Titration of MT shrinkage rates with ADP

We measured average shrinkage rates of MTs in the optimised kinesin-clamp over a range of ADP concentrations. We found that shrinkage rates saturated at concentrations above and including 50 µM (Figure 3.13A). No significant difference was found between the shrinkage rates of the plus- and minus-ends of MTs ($p = 0.06$, F-test; see Table 3.5 for a comparison of curves fitted). Plus-end trails were found to have the greatest shrinkage rates, reaching $9.0\,\mathrm{dimer\,PF^{-1}\,s^{-1}}$ at saturating concentrations of ADP.

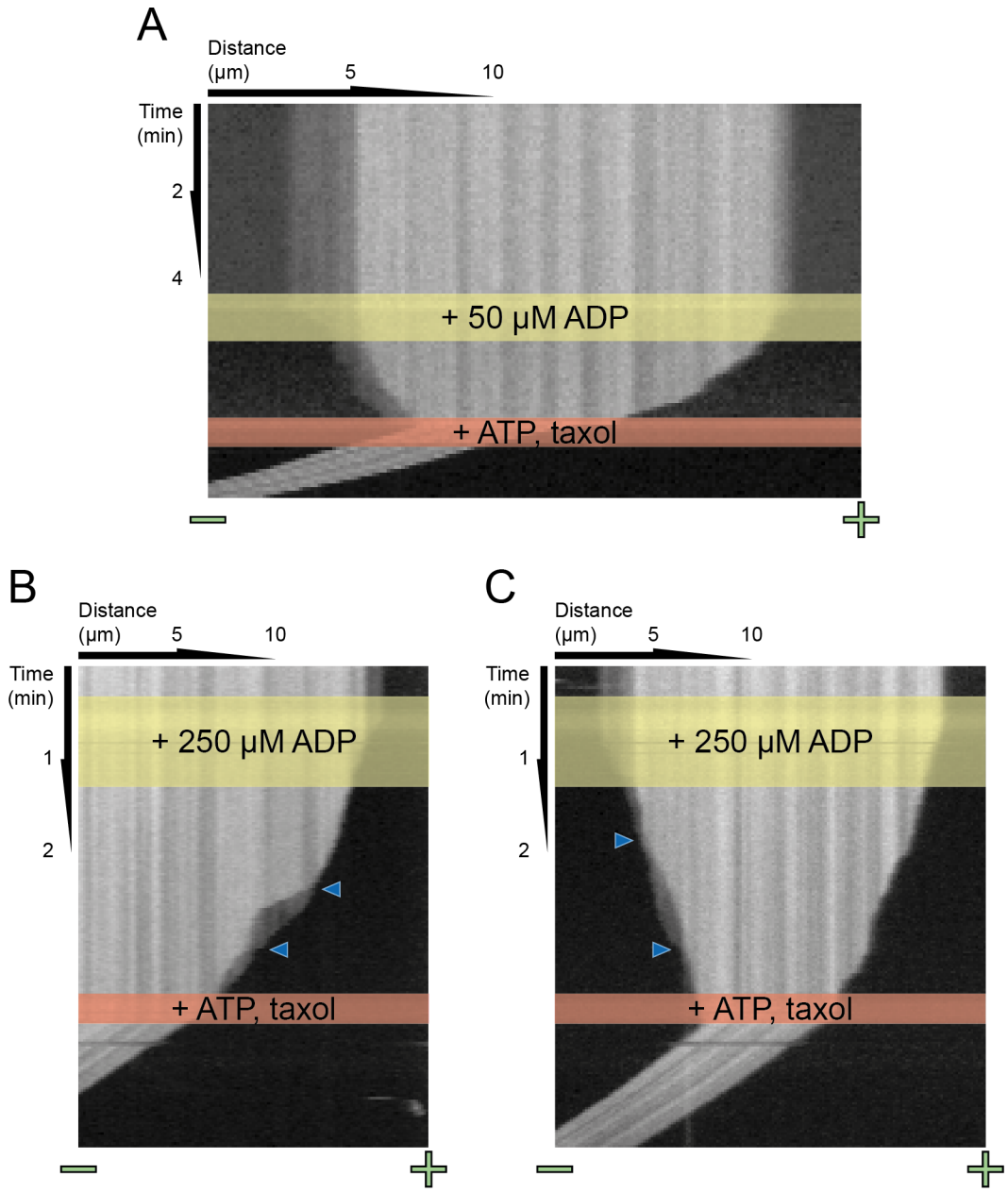

Figure 3.11: Representative kymographs of trail dynamics. MTs are bound in the absence of nucleotides in a kinesin-clamp. ADP is then added to promote MT disassembly. Finally, ATP and taxol are added to determine MT polarity; kinesin-propelled motility pushes MTs in the minus-end direction. **A.** Trails are typically present upon initial tight binding of MTs in a kinesin-clamp. They shrink at variable rates and they often remain during shrinkage. **B, C.** Both plus- and minus-end trails occur at MT tips in a kinesin-clamp. Trails undergo substantial length fluctuations. Lengthening-shortening cycles are marked by blue triangles. Lengthening typically coincides with a burst of rapid MT shrinkage. MT shrinkage subsequently slows down and the trail shortens. Thus, the average shrinkage rates of MTs and trails are remarkably similar. Trails do not always occur at both ends of a MT (C).

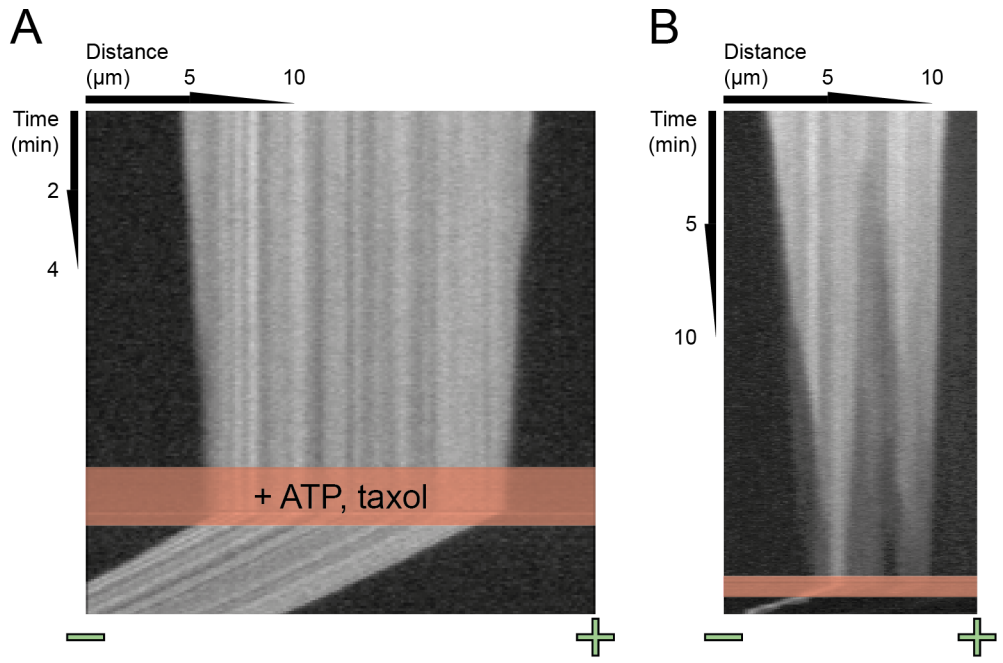

Figure 3.12: Kymographs showing infrequent kinesin-clamp behaviour. **A.** A MT with no observable trails ($2\,\mu M$ ADP present). **B.** Trails can be seen to emerge from the centre of the MT and spread towards the ends ($10\,\mu M$ ADP present).

Minus-end trails showed a significantly different response to ADP concentrations ($p = 0.0001$) and reached a maximum shrinkage rate of just $4.4\,\text{dimer}\,\text{PF}^{-1}\,\text{s}^{-1}$. This suggests that plus-end trails are less stable than minus-end trails, which could explain why trails are much more prominent at minus-ends.

The behaviour of minus-end MTs and minus-end trails are indistinguishable in our data for mean shrinkage rates (Figure 3.13A, Table 3.5). It is clear to see from in the kymographs that each of these tip structures can show high variability in a single trajectory (Figure 3.11C). Trail trajectories are constrained, for they cannot shrink beyond their MT stems. Therefore, if stochastic shrinkage rates lead to trail formation but on average the trails depolymerise faster than MTs then trails would form, grow and eventually shrink back to the MT. Mean shrinkage rates would be equal for MTs and trails. We therefore investigated the fraction of time that MTs and trails spend shrinking at different rates in order to help elucidate how their behaviours differ. Trajectories in kymographs were traced manually to generate piecewise-linear shrinkage rates. Shrinkage rates were then plotted in histograms that were weighted according the the time spent at each rate. This preliminary analysis was carried out

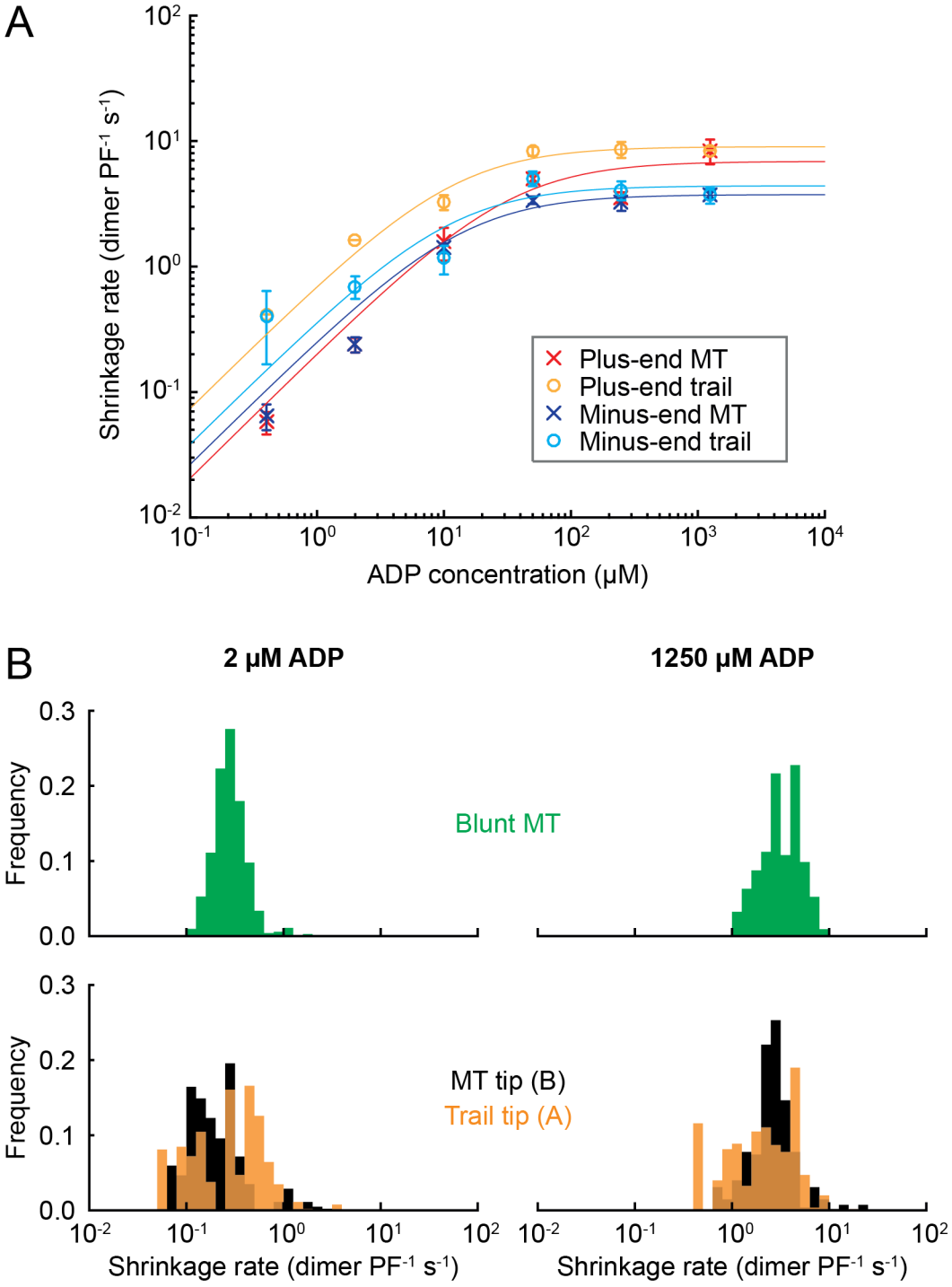

Figure 3.13: Shrinkage rates of MTs in kinesin-clamps. **A.** Mean shrinkage rates of MTs. Error bars show mean ± SEM. Rates (with *n*-values) are summarised in Table 3.4. Fitted curves are summarised in Table 3.5. **B.** Time-weighted histograms of shrinkage rates for MT minus-ends in the presence of 2 and $1250\,\mu\mathrm{M}$ ADP. Data has been further separated into the shrinkage of blunt MTs (*top*) and MTs with trails (*bottom*). Mean ± standard deviation for the time-weighted data is 0.30 ± 0.09, 3.51 ± 12.10 (blunt MTs); 0.38 ± 0.14, 2.65 ± 6.89; 0.26 ± 0.07, 3.05 ± $9.18\,\mathrm{dimer\,PF^{-1}\,s^{-1}}$ for MTs shrinking in the presence of 2 and $1250\,\mu\mathrm{M}$, respectively.

for both ADP-limited (2 µM) and ADP-saturating (1250 µM) conditions. No clear difference between minus-end MTs and minus-end trails emerged from this analysis; more data would required to make a conclusive statement. To summarise, the dynamic behaviours of minus-end trails and minus-end MTs are indistinguishable in the current data.

3.5 Conclusions

We optimised a kinesin-clamp assay to investigate the mechanisms of kinesin-regulated MT depolymerisation.We have shown that kinesin-1 motor domains have the ability to dramatically inhibit the shrinkage of GDP-tubulin MTs. We modulated the density of tightly-bound kinesin heads on the MT lattice, which was found to successfully fine-tune rates of MT depolymerisation.

Shrinkage rates were measured as low as 0.06 and 0.07 dimer PF^{-1} s^{-1} respectively for plus- and minus-ends of MTs in low-nucleotide conditions (0.4 µM ADP). Rates were significantly increased in the presence of high concentrations of ADP.

In the optimised version of our assay, before MTs are subjected to the kinesin-clamp, they are diluted to concentrations that promote rapid depolymerisation. The GTP-cap is consequently lost, meaning our results apply to intrinsically unstable GDP-MTs. Our results show that in the absence of nucleotides, kinesins can bind to rapidly depolymerising MTs and inhibit shrinkage rates by approximately two orders of magnitude. Therefore, we predict that tightly-bound kinesin could serve as a potent MT rescue factor.

We discovered novel tip structures that emerge at the tips of MTs bound in a kinesin-clamp. These structures, which we call MT 'trails', have the property of shrinking endwise. We propose that trails correspond to the fraction of the MT lattice (i.e. the number of PFs) that interact directly with the kinesin surface (Figure 3.6). It follows that MTs can be stabilised simply by maintaining the structural integrity of a subset of PFs. By quantifying the fluorescence intensities of data presented in this chapter, it is theoretically possible to estimate the fraction of the MT that comprises a

trail, putting an upper bound on the number of PFs that must be maintained in order to stabilise a MT.

Table 3.4: Shrinkage rates of MTs in an optimised kinesin-clamp ($\mathrm{dimer\,PF^{-1}\,s^{-1}}$). Data corresponds to that plotted in Figure 3.13A. Values given are mean ± SEM (n).

ADP concentration	Plus-end		Minus-end	
(µM)	MT	Trail	MT	Trail
0.4	0.06 ± 0.01 (6)	0.42 (1)	0.07 ± 0.02 (6)	0.40 ± 0.24 (4)
2	0.24 ± 0.03 (15)	1.62 (1)	0.24 ± 0.03 (13)	0.69 ± 0.14 (6)
10	1.57 ± 0.46 (10)	3.26 ± 0.44 (2)	1.40 ± 0.12 (11)	1.16 ± 0.30 (10)
50	5.08 ± 0.38 (22)	8.28 ± 0.69 (4)	3.39 ± 0.23 (20)	5.04 ± 0.68 (17)
250	3.56 ± 0.35 (18)	8.58 ± 1.25 (2)	3.22 ± 0.44 (3)	4.07 ± 0.70 (11)
1250	8.40 ± 1.87 (8)	8.42 (1)	3.74 ± 0.26 (12)	3.69 ± 0.53 (4)

Table 3.5: Comparison of ADP-induced MT shrinkage response curves. Rectangular hyperbolae (Michaelis-Menten curves) were fitted by least-squares to the mean values presented in Figure 3.13A and Table 3.4. Parameters for these fits are given below. For each pair of datasets, we tested the null hypothesis that a single curve, rather than two distinct curves, is the correct model to explain the data. These comparisons were performed using an F-test. p-values are given below.

	Fitted parameters		**p-values**			
	$V_{\max}$ ($\mathrm{dimer\,PF^{-1}\,s^{-1}}$)	K_m (µM)	Plus-end MT	Plus-end trail	Minus-end MT	Minus-end trail
Plus-end MT	6.9	33.4	-	-	-	-
Plus-end trail	9.0	12.1	0.02	-	-	-
Minus-end MT	3.7	14.0	0.06	0.000002	-	-
Minus-end trail	4.4	11.4	0.3	0.0001	0.6	-

4

Quantitative fluorescence analysis of MTs in a kinesin-clamp

The number of PFs that are bound by kinesin in a clamp assay has implications for the stabilising ability of kinesin and also the mechanical properties of MTs. If maintaining the structural integrity of a subset of PFs affects the stability of entire MTs, it is important to put an upper bound on the number of intact PFs that are needed to produce such an effect. Equally, knowing how few PFs can be stabilised in isolation would shed light on the efficacy of this mechanism for directly inhibiting subunit loss.

In order to address this problem, we quantified fluorescence intensities of MTs in the optimised kinesin-clamp assay. Flat-field correction was applied to our images in order to ensure that fluorescence intensities were spatially homogeneous (see Chapter 2). Once such corrections have been applied correctly, image pixel intensities are proportional to the number of fluorescently-labelled molecules that are illuminated. Therefore, by quantifying the ratio of fluorescence intensities of MTs to trails, we could estimate the number of stabilised PFs that comprise a trail.

4.1 A stepped tip function for approximating fluorescence intensity profiles

The fluorescence profiles of MTs with trails typically show a distinct fluorescence profile (Figure 4.1A). Trails are easily identified as a shelf-like plateau at an intensity between

those of the background and the MT. In order to quantify the relative signal of trails to MTs, we designed a simple function to approximate such fluorescence intensity profiles.

We propose a 'stepped tip' function, Υ, to approximate the underlying structure of MTs in the kinesin-clamp. A diagram of the function is shown in Figure 4.1B (black line). It consists of three piecewise-linear segments resembling steps. The first segment (on the interval $(-\infty, a)$), represents background fluorescence levels (I_{bgd}). The second (on $[a, b)$) corresponds to the trail. We allow this segment to have a non-zero gradient to accommodate for any tapering that may occur. The third and final step (on $[b, \infty)$) represents the signal of the MT (I_{tube}). The stepped tip function, Υ can be written formally as

$$\Upsilon(x) = \begin{cases} I_{bgd} & \text{if} \quad x < a \\ \frac{(x-a)(I_b - I_a) + I_a(b-a)}{b-a} & \text{if} \quad a \le x < b \\ I_{tube} & \text{if} \quad x \ge b, \end{cases} \tag{4.1}$$

where $a \le b$, $I_{bgd} \le I_a \le I_b \le I_{tube}$ and I_a and I_b denote the fluorescence at points a and b, respectively.

Images acquired by microscopy correspond to a convolution of the ground truth with the point-spread function (PSF) of the microscope. The stepped tip function is designed to approximate the ground truth, so it must be convolved with the PSF before fitting to the data. The PSF can be calculated theoretically (for a perfectly in-focus sample) and well approximated by a Gaussian function [159].

We generated a theoretical PSF for our selected fluorophore (Alexa Fluor-488; 525 nm emission maxima) and microscope arrangement (1.3 NA, 128 nm pixel size). The PSF was averaged over its cross-section to mimic the way our kymographs are generated. We then fit a Gaussian function, f to approximate the PSF for our data. We convolved f with the stepped tip function, Υ, to obtain a function that is suitable for fitting to the trails seen in kymographs. A diagram of the convolved function and an example fit to data is shown in Figure 4.1B (blue line). The equation takes the following form:

$$[\Upsilon * f](x) = I_{bgd} + p[f(x-a) - f(x-b)] + q[F(x-a) - F(x-b)] + (I_{tube} - I_{bgd})F(x-b), \tag{4.2}$$

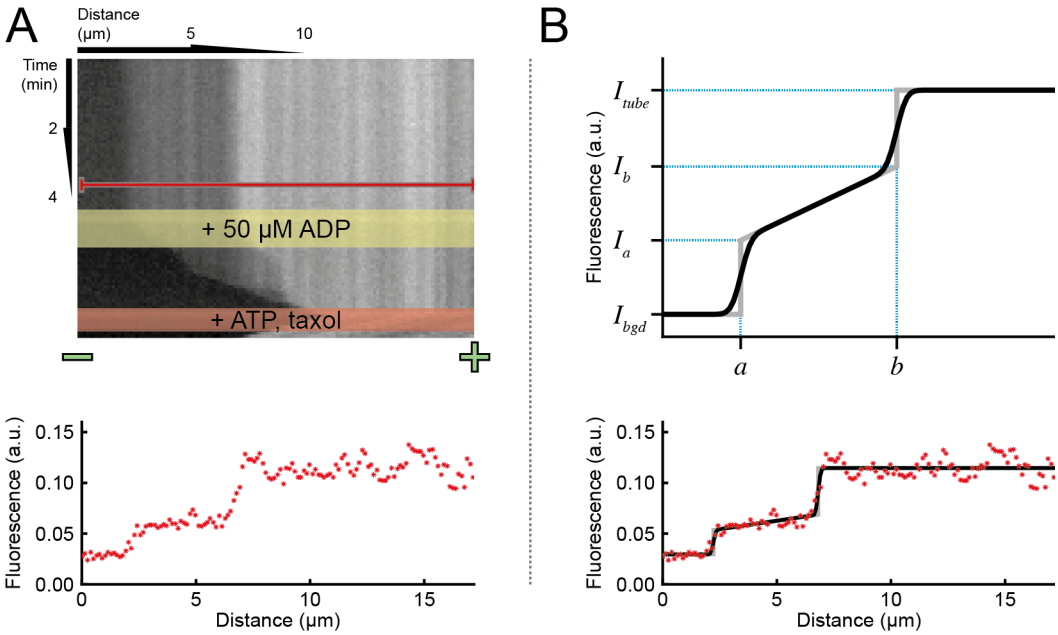

Figure 4.1: A stepped tip function for approximating fluorescence intensity profiles. **A.** A kymograph of a MT with a long trail (*top*). The intensity profile of the MT is plotted for a single time-point (*bottom*), corresponding to the region marked by a solid red line in the kymograph. **B.** The proposed function for approximating MT intensity profiles (*top*). From left to right, the three steps of the function correspond to intensity levels of the background (I_{bgd}), the trail (from I_a to I_b) and the MT (I_{tube}). The grey line shows the basic function, Υ. The black line depicts Υ convolved with a Gaussian approximation to the point-spread function. The convolved model well represents MT trail profiles, as demonstrated by a fit to the line-scan from (A) (*bottom*).

where

$$p = \frac{(I_b - I_a)\sigma^2}{b - a} \tag{4.3}$$

and

$$q = \frac{(I_b - I_a)(x - a) + (I_a - I_{bgd})(b - a)}{b - a}. \tag{4.4}$$

The function F denotes the integral of f, given by

$$F(x) = 0.5\left(1 + \mathrm{erf}\left(\frac{x}{\sigma_{\mathrm{PSF}}\sqrt{2}}\right)\right) \tag{4.5}$$

(assuming f has been normalised); erf is the Gaussian error function and σ_{PSF} is the standard deviation of the PSF.

4.2 Ensuring a robust fit

The stepped tip function fits well to the profile of MTs that have long trails. However, for MTs with short (or non-existent) trails, the parameters become highly sensitive to small fluctuations in the data (Figure 4.2A). It is therefore unreliable to quantify the proportion of the signal that corresponds to a trail for such intensity profiles. A simple fix to improve the reliability of the data would be to threshold according to the length of the trails.

The stepped tip function reports two jumps in the fluorescence intensity by definition. One jump corresponds to the tip of the trail and the other to the tip of the MT. A problem can then arise when fitting to data with one clear jump in the intensity. If a function with a single jump (i.e. when $I_a = I_b = I_{tube}$) well approximates the data then an unconstrained stepped tip function will naturally detect a second jump within the noise of the MT signal (Figure 4.2B). In such cases, it is not possible to say with any level of certainty whether there is indeed a 'trail' or whether the prediction is incorrect. A stricter definition of a trail is therefore needed. The trails that are detected in these cases can be several microns long, so thresholding against the length is an unsuitable approach.

The case when $I_a = I_b = I_{tube}$ represents a blunt MT tip with no trail. In this case, the convolved function from Equation 4.2 is reduced to

$$[\Upsilon * f](x) = I_{bgd} + (I_{tube} - I_{bgd})F(x - a) \tag{4.6}$$

$$= I_{bgd} + 0.5(I_{tube} - I_{bgd})\left(1 + \operatorname{erf}\left(\frac{x - a}{\sigma_{\mathrm{PSF}}\sqrt{2}}\right)\right). \tag{4.7}$$

It must be noted that the transition point from the trail to the MT (point b) does not factor into this equation. The detected trail length $(b - a)$ is therefore a highly unstable measurement when fitting to blunt MT tips. This provides an intuitive explanation for why the model predicts long trails in such circumstances.

Equation 4.7 is a function that has been applied previously to track the tips of dynamic MTs [44, 160, 161]. However, rather than treating the standard deviation as

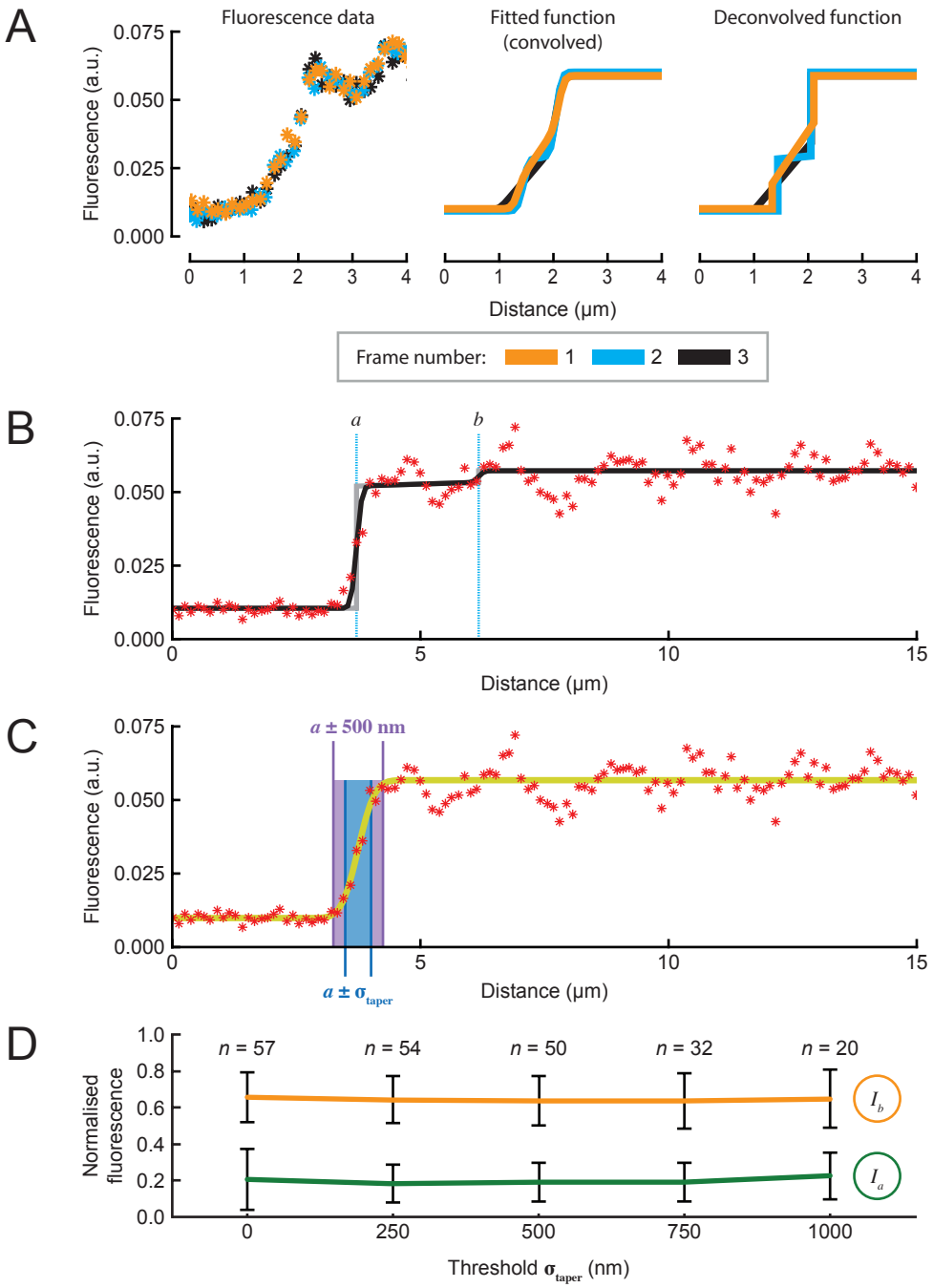

Figure 4.2: A method to ensure robust estimation of trail geometries. **A.** The stepped tip function is highly sensitive to small fluctuations in the signal at blunt MT tips. From left to right: intensity profiles, convolved fits and the predicted geometry of MTs for three consecutive frames of an image sequence. **B.** Long trails are predicted for profiles that appear to resemble blunt-ended MTs. The large jump in the fluorescence signal is accommodated by the end of the estimated trail (a). The trail-MT transition point (b) is subsequently fitted within the noise of the MT signal. The length of the predicted trail is highly sensitive to small fluctuations in the signal. **C.** We fitted a robust function with a single-intensity-jump (Equation 4.8) to MT tips as a 'counter fit'. If the MT tip was sufficiently blunt ($\sigma_{\text{taper}} < 500\,\text{nm}$) then the stepped tip function was rejected for describing the MT geometry. The MT tip is denoted by x and the blue and purple regions demonstrate the selection criteria. In this case (same data as in (B)), $\sigma_{\text{taper}} < 500\,\text{nm}$, so the stepped tip function is rejected. **D.** Parameters of the fitted function for a range of taper threshold values σ_{taper}.

a constant (σ_{PSF}), which exclusively describes blunt MT tips, the authors define it as a variable to accommodate for tapering (σ_{taper}). We refer to this function as a taper function, G, given by

$$G(x|a, \sigma_{\text{taper}}) = I_{bgd} + 0.5(I_{tube} - I_{bgd})\left(1 + \text{erf}\left(\frac{x-a}{\sigma_{\text{taper}}\sqrt{2}}\right)\right). \tag{4.8}$$

Due to it fitting to only one jump in the intensity, the taper function fits robustly to MT ends. Furthermore, σ_{taper} provides a measure of any tapering that occurs.

As we have shown, overfitting the stepped tip function occurs when MT tips are blunt. The taper function provides a robust method to assess how blunt MT tips are. We therefore propose the taper function as a 'counter fit' to the stepped tip function. If $\sigma_{\text{taper}} \leq 500\,\text{nm}$ then we reject the stepped tip function (Figure 4.2C). Otherwise, we accept the stepped tip function to describe the geometry of the MT tip. We found 500 nm to be an effective threshold for ensuring a robust fit. Results were not biased by this criteria; trail intensity parameters were in fact invariant to the threshold value set (Figure 4.2D).

4.3 Quantitative characterisation of tip structures

4.3.1 Quantification of trail intensities

For each time point in our kymographs, we fitted the stepped tip function and normalised the data (Figure 4.3A). Normalisation was achieved by subtracting the fitted values for the background signal (I_{bgd}) and dividing by the intensity of the MT ($I_{tube} - I_{bgd}$). Normalised fluorescence readings may therefore be considered as fractions of a MT, providing a direct readout for the proportion of the MT that forms a trail.

Throughout the no-nucleotide phase of experiments, trails were found to maintain a constant geometry (Figure 4.3B). We averaged the fitted model parameters for the no nucleotide phase of each kymograph. A histogram of the parameters I_a and I_b for the no-nucleotide stage is shown in Figure 4.3C. As described earlier, I_a and I_b represent

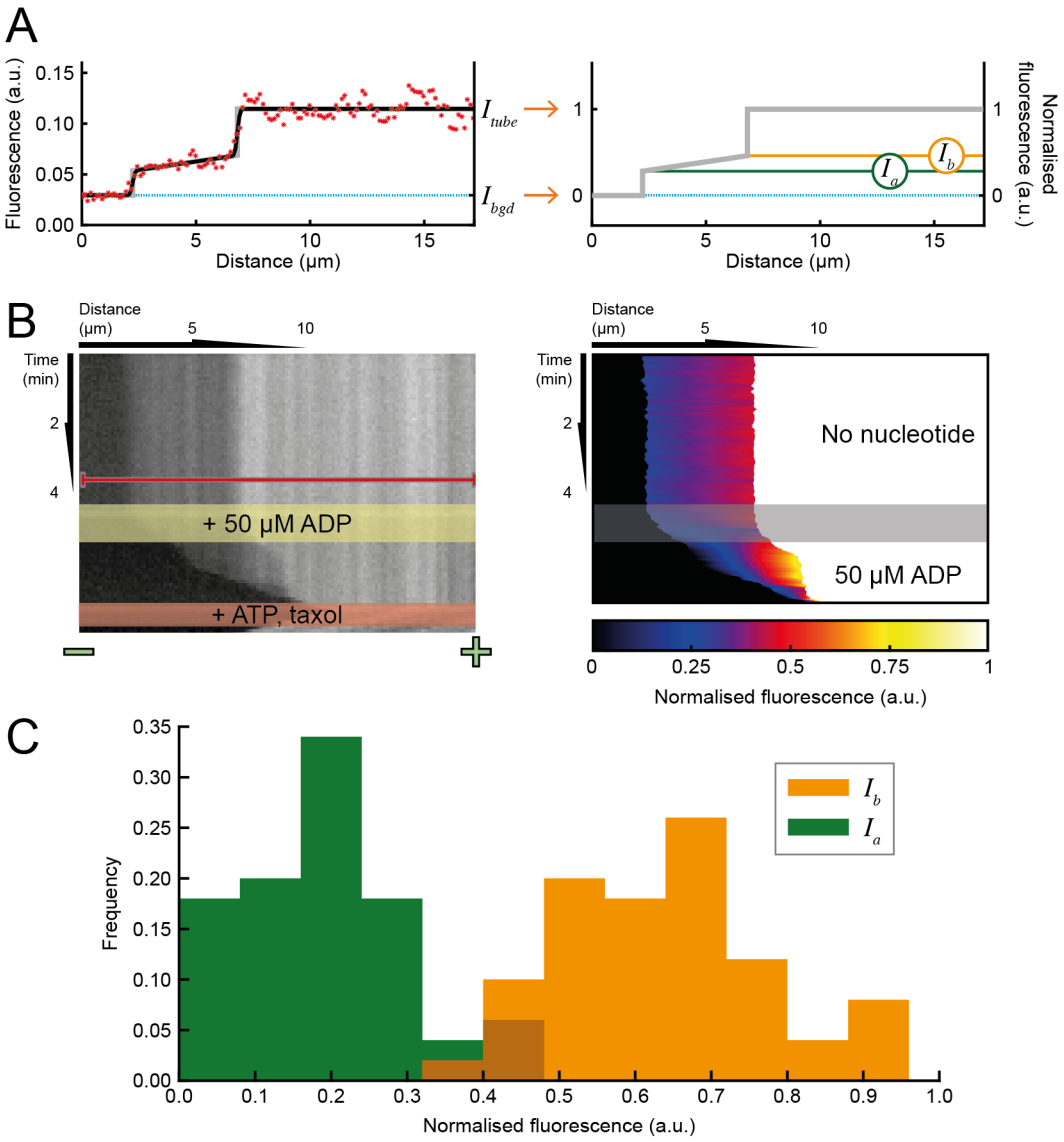

Figure 4.3: Quantification of trail intensities. **A.** Intensity profiles were normalised by subtracting the background and dividing by MT intensities estimated by the stepped tip function. The normalised values of I_a and I_b represent the fraction of the MT that comprises a trail at its end and its base, respectively. **B.** Normalisation of a kymograph. The stepped tip function was fitted to each time point of the raw data (*left*, red line corresponds to the line scan in (A)). Normalised values for the stepped tip function were used to generate the kymograph on the right. **C.** The parameters I_a and I_b were averaged across all time points belonging to the no-nucleotide phase. Each entry corresponds to the mean profile of a microtubule in the no nucleotide phase of the experiment. Mean ± standard deviation is 0.19 ± 0.11 and 0.64 ± 0.13 for I_a and I_b, respectively ($n = 50$).

the fraction of the MT that comprises the tip and base of the trail, respectively. The average intensity at the trail tip is 19% of a MT, whereas the base of the trail makes up 64% of a MT. Previous studies have shown that MTs grown under similar experimental conditions to ours primarily have 13 or 14 PFs [9, 129]. Assuming this to be the case for our MTs, we predict that trails taper upwards from 2-3 PFs at their tips to 8-9 PFs at the transition point to the MT. Additionally, the greatest values we measured for I_a would correspond to 5-6 PFs, consistent with our prediction that the kinesin-clamp is unlikely to interact with more than 5 PFs simultaneously (recall Figure 3.6).

We propose that the fraction of the MT lattice that is addressed by the kinesin-clamp is reflected in parameter I_a, the fraction at the trail end. The transition point to the MT provides additional contacts to stabilise the trail, and as such, it is unsurprising that trails are more substantial at this point (Figure 4.3C). It is important to establish a relationship between the two transition points to better understand how the fraction of the lattice that interacts with the kinesin affects the geometry of the trail.

4.3.2 Classification of trail structures

We found that trails adhere to a constrained geometry (Figure 4.4A). Out of the 50 trails that were analysed only 6 of them had average intensities greater than 50% of a MT. Remarkably, we found a negative correlation between parameters I_a and I_b. That is, we observed that trails with greater tip intensities tended to have a flatter profile than those with low tip intensities. Therefore, trails that arise due to many interactions with kinesins have a uniform intensity, whereas fewer interactions give rise to trails tapering up to the full intensity of the MT. This suggests that the kinesin-clamp has conflicting mechanisms in action. Not only does the clamp stabilise MTs and trails, but it also mitigates the additional support that is provided by MT at the trail-MT interface.

It must be noted that this description of how 'flat' trails are accounts only for the difference between I_a and I_b, and not the gradient. We checked for correlations between the length of the trail and I_a and I_b. Surprisingly no correlation was found, suggesting

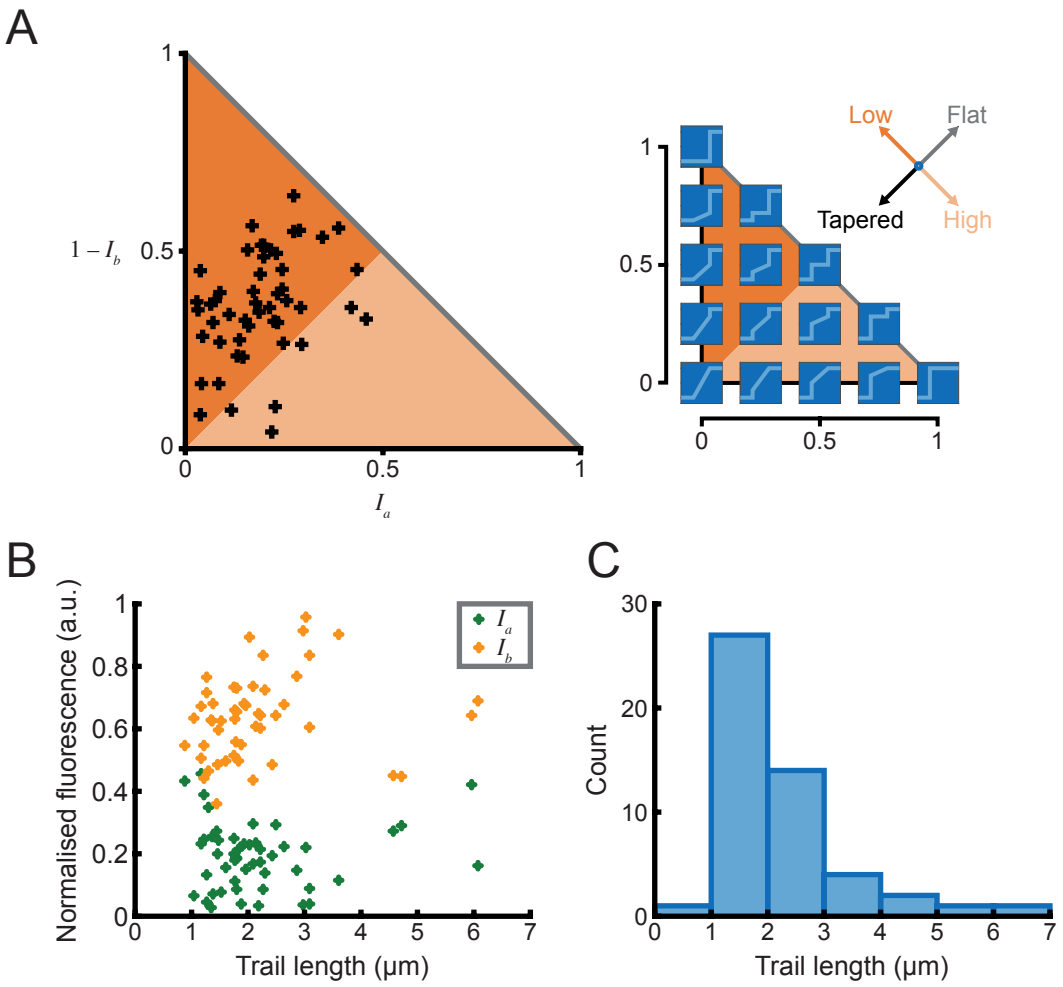

Figure 4.4: MT trail geometries. **A.** Values for $1 - I_b$ are plotted against I_a for visualising the distribution of MT trail types (see diagram to the right). These values correspond to the magnitude of the jumps in intensity at the trail-MT transition and the end of the trail, respectively. The origin therefore represents completely tapered MT ends with no single intensity jump. The colour divide marks the transition from trails that have average intensities above or below 50%. As trails approach the grey line ($I_a = I_b$), they have a flatter profile. There is a significant correlation between the two intensity jumps; $r = 0.36$ (Pearson's correlation), $p = 0.01$. **B.** Comparison of intensity parameters and trail length. No significant correlations between I_a or I_b and the trail length were found ($p = 0.70$ and 0.22 for I_a and I_b, respectively). **C.** Distribution of trail lengths. Trails below $1\,\mu\mathrm{m}$ were rarely counted due to the thresholding technique we apply to improve the robustness of model fitting.

that the number of PFs in the trail does not influence its length (Figure 4.4B). Neither is it the case that MT trails are consistent in length (Figure 4.4C). Measurements of trails shorter than ~1 µm are discarded due to the criteria we set for robust model fitting (see Section 4.2), so results are limited to higher values. Trail lengths (in the absence of nucleotides) appear to be exponentially distributed.

4.4 Fluorescence controls

4.4.1 Normalisation to fluorescence controls

The stabilised colour-barcoded MTs that were included in the optimised kinesin-clamp experiments provide a means to control for fluorescence intensities. The fluorescence controls were assembled from the same stock of fluorescently-labelled tubulin. Therefore, assuming that they contain approximately the same number of PFs as the dynamic MTs, their fluorescence intensities should be equivalent. We selected a third function for quantifying the intensity of the fluorescence controls. This function is an extension of the taper function where both ends of the MT are included (see Figure 4.5). Its equation is given by

$$H(x|a_1, a_2, \sigma_1, \sigma_2) = I_{bgd} + 0.5(I_{tube} - I_{bgd}) \left(\mathrm{erf}\left(\frac{x - a_1}{\sigma_1 \sqrt{2}} \right) - \mathrm{erf}\left(\frac{x - a_2}{\sigma_2 \sqrt{2}} \right) \right), \qquad (4.9)$$

where a_1 and a_2 denote the MT tips, and σ_1 and σ_2 are the corresponding standard deviations.

Once this function had been fitted to the data, we calculated the fluorescence intensity of each segment of the stabilised control MTs ($I_S = I_{tube} - I_{bgd}$, Figure 4.5B). All of the values were then averaged for each flow cell $\bar{I_S}$, which was taken to represent the fluorescence intensity of a single MT. We then calculated the fluorescence intensity of each dynamic MT ($I_{MT} = I_{tube} - I_{bgd}$, Figure 4.5A) from parameters fitted using the stepped tip function. For individual MTs, the fraction $I_{MT}/\bar{I_S}$ should be equal to one, whereas for bundles it should be greater.

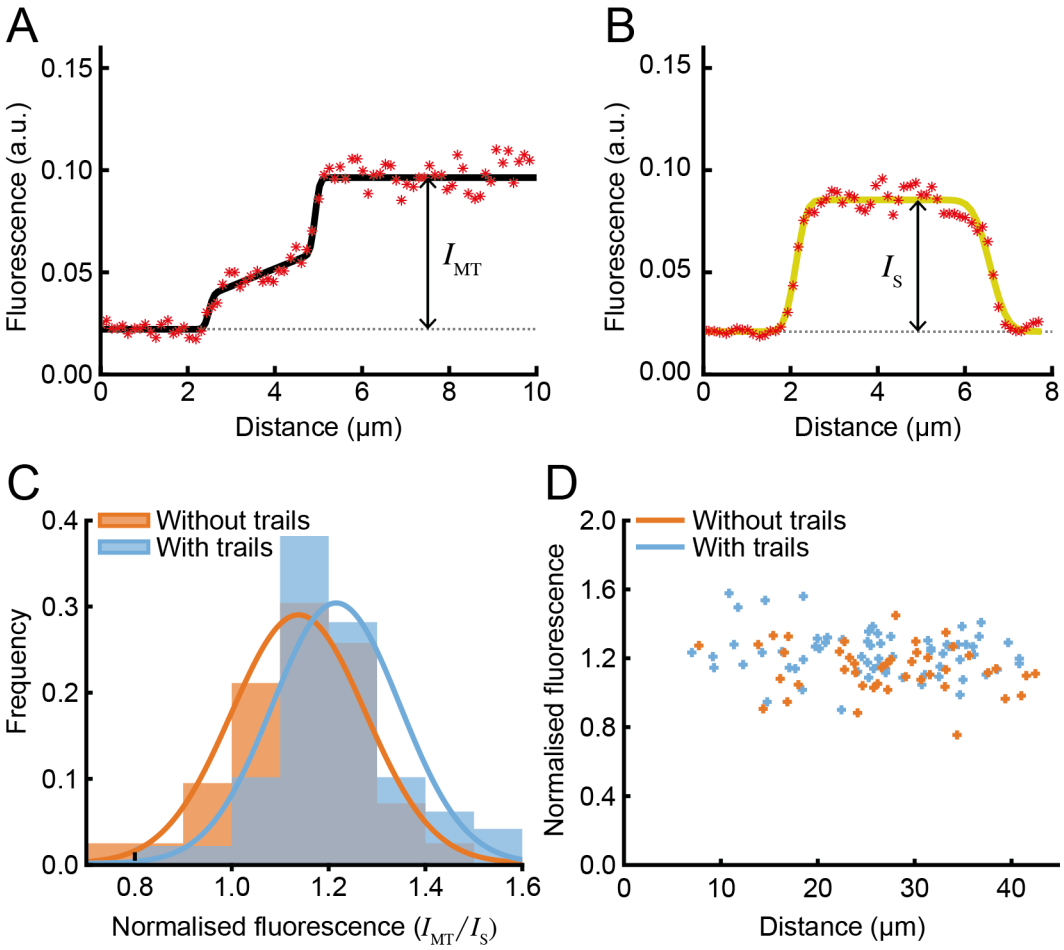

Figure 4.5: Normalisation of fluorescence intensities to controls. **A.** Intensity profile of a MT with a trail. The calculated intensity of the MT is labelled I_{MT}. **B.** Intensity profile of a segment of a fluorescence control. The intensity of controls, labelled I_{S} were averaged before finding the ratio of MT intensities to control values ($I_{\mathrm{MT}}/\bar{I}_{\mathrm{S}}$). **C.** Values of MT intensities normalised to controls. MTs with trails had higher intensities than those without trails (1.22 ± 0.13 (50) compared to 1.14 ± 0.14 (43); mean ± standard deviation (n)). MTs with trails have significantly greater intensities ($p = 0.003$, one-tailed t-test). **D.** MT intensities plotted against the radial distance from the brightest point of illumination. No significant correlation was detected ($r = -0.18$, $p = 0.25$ for MTs without trails and $r = -0.15$, $p = 0.25$ for MTs with trails (Pearson's correlation)).

The fluorescence intensities of MTs with and without trails were 1.22 and 1.14 when normalised to the controls, respectively (Figure 4.5C). These numbers unequivocally demonstrate that our results are from single MTs rather than bundles. The values for MTs with trails are significantly greater than MTs without trails (p = 0.003, one-tailed t-test). MTs with more PFs may therefore have a greater propensity to produce trails. This prediction could be tested more precisely in future experiments by using EM or AFM to determine PF numbers precisely.

It must be noted that the intensities of dynamic MTs are greater than control levels. This is surprising because GMPCPP-tubulin (used for producing the controls) has been reported to polymerise into 14-PF MTs [11], whereas dynamic MTs polymerised under similar conditions to ours typically have 13-14 PFs [9, 129]. It is possible that fluorescently-labelled tubulin is more readily incorporated into the lattice when polymerised with GTP rather than GMPCPP. Indeed, the tubulin labelling procedure we adopted reacts fluorophores with GTP-MTs. Therefore, we know that the labelled tubulin is assembly-competent with GTP but the proportion of lattice incorporation of fluorescent tubulin may not be the same with GMPCPP.

An alternative possibility is that the assembly procedure for the controls is not optimal for this application. It has been shown that the number of PFs can change along the length of MTs assembled *in vitro* [15]. Such lattice defects produce weak spots with the potential for tubulin dimers to bind and unbind from PFs with exposed ends in middle of the lattice [162]. At low tubulin concentrations, one might imagine that the unbinding process is favoured, leading to a gradual reduction in PF numbers.

A third consideration is that photobleaching could occur during the phase of end-to-end annealing in our protocol for the preparation of the controls. This seems unlikely because the solution is kept well covered away from light during this process. Each of the speculated reasons for the discrepancy between the intensity of dynamic MTs and controls could be formally tested. However, our results already provide robust evidence to control against MT bundling so we have not investigated further.

4.4.2 Assessing the effectiveness of flat-field correction

The reliability of quantitative fluorescence analysis is highly dependent on the assumption that there is a uniform excitation response to illumination across the field of view. In reality, illumination is always non-uniform. Image processing known as flat-field correction is commonly applied to resolve this issue [163]. We applied flat-field correction to all of our images prior to analysis (see Chapter 2).

To check that our results are spatially unbiased, we did the following analysis. A uniform sample (Alexa Fluor-488 dye in solution) was illuminated using epifluorescence. The centre of the illumination was then found by fitting a 2D Gaussian curve to the signal. Distances from the peak of the Gaussian to centroids of kymograph locations were then plotted against the corresponding MT intensities (normalised to fluorescence controls). The results are shown in Figure 4.5D. Reassuringly, we found no significant correlation between the kymograph locations and the normalised MT intensities.

4.5 Conclusions

We developed a novel function to approximate the intensity profiles of MTs imaged by fluorescence microscopy. The parameters have a simple physical interpretation, granting a deeper insight into the nature of MT trails. Using this approach, we quantitated the geometries of trails and found that the vast majority (88%) of the trails we measured had average intensities equivalent to less than half of that of a MT. Moreover, trails were typically found to be tapered structures, consisting of 19% of a MT at the tip and 64% of a MT at the base.

By comparing the fluorescence intensities of dynamic MTs to the stabilised fluorescence controls, we were able to validate that the trail formations in these experiments were not artefacts generated by MT bundling. That is, the trails observed in the optimised kinesin-clamp assay are indeed substructures at MT tips. Following on from this analysis, we found that MTs without trails at their ends had only 93% of

the fluorescence signal of those with trails. This is approximately the ratio one would expect for having one fewer PF (assuming in the range of 12-15 PFs), potentially providing a clue for the mechanism of trail formation.

We propose that the number of MT PFs that interact with the kinesin surface is reflected in the relative intensity of the tip of the trail. The average fraction of a MT found at the trail tip then translates to approximately 3 PFs. Surprisingly, we found that the length of the trail and its fluorescence intensity were uncorrelated. This suggests that the number of PFs bound by the kinesin surface has little influence on the trail formation process.

5

Effects of kinesin-1 motor domains on MT shrinkage in solution

5.1 Introduction

There are two possible mechanisms for the stabilisation of MTs in the kinesin clamp. Our hypothesis from Chapter 1 is that PFs interacting with the kinesin surface are immobilised in a straight and stable conformation. This support is then transmitted circumferentially through the MT lattice. With this view, kinesins serve only as a tether linking the MT to the coverslip. An alternative model that is consistent with the kinesin-clamp data is that the motor domains themselves can stabilise MTs.

There have been conflicting reports as to whether kinesin-1 affects MT dynamics *in vivo* [113, 144]. However, the evidence in favour of kinesin-regulated MT dynamics suggests it is the transport of the motor (JNK kinase), and not the motor itself, that is important [113]. Additionally, kinesin-1 has been shown to transport tubulin to growing MT ends via the cargo-linking protein CRMP-2 [112].

Kinesin has also been reported to have no effect on MT dynamics *in vitro* [145]. Curiously, spheres coated with kinesin-1 have been shown to track the tips of depolymerising MTs and regulate shrinkage rates in an ATP-dependent manner [164].

Katsuki et al. showed that intrinsically unstable A-lattice MTs can be stabilised by tethering them to a rigid substrate, even if the linkers used (anti-fluorophore antibodies) are not kinesins [23]. Therefore, the literature strongly supports the view of

kinesin-1 having no direct effect on MT dynamics. The kinesin-clamp could therefore be explained by our original hypothesis that holding PFs straight against a rigid substrate (glass coverslip) imparts stability upon the lattice.

5.2 Effects of kinesin-1 on MT depolymerisation away from the surface

5.2.1 Controlling for surface effects

An assay for investigating the depolymerisation of kinesin-decorated MTs in solution (away from the surface) was required in order to control against any surface-related stabilising effects in the kinesin-clamp.

GMPCPP-stabilised MT seeds were attached to a glass coverslip before blocking the surface and growing dynamic MT extensions by adding GTP-tubulin (Figure 5.1A). Conditions were optimised such that MTs could be seen to flex and bend (driven by thermal motions), indicating that they were free from the surface. GTP-tubulin was depleted by flowing buffer through the flow chamber, just like in the kinesin-clamp assay. However, the buffer was supplemented with monomeric kinesin (K340-His) to test whether kinesin affects the shrinkage rate.

We optimised conditions to minimise potential effects of MTs binding to the surface; efforts were made to repel the MTs from the coverslip, meaning that a microscopy technique with a large depth of field was necessary to image these experiments. Both epi-fluorescence and dark-field illumination satisfy this requirement. However, fluorescence imaging gives a linear response to the fraction of fluorescently labelled protein so unpolymerised tubulin generates a high background signal if illuminated by epifluorescence. TIRF illumination is commonly used to overcome this problem, since it only penetrates the sample to approximately 200 nm. Such a shallow depth of field renders the technique unsuitable for our experiments. Dark-field illumination provides a nonlinear response, generating a large signal for MTs in contrast

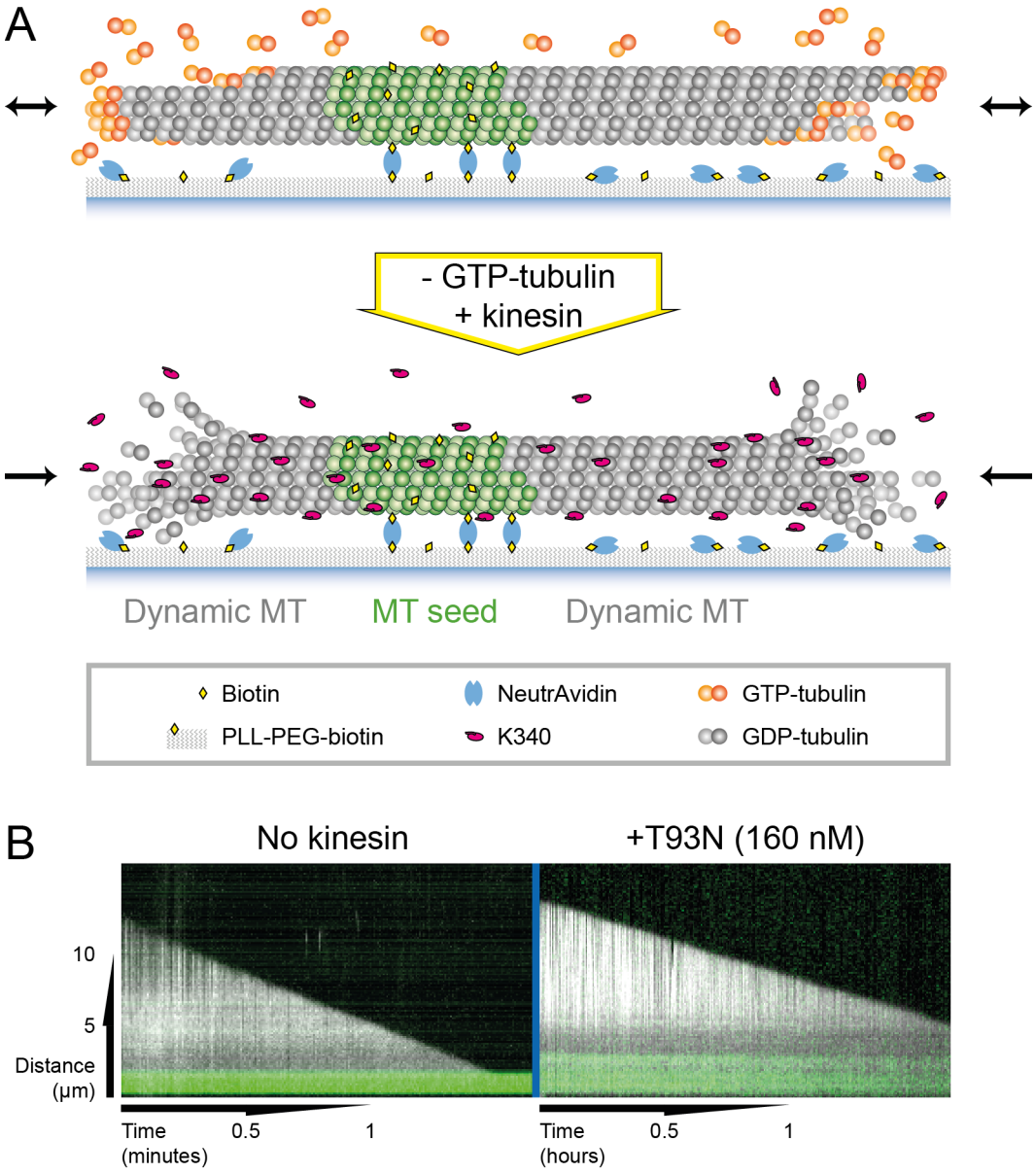

Figure 5.1: Tubulin depletion assay. **A.** Schematic of the tubulin depletion assay. Dynamic MTs were grown from stabilised seeds. GTP-tubulin was washed out of the flow-chamber with a kinesin-containing (K340) buffer. **B.** Two kymographs of depolymerising MTs in the absence of tubulin. *Left*: No kinesin was added to the buffer. *Right*: $160\,\mathrm{nM}$ of a non-stepping kinesin mutant (T93N) was added to the buffer.

to unpolymerised tubulin. We therefore selected dark-field for imaging dynamic MTs and epifluorescence for fluorescently labelled (Alexa Fluor-488) seeds.

Initially, we used anti-fluorophore (Alexa Fluor-488) antibodies to bind seeds to the coverslip. We found that MTs had a slightly lower affinity for the surface when a low concentration of antibodies was used ($0.05\,\mathrm{mg\,ml^{-1}}$ rather than $1\,\mathrm{mg\,ml^{-1}}$). Seeds were immobilised effectively at this concentration. However, upon addition of kinesin, MTs were found to bind rigidly to the coverslip. This was the case even when very low concentrations (40 nM) of kinesin were used, demonstrating that the kinesin has a high affinity for the surface. Increasing the concentration of blocking agent had no effect, suggesting that kinesin binds non-specifically to the antibodies.

We tried an alternative method of attaching the seeds to the cover-slip. We found that by attaching biotin-labelled seeds to a PLL-PEG-biotin-coated coverslip via NeutrAvidin linkers, dynamic MT extensions were free from the surface even in the absence of blocking agents. Upon addition of 40 nM kinesin, MTs were seen to be free from the surface but occasionally showed signs of sticking. At higher concentrations, MTs would be immobilised. We found Tween20 to be an effective blocking agent for this arrangement. Using 0.1% Tween20 (v/v) prevented MTs from sticking to the surface over the full range of kinesin concentrations we tested (up to 160 nM).

5.2.2 Shrinkage rates of kinesin-bound MTs away from the surface

Remarkably, we found that shrinkage rates were inhibited dramatically upon addition of kinesin, demonstrating that the kinesin motor domain has an intrinsic ability to stabilise the MT lattice (Figure 5.1B). We used a kinesin mutant (T93N) with an inhibited ability to coordinate nucleotides to resemble the no-nucleotide state of kinesin. The unmutated construct (K340) was used initially but preliminary measurements were highly variable. Our kinesin-clamp data suggests that kinesin-regulated MT depolymerisation is highly sensitive to low doses of nucleotides. We therefore envisage that the variability in our results was due to residual nucleotides in the flow chamber.

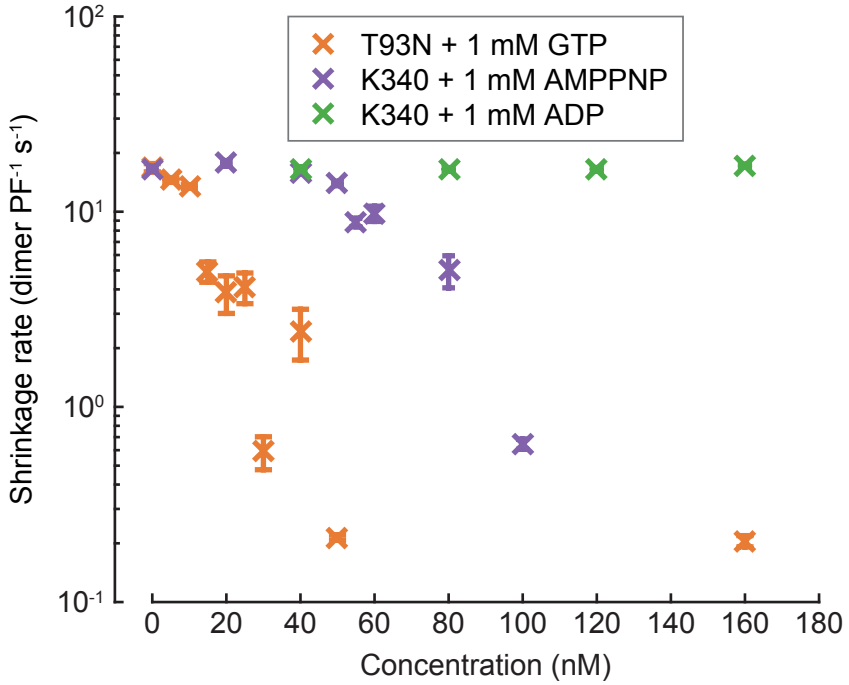

Figure 5.2: MT shrinkage rates in the presence of kinesin-1. Rates were measured in the absence of GTP and tubulin unless stated otherwise. 'No flow-through' refers to the shrinkage of MTs when GTP-tubulin was not depleted (so in the presence of 1 mM GTP and 15 µM tubulin). Kinesin concentrations used and sample sizes are as follows. T93N + GTP: concentration=0,5,10,15,20,25,30,40,50,160 µM; n=20,38,33,27,35,53,40,17,29,25. K340 + AMPPNP: concentration=0,20,40,50,55,60,80,100; n=28,25,14,20,70,18,16,34. K340 + ADP: concentration=40,80,120,160; n=34,41,44,49. Error bars show mean ± SEM.

During optimisation of the assay we also tested the use of apyrase as a means to maximise the efficiency of nucleotide depletion. Apyrase is an enzyme that hydrolyses nucleotide triphosphates and diphosphates into monophosphates. This technique is commonly used to drive kinesin into a tightly-bound state [158]. We found that large tubulin aggregates formed rapidly upon addition of apyrase so we rejected this approach.

Tubulin denaturation in the absence of nucleotides is a likely cause of the aggregation that we observed. A benefit of using T93N is that we could control for this. Due to its insensitivity to nucleotides, we were able to include GTP in the buffer and observe (a stable homologue of) the no-nucleotide state of kinesin simultaneously.

We varied the concentration of T93N from 0 to 160 nM and measured the shrinkage rates. Amazingly, the difference in shrinkage rates spanned approximately three orders of magnitude (Figure 5.2). Clearly, kinesin-induced MT stabilisation is

highly sensitive to nucleotides, so we asked how the effect changes as kinesin progresses through the ATPase cycle.

We included saturating levels of a slowly-hydrolysable ATP analogue (AMPPNP) to study the ATP-bound state of the cycle. Pleasingly, we observed a similar response for AMPPNP-bound kinesin as we did for the T93N mutant. Nucleotide-free and ATP-bound kinesin, referred to hereafter as 'strong-state' kinesin, binds tightly and stereospecifically to the MT lattice. We found no measurable effect for weak-state (ADP-bound) kinesin. We conclude that only the kinesin strong states stabilise MTs.

5.3 Kinesin structurally modifies the MT lattice

The depletion step of the experiments described above sees that buffer (with or without kinesin) is flowed through the flow chamber. If the buffer is exchanged quickly, the hydrodynamic flow exerts forces that bend any MTs that are not aligned with the flow direction. When no kinesin is added to the buffer, MTs are seen to resume a straight conformation in seconds after the flow is stopped (Figure 5.3). Strikingly, we found that low doses (15 nM) of strong-state kinesin trapped MTs in a curved state.

MT curvature is not only stabilised by kinesins but it also increases over time. This effect is more pronounced at higher kinesin concentrations (e.g. 30 nM). At even higher concentrations ($\geq$ 50 nM) MTs would re-straighten after the flow was stopped. These concentration-dependent behaviours could be seen for all MTs in a given field of view. The amplification of MT curvature by kinesins was however most pronounced for the MTs initially grown opposing the flow direction (Supplementary Movie 1). These MTs naturally experience the greatest bending forces. MTs that are aligned with the flow direction experience little bending even in the presence of 30 nM kinesin. Therefore, strong-state kinesin does not induce bending without the aid of additional factors. Rather, it recognises and amplifies the conformational bias that is initiated by the hydrodynamic flow.

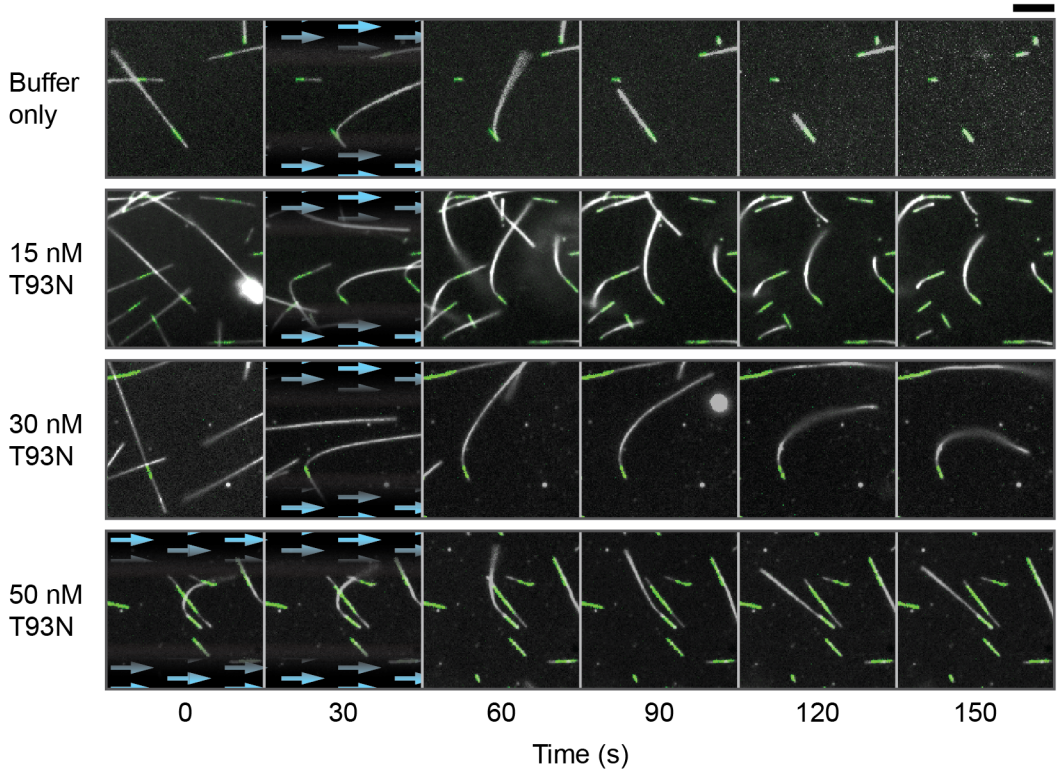

Figure 5.3: Nucleotide-free kinesin motor domains recognise and modify the curvature of bending microtubules. Time-lapse images of microtubule bending experiments for a range of kinesin concentrations are shown. Blue arrows highlight the presence and direction of fluid flow. Dynamic microtubules appear in white (dark-field) and fluorescent seeds in green (epi-fluorescence). Scale bar is $5\,\mu\mathrm{m}$.

5.4 Conclusions

We examined the influence of monomeric kinesin-1 on the shrinkage rate of MTs in solution (free from the glass surface). We found that kinesin-1 has the ability to reduce shrinkage rates by approximately two orders of magnitude. We therefore envisage that strong-state kinesin could promote MT rescue and thereby promote lengthening of dynamic MTs. Future experiments will test this hypothesis.

The MT-stabilising property of kinesin is tightly linked to the ATPase cycle. As a kinesin molecule takes a step, it transiently enters the ADP-bound state and permits tubulin dissociation. Moreover, kinesin-1 does not pause when it reaches the MT tip; it literally walks off the end. This may explain why kinesin-1 has previously been shown to not affect MT dynamics *in vitro* [145].

As well as inhibiting MT shrinkage, our data support the view that strong-state kinesin modifies MTs structurally. The underlying mechanisms of kinesin-MT interactions are discussed further in Chapter 6.

6

Discussion

We discovered that kinesin-1 can stabilise GDP-MTs and used *in vitro* techniques to probe the mechanism.

It has previously been reported that kinesin-1 has no effect on MT dynamics [145] but there are nonetheless hints in the previous literature that kinesin in low nucleotide conditions can stabilise MTs. Kinesin-coated beads are able to track MT tips and regulate shrinkage rates in an ATP-dependent manner [164]. However, many mechanisms could account for this behaviour [165]. Further, kinesin promotes the formation of long PFs in the presence of taxol [166, 167], although taxol alone has been reported to have similar effects [168]. Very recently, GMPCPP-MTs have been reported to shrink more slowly in the presence of kinesin monomers but the rates were not measured explicitly [146].

Our own results show that kinesin-1 has the ability to function as a highly effective stabiliser of GDP-MTs. This function is attributed to the strong states, the nucleotide-free and ATP-bound phases of the stepping cycle.

In the following sections we discuss the implications of our findings in light of published data, suggest reasons for discrepancies in the literature and speculate about how cells might exploit kinesin-MT interactions for the regulation of MT dynamics.

6.1 Strong-state kinesin-1 inhibits MT depolymerisation

We have shown that both monomeric and dimeric kinesin-1 dramatically inhibits the shrinkage of GDP-MTs when bound tightly to the MT lattice. The fact that

kinesin dimerisation is not required for MT stabilisation shows that the underlying mechanism does not require cross-linking of the cognate kinesin binding sites on tubulin dimers. There are many published EM reconstructions of kinesin-MT complexes that localise this binding site [61, 62, 141, 142, 146, 166, 167]. Recent crystal structures of kinesin-tubulin complexes provide additional resolution [139, 140]. The binding site is centred on the interface between α- and β-tubulin, and is formed largely by the C-terminal hairpin of α-tubulin (the helices 11 and 12, together with the loop that connects them). Recent work identifies specific residues on the kinesin motor domain and on tubulin whose interaction is required for MT activation of the kinesin ATPase [169]. The site at which strong-state kinesin motor domains bind to tubulin is thus tightly localised. The most recent EM reconstructions with kinesins bound to these sites on the MT underline that there are no obvious contacts between kinesin motor domains in either the lateral or longitudinal directions. On this basis we regard it as unlikely that strong-state kinesins stabilise MTs by linking tubulins together, either longitudinally or via lateral linkage of PFs.

Our current model envisages that strong-state kinesins stabilise MTs by inducing allosteric conformational changes in lattice-bound tubulin. This idea has been previously suggested based on low-resolution (17 Å) structural data of the MT-kinesin complex [166]. The authors speculated that kinesin stabilises the longitudinal inter-dimer contacts along PFs. Further, there have been at least two reports claiming that long taxol-GDP-PFs are stable in the presence of kinesin-1 [166, 167]. However, such results should be interpreted with caution because taxol alone can stabilise individual PFs [168].

Very recently, kinesin-1 has been shown to induce conformational changes in GMPCPP-MTs [146]. Kinesin causes the C-terminal helices (H11-H12) of α-tubulin to be compacted towards the MT lumen, which in turn causes a rotation in the intermediate domain of α-tubulin (Figure 6.1). There is also evidence that kinesin binds preferentially to GTP-MTs over GDP-MTs, suggesting a potential conformational selection mechanism by which kinesin binding might drive GDP-tubulin into a more GTP-like tubulin conformation [170].

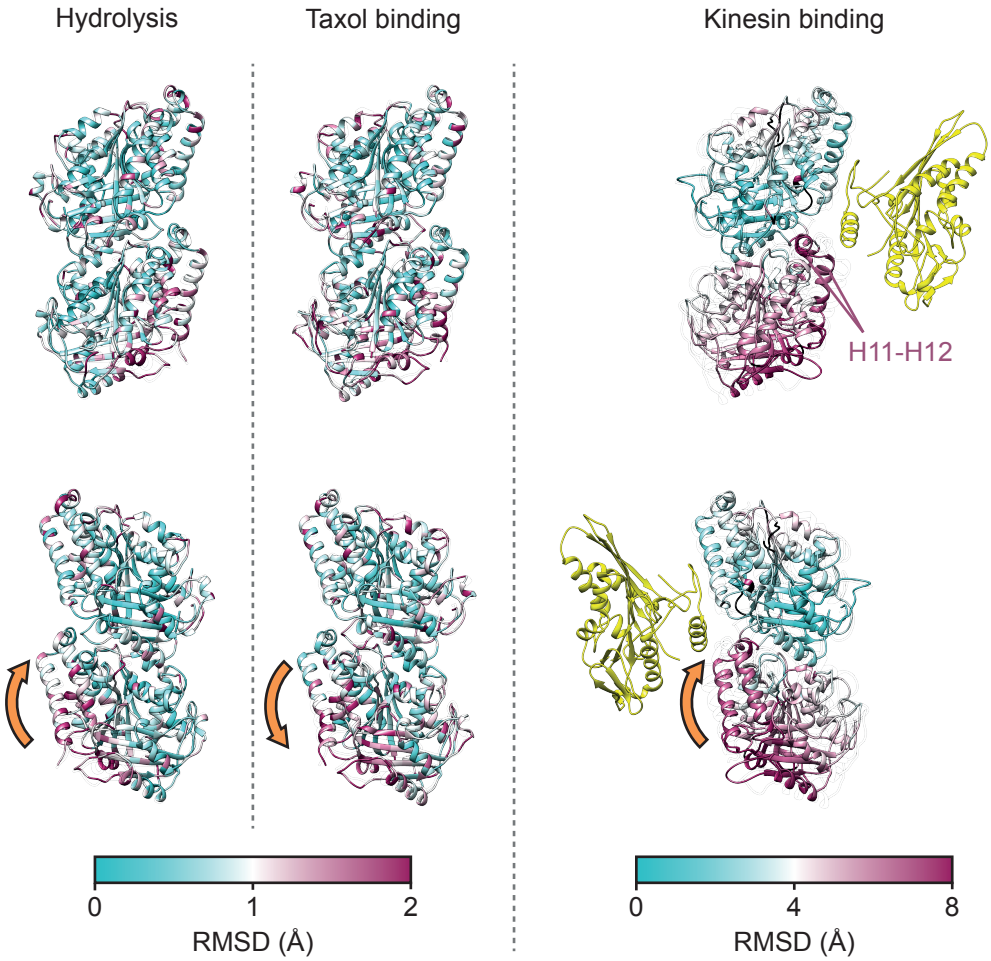

Figure 6.1: Conformational changes in the MT lattice. Pairwise comparisons of (polymerised) tubulin structures were compared by aligning β-subunits and calculating the average root-mean-squared deviation (RMSD) of each residue. Three transitions are shown. The first state is faintly outlined and the second state is coloured according to the RMSD of the transition. Two views are shown (*top* – left-side view; *bottom* – right-side view; aligned such that the MT plus-end is at the top of the page in each case). Structures used for the transitions are as follows. *Left* – 3J6E (kinesin-GMPCPP-MT) to 3J6F (kinesin-GDP-MT); *Middle* – 3J6F (kinesin-GDP-MT) to 3J6G (kinesin-GDP-taxol-MT); *Right* – 3J6H (GMPCPP-MT) to 3J7I (kinesin-GMPCPP-MT). Kinesin is shown in yellow.

The intermediate domain of α-tubulin similarly rotates and compacts upon GTP hydrolysis [61, 62]. Kinesin has however been reported to dampen such conformational changes [61]. Interestingly, the motions associated with GTP hydrolysis can be partially reversed by adding the MT stabilising drug taxol (Figure 6.1, [61]). Moreover, upon binding kinesin to GMPCPP-MTs, tubulin conformation is driven towards a more 'taxol-like' state, suggesting that kinesin and taxol might support similar conformations of tubulin in the MT lattice [146]. It must be noted however, that conformational changes are incurred upon binding of kinesins to taxol-stabilised GDP-MTs [166], so the conformational changes induced by kinesin and taxol are distinct.

Unfortunately, no high-resolution structures have been reported for GDP-MTs that are not bound to either taxol or proteins that interfere with MT structure. Such data will be key to building a comprehensive picture of the molecular mechanisms underlying GTP hydrolysis and kinesin- and taxol-regulated MT stabilisation. A technical limitation in acquiring a MT structure is the identification of the A-lattice seam. This means that MTs have to be either perfectly helical (e.g. have a 15_4 structure) or be decorated with 'marker proteins' (such as kinesins). A structure of GDP-MTs decorated with EB3 was recently reported [62]. However, EB3 brought GMPCPP- GDP- and GDP-taxol-MTs to the same conformation (different from taxol or kinesin), ruling this out for representing the unmodified structure of GDP-MTs.

Kinesin binding to GMPCPP-MTs induces a striking conformational change in the C-terminal hairpin of α-tubulin (H11-H12, Figure 6.1). Indeed, some the most extensive movements reported are in the compaction of the hairpin towards the MT lumen. This motion is distinct from the effects that have previously been suggested for taxol-induced MT stabilisation. Remarkably, the hairpin is in fact shifted similarly in both α- and β-subunits of tubulin. Longitudinal contacts between tubulins in a PF involve bonds that join consecutive hairpins. Conformational changes in this region could therefore alter longitudinal bond strengths.

Based on our data and on these previous reports, we propose a mechanism whereby strong state kinesin-1 operates in a converse manner to the kinesin-13 motor protein, MCAK (Figure 6.2). MCAK binds to the same face of tubulin as kinesin-1.

The depolymerase mechanism of MCAK promotes a highly curved conformation of tubulin that is incompatible with the MT lattice. In this way, MCAK extracts GTP-tubulin from the MT tip and subsequently triggers catastrophes. We propose that strong-state kinesin-1 drives tubulin into a stable and shrinkage-resistant conformation. A prediction of our model is that strong-state kinesin-1 could be a potent MT rescue factor.

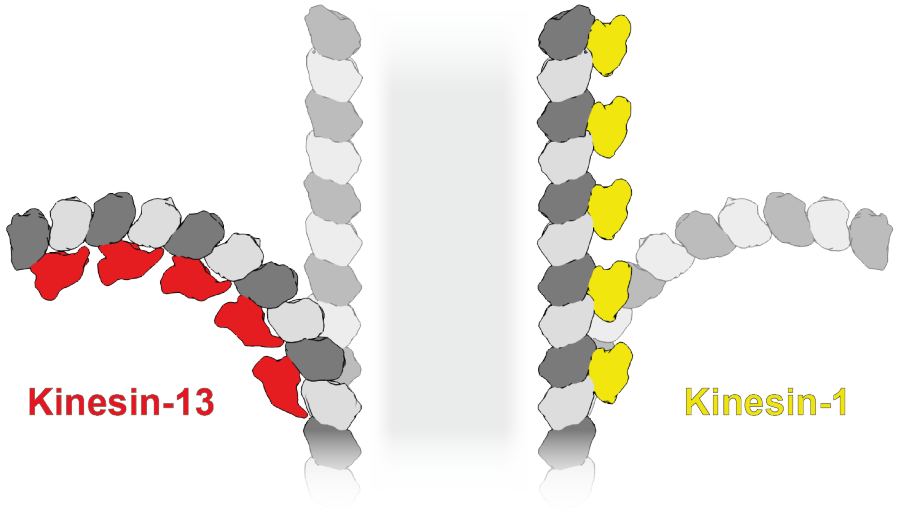

Figure 6.2: Proposed mechanism for kinesin-regulated MT dynamics. The kinesin-13 motor protein MCAK promotes MT catastrophe by inducing PF curling. We propose that tightly-bound kinesin-1 has the opposite functionality; it favours a straight, GTP-like conformation of tubulin that enhances MT stability.

6.2 Strong-state kinesin recognises curved MTs and modifies the extent of bending

We showed that strong-state kinesin not only inhibits MT shrinkage but it also stabilises and enhances the curvature of bending MTs.

One explanation for these observations might be that inter-PF shearing occurs as MTs bend, and this is locked in place by the kinesin. This however would not explain why MT curvature increases over time in the presence of kinesin. Additionally, the rearrangement of lateral bonds in curved MTs has been reported to be small [171]. An alternative mechanism would be that MT lattice defects, which have been shown to

accumulate during hydrodynamic flow and soften MTs [162], could contribute towards this phenomenon. However, this alone would not explain how MTs are restored to a straight conformation at saturating kinesin concentrations.

To explain our observations we propose that strong-state kinesin recognises the conformational bias of bending MTs; the outermost (convex) side is stretched relative to the innermost (concave) side of the bend. Kinesins have previously been reported to show conformational selectivity, binding preferentially to GTP-MTs compared to GDP-MTs [170]. We envisage that kinesin binding then locally enhances the lattice deformation, promoting additional recruitment of kinesins and thereby driving further MT bending (Figure 6.3). Kinesin binding could also occur, to a lesser extent, on the opposite side of the lattice. At saturating kinesin levels, this would gradually drive the microtubule back into a straight conformation.

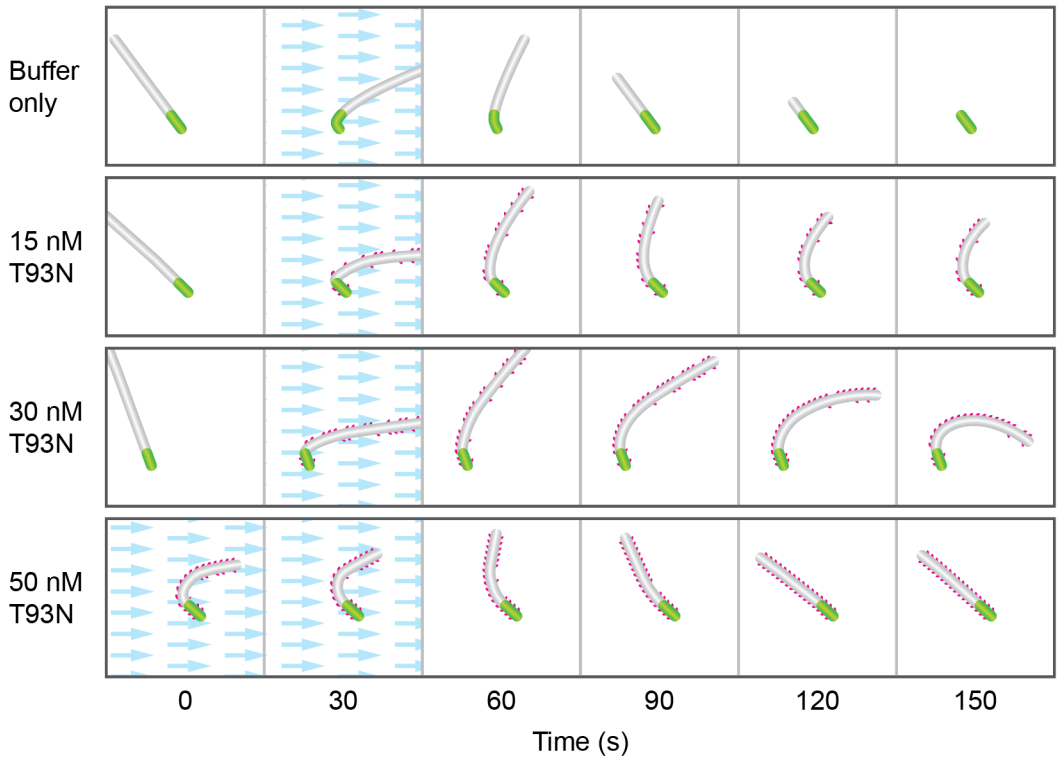

Figure 6.3: Proposed mechanism for kinesins remodelling MT conformations. Boxes represent our interpretation of the frames shown in Figure 5.3. T93N binds preferentially to one side of bending MTs (shown as the longer, outside edge). The favoured conformation is enhanced by kinesin, creating a positive feedback loop that is most pronounced at $\sim 30\,\mathrm{nM}$. Once the preferred binding sites are saturated, further increases in concentration ($\geq 50\,\mathrm{nM}$) drive kinesins to bind at less favourable sites, thus mitigating the asymmetry.

Note that MTs do not bend in the presence of kinesin if they are aligned with the

direction of flow. Therefore, the initial induction of MT curvature is due to the flow, not the kinesin. To maintain the asymmetry, kinesins must bind preferentially to one side of the MT (Figure 6.3). We suggest that this is the longer, outside edge based on observations that kinesin binds more readily to a straighter, elongated conformation of tubulin [170] and it suppresses compaction of tubulin that occurs upon GTP hydrolysis [61]. However, the possibility of binding preferentially to the inner surface cannot be excluded.

Another factor to consider is the bi-stability of tubulin curvature; both straight and curved conformations of tubulin are reported to reside in local energy minima [172]. Crystal structures further reveal that a curved conformation is readily adopted by tubulin, regardless of the nucleotide state [54]. It has been previously suggested that the bi-stability of lattice-bound tubulin can lead to MTs favouring a slightly curved conformation [173]; as tubulin on the convex side of the lattice straightens up it approaches an energy minimum and the tubulin on the concave side simultaneously approaches a lower energy state.

This has implications for the MT bending that we observed. Rather than kinesin elongating tubulin, we might consider that kinesin relieves some of the mechanical stress on the convex side of a bending MT. Kinesin-1 has in fact been reported to 'soften' tubulin [174]. Relieving the mechanical stress could contribute to further bending. The more kinesin that binds to the lattice, the easier it is for the tubulins on the concave side of the MT to release energy by adopting a curved conformation. Again, a feedback loop arises as the affinity of kinesin for the MT lattice changes with curvature.

Clearly, it would be of interest to identify which side of the curved MT lattice kinesin-1 truly binds to. Clarification of this should come from electron microscopy or possibly even super-resolution fluorescence microscopy. An exciting prospect, given the proposed conformational specificity of kinesin-1 and kinesin-13, would be to investigate their behaviour in a two-motor competition experiment. We suspect that MCAK will bind to MTs that have been bent by kinesin-1. This is highly speculative however because the curvature induced by kinesin-13 is much greater than that of the MT

bending we observed [115].

The polymorphic conformations of tubulin and associated feedback loops have attracted much attention. MTs in gliding assays have been reported to occasionally enter a circular trajectory from which they often don't escape. A recent computational model has shed light on this phenomenon, again proposing that MTs are able to adopt metastable curved conformations [175]; mechanical hysteresis of MTs may result from collective behaviour of tubulins in the MT lattice. Our results suggest that the specific interaction with kinesin also plays a critical role in this phenomenon.

Several instances of non-uniform binding of kinesins to MTs have been reported in the literature. Kinesin-1 has been shown to fully-decorate subgroups of homogeneous MT populations *in vitro*, whilst not binding to others in the same sample [176]. The same effect has been reported to a greater extent for Vik1-Kar3 [177]. There is also evidence to suggest that both the on- and off-rates of kinesin-MT binding kinetics are biased in the neighbourhood of pre-bound kinesin [178]. Most interestingly, kinesin-1 appears to induce conformational changes in the MT lattice, which demonstrate cooperative binding, spanning lengths of several microns [179]. The prospect of sending mechanical signals along the MT lattice has attracted much attention from theorists [180, 181]. The extent to which these processes might play a role in MT mechanics and MT-kinesin interactions is currently unclear. However, these observations collectively paint a picture where the allosteric effect of kinesin binding to the MT lattice is not localised to a single tubulin dimer.

6.3 Kinesin-clamps bind to a subset of PFs but stabilise the entire MT lattice

Continuing along the theme of kinesins binding to one side of the MT lattice, we discuss the potential mechanisms underlying the kinesin-clamp phenomenon.

6.3.1 Is the clamp-induced MT stabilisation specific to kinesin?

We originally hypothesised that tethering a MT to a rigid substrate would stabilise it; PFs bound to the surface are maintained in a straight conformation, enhancing the stability of the neighbouring PFs and therefore also the remainder of the MT (by argument of induction). We have shown that this mechanism is not fundamental to the stabilisation of MTs by kinesin, for strong-state kinesin inhibits MT shrinkage in solution. However, MTs shrank slower in kinesin-clamps than when they were free from the surface, both in the presence of low ($\leq$ 400 nM) and high ($\geq$ 1 mM) ADP concentrations (compare Figure 3.13 and Figure 5.2). Therefore, there must be at least one mechanism contributing to the stabilisation of MTs in a kinesin-clamp in addition to direct effect attributed to strong-state kinesin motor domains.

We suggest two possibilities. First is the mechanism we originally proposed; MTs are stabilised by binding to a rigid substrate, potentially due to surface-bound MTs having fewer degrees of freedom. Measuring the shrinkage rates of GDP-MTs firmly attached to a flat surface by alternative linkers would shed light on this. We did try to control for this possibility by binding biotin-labelled MTs to a functionalised surface via NeutrAvidin linkers. However, such experiments are technically challenging because tubulin appears to outcompete MTs for available binding sites. Moreover, we have preliminary data that demonstrates the ability of NeutrAvidin to stabilise biotin-labelled MTs in solution, presumably by cross-linking tubulins in the lattice. This could provide an explanation for previously reported ability of antibodies to stabilise MTs in a clamp-like arrangement [23]. A next step in obtaining suitable controls should therefore involve the use of monovalent linkers (e.g. monomeric streptavidin [182]) to bind the MTs to the coverslip.

A second possible mechanism is that the on-rate of kinesin-MT interactions is increased in the kinesin-clamp relative to MTs that are free from the surface. Kinesins are tethered near to their MT-binding sites in a kinesin-clamp. In this arrangement kinesins cannot diffuse away from their binding sites after detaching

(translationally and, to some extent, rotationally), which is a key difference from kinesin-MT interactions away from the surface.

In any case, it is clear that the stabilisation provided by the kinesin-coated surface is transmissive through the MT lattice; stabilising one side of the lattice maintains the integrity of the entire MT.

6.3.2 The behaviour of MT trails

What causes MT trails to form in our assays? It is clear first of all that trails do not always form – some MTs, bound on their lower surface by kinesins, have their shrinkage rate inhibited, yet shrink nonetheless blunt-ended (at the resolution of the light microscope), without leaving a trail. Equally, it is clear that in those MTs that do form trails, the two ends behave differently – trails are much more likely to form at minus ends than plus ends. Finally, in those MTs that form trails, shrinking trails can sometimes catch up to their parent tubes, reforming a blunt ended, slowly-shrinking tube. In some instances MTs that undergo blunt-ended shrinkage can form new trails, and these new trails can again shorten to sub-resolution lengths. Kinesin in solution slows shrinkage but does not create trails, so it is clear that the formation of trails is due to the specific geometry of the kinesin-clamp. How might this cause the MT structure to split apart?

Trail-like observations have been reported in the literature. Short trails (< 10 dimers long) have been observed by AFM at the ends of taxol-stabilised MTs bound to positively charged coverslips [183]. Such trails took the form of flat PF sheets, presumably due to strong interactions with the negatively charged surface of tubulin. Although the flattening of trails likely plays a role in the kinesin-clamp experiments, we find that they are actually tapered structures. We envisage that the MT provides an additional source of stability for the trail, such that trails with more PFs are stabilised in the proximity of the MT, in turn creating a taper.

There are many reports of MT tips having tapered geometries during phases of growth [19, 44]. However, shrinking MTs have relatively blunt tips due to the rapid

(potentially oligomeric) dissociation of GDP tubulin once lateral contacts in the lattice have been broken. However, the emergence of trails demonstrates that it is possible to stabilise subsets of PFs at MT tips, differentially regulating opposing sides of the MT lattice such that tapered structures can form even during shrinkage. The trails that we observe are distinct from previously reported tapering of MT ends; we consistently detect a large drop in image intensity where the trail meets the MT. Moreover, the trails we observe reach lengths exceeding 6 µm, which is far greater than reported in the aforementioned publications.

Several factors may contribute towards the process of trail formation, which we address in the following sections.

6.3.3 How is mechanical stress accommodated by the MT lattice in a kinesin-clamp?

As discussed earlier, the allosteric effects of kinesin binding to the MT lattice may include an elongation of tubulin. For example, an increase in tubulin length by 1% would lead to a shear between affected and unaffected PFs of one dimer per 800 nm, provided the density of kinesin is high enough to address every tubulin dimer along a PF. The extension of just one side of the lattice would surely yield an increase in the internal stress of the MT, potentially leading to a rift that promotes the formation of trails.

Whether significant effects could arise by this phenomenon depends on the magnitude of the length change and also the extent to which MTs are able to distribute energy (both longitudinally and laterally) around the lattice.

The geometry of MT tips (imaged by cryo-EM) have been well reproduced by assuming that tubulin has an intrinsic bending energy, whilst inter-PF contacts in the MT lattice promote tubulin straightening [184–187]. Deep in the MT lattice, the GDP-tubulin bending energy is distributed evenly across the subunits. However at MT tips, each tubulin has fewer axial neighbours to 'share the load' with, creating a gradient of strain near the MT tip ([186], Figure 6.4). The heightened instability at MT

tips is proposed as the basis for MT catastrophe, which may be inhibited by enhancing lateral contacts (i.e. with a GTP-tubulin cap). These models of MT mechanics also predict that tapering of MT tips allows the bending energy of GDP-tubulin to be distributed more evenly [187].

The upshot of these models is that energies are distributed throughout the MT lattice in a highly elastic manner. Altering the mechanics of a subset of PFs would then produce a large redistribution of energy. This has large implications for the kinesin-clamp, even assuming there are no associated length changes.

We have shown that the stabilisation of PFs in a kinesin clamp is transmitted circumferentially around the MT lattice. Therefore, by extrapolation of the modelling results discussed above, one would predict a stress gradient not only axially but also circumferentially. The least stable PFs would surely be those furthest from those interacting with the clamp.

It must be noted that individual MTs and trails show high variability in their shrinkage velocities, whereas in experiments where MTs are free from the surface they shrink at a constant rate. The most intuitive explanation is that uneven kinesin densities lead to the variability seen in kinesin-clamped MTs; shrinkage rates are governed by the density of strong-state kinesins at the MT (or trail) tip. This is consistent with data suggesting that motile kinesin-1 does not influence MT dynamics despite always having one head bound firmly to the MT lattice [145]; kinesin-1 spends little time at the MT tip before it walks off the end, so no effect on shrinkage is seen.

Conformational changes induced by kinesin binding could additionally have far-reaching effects, as suggested previously by Muto et al. [179]. A kinesin-clamp assay with a micro-patterned and fluorescently-labelled kinesin surface could be used to establish whether such effects play a role; the shrinkage rate as a MT approaches a dense kinesin patch would reveal whether the enhanced stability is transmitted axially.

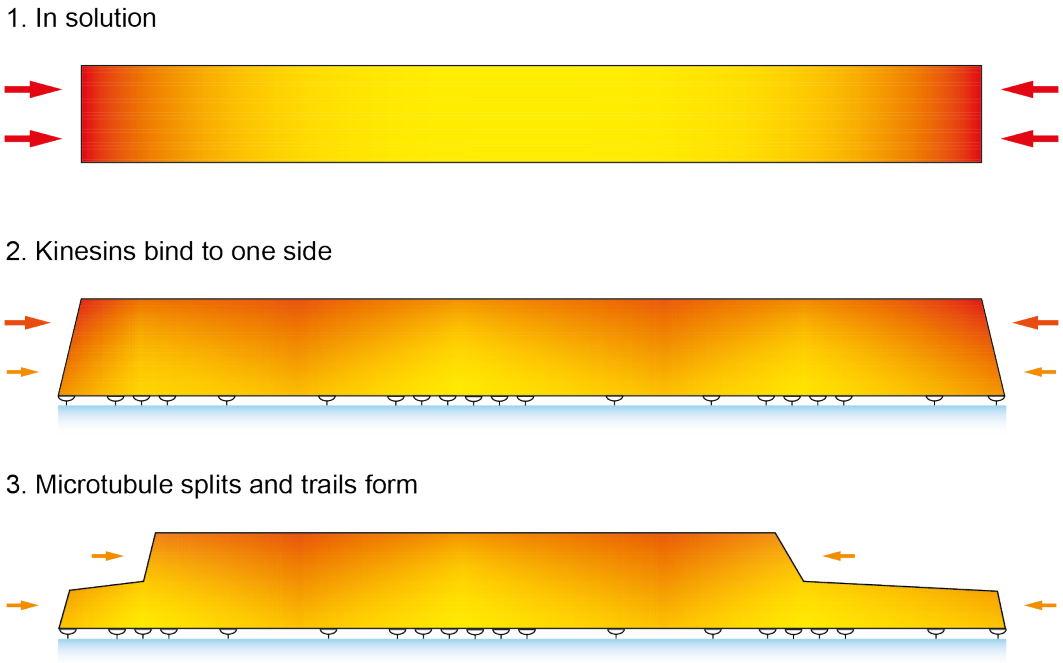

Figure 6.4: Model for trail formation in the kinesin-clamp. Unstable regions are highlighted in red. **1.** MTs are naturally less stable at their ends because there are fewer lattice contacts to distribute the intrinsic bending energy of GDP-tubulin. Shrinkage proceeds rapidly. **2.** Binding to the kinesin surface provides additional support on the lower PFs, leading to a circumferential gradient of stress in the MT. Further heterogeneity arises from uneven binding patterns. Kinesin-binding may additionally stretch the MT lattice. **3.** The MT breaks in regions of high stress, shrinking faster than the kinesin-bound PFs. Upon reaching a region of enhanced stability, determined by the density of kinesins on the surface, the shrinkage rate decreases. Rates of shrinkage are tightly coupled to the kinesin patterning.

6.3.4 Model for trail formation in the kinesin-clamp

We propose that in the kinesin-clamp assay, mechanical stress is distributed non-uniformly through the MT lattice. The distribution of this stress is largely determined by the patterning of kinesins on the MT. The least stable regions of the MT are those furthest from kinesin-bound dimers. Our model envisages that kinesin not only stabilises the MT but also modifies the conformation of tubulin, potentially altering the axial spacing of the MT lattice.

The PFs that harbour the greatest mechanical stress peel away from the rest of the MT, which is our proposed mechanism for trail formation. As the shrinking MT tip approaches a region of high kinesin density, it experiences greater support and hence slows down (Figure 6.4).

Curiously, we found that MTs that did not form trails had a 7% lower fluorescence signal than those with trails. This change corresponds to a difference of approximately 1 PF. The number of PFs in a MT determines their orientation with respect to the MT axis. For example, PFs in 13_3 MTs run parallel with the MT axis, whereas PFs in 14_3 MTs are slightly skewed to produce a super-helical structure [18]. This small difference could change a MTs propensity to produce a trail. Endwise-shrinking PFs in a super-helical arrangement could only shrink a finite distance before meeting the kinesin-coated surface, whereas straight PFs that are free from the kinesins surface would remain so.

Another unusual result is that trails and MTs depolymerise at similar rates to each other over a range of ADP concentrations and shrinkage rates. This reiterates that the stabilisation of the MT lattice is highly transmissive through lateral contacts. We thus propose that the PF shrinkage rate at any point in the MT depends on the ability of tipmost GDP-tubulin subunit to bend out of the lattice. If a tubulin heterodimer that is incorporated into the lattice has lateral neighbours that are in a straight and stable conformation, then it is unable to dissociate. At the tip of the trail, the rate at which tubulin can bend and dissociate from each PF tip corresponds to the local density and dissociation rate of kinesin. We propose that the same is true for the non-trail MT tip. That is, the stability of the non-trail part of the MT lattice is largely determined by how many kinesins are underlying.

The use of fluorescently labelled kinesin will be required in future work in order to assess the number of strong-state kinesins needed to stabilise a dynamic MT tip. Further insights to underlying mechanisms could also be obtained by imaging a kinesin-clamp with EM or AFM.

6.3.5 Why do trails form asymmetrically?

We found that trails form much more frequently at minus-ends than at plus-ends. The reason for this is unclear. MTs are intrinsically polarised and so are their interactions with kinesins. We discuss how this might contribute towards asymmetric trail formation

below.

Polarity of MT structure and dynamics

Lateral bonds in the MT lattice are clearly of high importance to MT dynamics. The breaking of these bonds allows GDP-PFs to splay outward, leading to inter-PF cracks propagating through the MT lattice during depolymerisation. A recent study has shown that mechanical strain can lead to crack propagation through the MT lattice [162].

The breaking of lateral bonds has long been proposed to be an asymmetric process with respect to MT ends, because it is thought that lateral α-α bonds are stronger than β-β bonds in B-lattice GDP-MTs [16]. The asymmetry of bond strengths was recently confirmed by molecular dynamics simulations [22]. Simulations are in good agreement with recent experimental results that investigate the relative stability of A- and B-lattice types [23].

Because the structure of the two ends is different, with α-α contacts outermost at the minus-end and peripheral β-β contacts at the plus-end, there is a potential structural basis for differences in MT stability at the two ends. GDP-MTs are less susceptible to catastrophe at the minus-end than the plus-end [75, 76], in agreement with the relative strengths of α-α and β-β bonds discussed above.

Polarity of kinesin-MT interactions

Our kinesin-clamp data suggests that MT plus- and minus-ends shrink similarly, as do minus-end trails. Plus-end trails shrink faster. The fact that the greatest difference is in the trails suggests that direct MT-kinesin interactions may contribute towards the polarity of trail formation.

Kinesin-induced conformational changes in MTs have been reported to span several microns [179]. This occurs in an asymmetric manner, demonstrated by subsequent binding of kinesins having a bias towards the plus-end [179]. Therefore, the stabilising

effect that kinesin confers to the MT lattice is likely to be asymmetric also.

Kinesin-1 has a greater propensity to detach if external forces pull in the direction of the plus-end than the minus-end [188]. Consequently, if kinesin does induce an elongated conformation in tubulin, the expansion of PFs in the kinesin clamp could give rise to complex binding patterns with a directional bias.

Either of these processes could contribute towards the trail formation bias towards the minus-end. MTs and kinesins are intrinsically polarised, so it is unsurprising that there is a distinct difference between the two ends. However, the mechanism of asymmetric trail formation is currently unclear.

6.3.6 Implications of the kinesin-clamp for MT dynamics

We showed that the whole MT displays enhanced stability when binding kinesins to 2-3 PFs on one side of the lattice. This demonstrates that there is a high degree of mutual stabilisation between PFs. It appears that, although intrinsically unstable, little energy is required to prevent the GDP-MT lattice from disassembling.

This has several implications for MT dynamics. Firstly, the GTP cap at growing MT tips is often considered to be a complete ring of GTP-tubulin. Indeed, statistical arguments based on experimental data suggest that a single layer of GTP-tubulin at the MT tip is both necessary and sufficient to protect a MT against catastrophes [45, 47]. Predictions from these studies are that a single exposed GDP-tubulin at the tip of a MT could initiate a catastrophe. Conversely, computational models suggest that this is not necessarily the case [32, 42]. Additionally, analysis of MT lifetimes suggests that MT catastrophe is a multi-step (estimated 3-step) process, possibly due to uncapping of several PFs [77, 78]. Our kinesin-clamp experiments show that terminal GDP-tubulin dimers can be retained in the MT lattice, in agreement with the latter reports.

Mutual PF-PF stabilisation also has implications for the dynamics of MTs in bundles. Kinesins can cross-link two MTs that are in close proximity of one another, thereby decorating one surface of each MT. In this way, bundles present a similar

geometry to the kinesin-clamp. Moreover, each MT will serve as a supportive splint for the other, inhibiting bending in a manner analogous to the coverslip. Our data suggest that binding kinesins to one side of the MT surface in this way could have a significant impact on shrinkage rates of MTs in bundles. One might speculate that MTs could be grown from intact PF templates off the side of MTs by the same mechanism.

6.4 Relevance of MT stabilisation by strong-state kinesins *in vivo*

As kinesins take steps, they cycle through multiple nucleotide states corresponding to both strong and weak MT-binding. Our results suggest that the strong-state kinesin inhibits MT shrinkage to a great extent, whereas weakly bound ADP-kinesin has little effect. Repeated cycling through weak binding modes could explain why, until recently, kinesin-1 was regarded to not influence MT dynamics. High concentrations of ATP are present in cells, allowing kinesins to continually cycle through both strong and weak binding states. So why are the MT-remodelling functions of strong-state kinesin relevant *in vivo*?

Kinesin motor domains are highly conserved, both in sequence and in structure (at least for structures that are currently solved), across the kinesin superfamily. In light of this, we discuss the implications of kinesin-regulated MT stability not just for kinesin-1 but also for other kinesin family members. Indeed, there is evidence to suggest that other strong-state kinesins can stabilise MTs [189].

Many factors can in principle influence the fraction of time that a particular kinesin spends in its strong states. The dwell times for the individual kinetic states of the MT-activated kinesin ATPase are sensitive to the species [134], post-translational modifications [190] and nucleotide states [191] of MTs. Furthermore, mechanical tension can increase the dwell time of kinesin in a nucleotide-free state [192]. Such forces naturally arise *in vivo* at kinetochores and MT bundles [110], cortical attachment sites [6], and through antagonistic motor activity on vesicles [193].

Over the following sections we discuss these mechanisms in greater detail.

6.4.1 End-binding modes

There is no evidence to suggest that kinesin-1 can sense when it has reached the tip of a MT. When it reaches the end, it simply walks off. The terminal tubulin dimer in a PF might become destabilised, and more prone to dissociate from the MT lattice, as the kinesin detaches. Therefore, in some circumstances the stepping frequency of kinesin-1 might become rate-limiting for MT depolymerisation.

In the absence of external forces, kinesin-1 can walk along ~100 tubulin dimers per second. This is 6 times faster than the shrinkage rate of MTs ($\sim 17\,\mathrm{dimer\,PF^{-1}\,s^{-1}}$). It is therefore unsurprising that low densities of walking kinesin-1 have been seen to have no influence on MT dynamics; kinesin residence time at the MT tip would be less than the lifetime of the tipmost GDP-tubulin dimer in a shrinking MT. However, at high concentrations of kinesin, the terminal binding sites on the MT lattice could become substantially occupied, potentially producing an effect. As we have shown, kinesin-mediated stabilisation is transmitted circumferentially through the MT lattice, such that stabilising one PF increases the stability of its lateral neighbour, as demonstrated by the kinesin-clamp experiments. Therefore, kinesin may only need to occupy a subset of the terminal tubulin dimers of a MT in order to maintain its structural integrity. Thus, kinesin concentrations at sub-saturating levels might still reduce MT shrinkage rates. Kinesin-clamp experiments using fluorescently labelled kinesin at low densities (or clustered on a micro-patterned surface) would be one way to investigate this possibility.

Some kinesins have the ability to sense the end of the MT. For example, CENP-E has a MT-binding domain that allows it to track MT plus-ends through phases of growth and shrinkage [194]. This increases the effective concentration of CENP-E at the MT tip. Other kinesins similarly dwell at MT ends, such as Kip2, Kip3, Eg5 and Kif15 [120, 123, 126, 127, 195, 196]. The tendency to linger at MT tips could enhance the ability for these proteins to affect MT stability. Indeed, several of them have been shown to influence MT dynamics [123, 126, 127, 195].

MT-binding regions of kinesins other than the motor domains can be responsible

for the increased residency at MT tips, as is the case for CENP-E [194]. However, a truncated kinesin-1 chimera with Eg5 motor domains has been shown to dwell at MT tips [127]. It has no known MT-binding regions except for the motor domains. Hence, the clearest explanation is that it stalls in a strong state when it reaches the MT tip. Notably, this chimera stabilises PF extensions at growing MT tips and accelerates MT polymerisation.

6.4.2 Crowding effects

In vivo, MTs become crowded as they interact with a plethora of MAPs and kinesins. Experimental data clearly demonstrate that stepping behaviour changes with kinesin density [197, 198]. When a motile kinesin has its path blocked, it dwells in a paused state, and if blocked for too long it may detach or transfer to a neighbouring PF [198]. An increased time spent in a paused state could amplify the stabilising ability of kinesin.

As the density of motile kinesin-1s on the MT lattice increases, kinesin velocity is largely unaffected but run lengths decrease [199]. The increased propensity for kinesin-1 to detach from the MT in crowded environments, and to walk straight off MT plus-ends, has in fact been proposed as a mechanism for avoiding traffic jams on MTs [195]. Therefore, the regulation of MT stability might be better suited to more processive kinesins. Conversely, transport kinesins (such as kinesin-1) move cargo by working in teams. Unsurprisingly, this dramatically increases run lengths [200, 201]. Thus, kinesin-1 may be a viable candidate for regulating MT dynamics *in vivo*.

Interestingly, the MT-end sensing ability of Kip3 (a kinesin-8) promotes crowding on the MT lattice [195]. Individual Kip3 molecules have no significant effect on MT stability [122]. Kip3 is highly processive so, unlike kinesin-1, it does not easily detach from MTs in the presence of roadblocks. The traffic progresses towards the MT tip, where Kip3s resist detachment. Kip3 congestion promotes MT disassembly, such that terminal motors are 'bumped off' the MT lattice, taking 2 tubulin dimers with them [122]. It is not clear whether the motors are physically pushed off the end of the MT;

it is possible that Kip3 induces allosteric changes in tubulin but must bind to adjacent dimers in the MT lattice to generate significant depolymerase activity. Kinesin-8 motor domains have in fact been reported to induce a degree of curvature in PFs [202].

Kip2 and Eg5 (a kinesin-5) both dwell at MT tips, presumably in a tight binding mode, and accelerate MT assembly [126, 127]. Eg5 is a tetrameric kinesin that cross-links and slides bundled MTs. Its processivity is greatly enhanced when bound to two MTs [203], so it may be that it is able to regulate MT dynamics differentially between regions of overlap. Kinesin-5s have been reported to influence MT dynamics but reports are mixed, from enhancing MT stabilisation to promoting disassembly [204, 205]. Recently, kinesin-5 was reported as a MT polymerase that stabilises PF extensions at growing MT tips [127]. Crowding dynamics may complicate the picture even further, as some kinesin-5s reverse their directionality at high densities [206].

6.4.3 Inhibition of ATPase activity

The rigor mutant (T93N) that we used in some of our experiments mimics the no-nucleotide state of the kinesin ATPase cycle. This was found to have the greatest effects on MT stability. A previous study injected T93N into live cells [144]. No changes in MT dynamics were reported, although the localisation of the protein was not identified and only MT growth rates (and not shrinkage) were reported. Therefore, it is hard at present to draw conclusions about the effect of T93N *in vivo*.

Interestingly, a Kip1 (kinesin-5) rigor mutant has been expressed *in vivo* [204]. Cells were not viable in the absence of wild-type protein. However, when both proteins were expressed, the rigor mutant was reported to stabilise MTs.

Recently, the crystal structure of the Kif14 (kinesin-14) motor domain was solved [189]. Surprisingly, it adopts a 'rigor-like' conformation when bound to ADP, with a conformation that is complementary to straight tubulin (MTs). Remarkably, although ADP was found to be in the nucleotide-binding pocket, Mg^{2+} was not. Disruption of Mg^{2+} coordination is in fact the primary consequence of the aforementioned T93N mutation [207]. Complementary to our results for T93N-bound MTs, Kif14 was shown

to inhibit MT shrinkage.

Vik1 and Cik1 are both derived from motor proteins but do not have a nucleotide-binding pocket. They both bind tightly to the MT lattice and form heterodimers with the kinesin Kar3 [177]. The non-motile counterparts are necessary for directional processive movement [208]. Although slight depolymerase activity has been reported for these heterodimers, they apparently stabilise MTs when crowded [177].

Another mechanism for inhibiting conformational changes associated with ATPase activity is with regulatory cofactors. Transport of mitochondria in axons is regulated by syntaphilin-kinesin-1 interactions [209]. Syntaphilin is a protein found to bind to kinesin-1 in axons. The syntaphilin-kinesin-1 complex shows little ATPase activity and binds to MTs. The authors propose a model whereby syntaphilin locks kinesin to the MT but prevents it from walking.

Dynein and kinesin share the same binding site on tubulin [210], so we must consider the possibility of dynein having similar MT-stabilising capabilities to kinesin. Dynein has been shown to affect MT dynamics both *in vivo* [211] and *in vitro* [6, 212]. It has been shown that Lis1 binds to dynein and acts as a 'clutch', allowing futile hydrolysis whilst retaining the MT-binding domain in a tight binding mode [213]. Interestingly, dynein-coated beads can inhibit MT depolymerisation in an ATP-dependent manner when retained at the plus-end with an optical trap [6]. The authors propose that the stabilising effect is due to tension generated by the dynein. An alternative explanation could be the stabilisation of MTs by dynein corresponds to a tight binding state. Dynein 'changes gear' as forces increase, improving the coordination between its steps [214]. This capability is also highly dependent on the availability of ATP.

6.4.4 External forces

As a transport motor, kinesin-1 naturally experiences external forces *in vivo* as it hauls cargo throughout the cell. Such forces have been shown to reduce ADP binding to kinesin heads [215]. Therefore, as resistive forces increase, kinesins are less likely

to enter a weak-binding state. Indeed, at high forces kinesin-1 spends considerably more time in a tightly bound state [192]. *In vivo*, cargo is frequently transported by both kinesin and dynein, which contribute opposing forces, potentially amplifying this effect [216]. However, the extent to which this 'tug-of-war' occurs is currently unclear [217]. We speculate that by entering the tightly bound state when under load, kinesins could have enhanced MT stabilising capabilities when transporting cargo, so that tension might increase the dwell time of kinesin-cargo complexes at MT tips and thereby enhance their influence on tip stability.

6.4.5 Specific kinesin-MT interactions

The kinesin ATPase cycle is highly dependent upon specific interactions with the MT lattice. It has been shown that depending on the precise combination of kinesin and tubulin species, ATPase rates vary dramatically [134]. Moreover, kinesin-1 has a higher tendency to bind to GTP-MTs than GDP-MTs [170], accompanied by an increase in ATPase activity [191].

Given that we have shown kinesin-1 to increase MT stability, it is clear that the mechanochemical cycles of kinesins and MTs are tightly coupled. Weak or tight binding modes of kinesin, and subsequent inhibition of depolymerisation, may therefore be fine-tuned by modifications in either tubulin or kinesin.

Kinesins have been shown to walk along specific subsets of MTs *in vivo* [218, 219]. The localisation correlates with post-translational modifications (PTMs) in tubulin. Indeed, tubulin PTMs have significant effects on the kinesin ATPase cycle [190]. Tubulin PTMs affect the recruitment of kinesins and MAPs to the MT lattice, and also modify the dynamical and mechanical properties of MTs [220]. PTMs may therefore have diverse consequences for the stabilisation of MTs by strong-state kinesins.

The MTs used to acquire the data presented in this thesis undoubtedly host a wide variety of PTMs. It would be interesting to examine how MTs with distinct PTMs would be affected by strong-state kinesin. We would predict that MTs with a greater affinity for kinesins, or those with modifications that reduce the stepping rate

of kinesins (e.g. a cleaved C-terminal tail on the β-subunit [190]), would be stabilised more effectively.

Recently published high-resolution structures of EB-MT complexes have suggested that the conformational changes that EB induces in the MT lattice can accelerate hydrolysis in GTP-tubulin [62]. Moreover, EB proteins, in addition to several other MAPs, have been shown to regulate the number of PFs in the MT lattice [13, 14, 43, 62, 87, 221]. It would be interesting to see if MTs polymerised in the presence of kinesin could be similarly affected, as our work suggests that kinesin induces conformational changes in tubulin.

6.5 Conclusions

We have shown that strong-state kinesin-1 is a highly effective inhibitor of GDP-MT shrinkage. We propose that an allosteric mechanism underlies this effect, whereby kinesin-1 stabilises a shrinkage resistant conformation of tubulin.

The density of strong-state kinesin required to stabilise the MT is currently unclear. Key experiments for future work should involve the use of fluorescently labelled T93N, such that the number of kinesins on the MT can be determined precisely. Moreover, we predict that strong-state kinesins could serve as effective rescue factors. Reconstituting MT dynamics in the presence of GFP-T93N would be an good way to test this hypothesis. Furthermore, a recent model has suggested that the most efficient route to accelerating MT polymerisation is to inhibit tubulin dissociation from MT tips [161]. We have shown that T93N is an effective MT stabiliser, so assessing MT growth rates in the presence of T93N could also provide a means to test this model.

To compliment the data presented in this thesis, an obvious experiment for future work is to characterise the influence of motile kinesins on MT dynamics. Although this has been studied previously and no effects were found, the authors were specifically looking for conditions in which dynamics are not affected [145]. These experiments should be repeated with varying concentrations of kinesin, and at varying nucleotide concentrations.

Our results suggest that kinesin structurally modifies MTs. We find that kinesin-1 can both recognise and induce conformational changes in the MT lattice, as demonstrated by the bending MTs we observe in the tubulin depletion experiments. Interestingly, we found that the kinesin-stabilised bending of MTs only occurs for a small range of kinesin concentrations. At high kinesin concentrations, MTs adopt a straighter conformation and appear to be much more flexible.

A quantitative analysis of MT bending has not been carried out because, due to the depth of our flow chambers and the imaging technique used, our data is unsuitable for analysis by traditional means [222, 223]. Moreover, the lack of automated microfluidics in our experimental setup means that the forces exerted on MTs during the flow-through stage of the experiment will vary from sample to sample. Small modifications to the experimental setup, or alternatively the use of an optical trap [224], would enable the mechanics of kinesin-bound MTs to be characterised. This should be a priority in future experiments, as it has large implications for the interpretation of our results. Furthermore, modifying the mechanics of MTs has clear significance for the roles of kinesins *in vivo*.

Considerations of MT mechanics as well as chemical kinetics are clearly necessary to capture the essence of MT dynamic instability [32, 42, 71]. Our data, and the work of others [62, 223], suggest that MAPs and kinesins could influence both mechanical and chemical kinetic aspects of MT dynamics. It would be interesting to see whether, like the conformational changes induced by EB proteins, kinesins have the ability to modify the structure of MTs or even affect the rate of GTP hydrolysis.

We have found that kinesin-1 affects MT stability differently as it progresses through the mechanochemical stepping cycle. This process could be regulated in many ways *in vivo*, suggesting that kinesin-1, and potentially other kinesins, will have different effects on MT dynamics depending on the detailed patterns of motors stepping and of forces deriving from the local physical environment at the MT tip.

It is of great interest to see how other kinesins influence MT dynamics as they progress through the kinetic states of the ATPase cycle. Kinesin family members have distinct cycles, respond differently to external loads and crowding effects and

show different characteristics in regions of MT overlap. Therefore, by the arguments presented in this thesis, the functionality of kinesins could be even more diverse than previously anticipated. The possibilities are legion.

Bibliography

[1] T J Mitchison and E D Salmon. Mitosis: a history of division. *Nature Cell Biology*, 3(1):E17–E21, January 2001.

[2] Timothy J Mitchison and Marc W Kirschner. Dynamic instability of microtubule growth. *Nature*, 312:237–242, November 1984.

[3] Marileen Dogterom, Jacob WJ Kerssemakers, Guillaume Romet-Lemonne, and Marcel E Janson. Force generation by dynamic microtubules. *Current Opinion in Cell Biology*, 17(1):67–74, February 2005.

[4] Alexey Khodjakov and Tarun Kapoor. Microtubule Flux: What Is It Good for? *Current Biology*, 15(23):R966–R968, December 2005.

[5] J Richard McIntosh, Ekaterina L Grishchuk, Mary K Morphew, Artem K Efremov, Kirill Zhudenkov, Vladimir A Volkov, Iain M Cheeseman, Arshad Desai, David N Mastronarde, and Fazly I Ataullakhanov. Fibrils connect microtubule tips with kinetochores: a mechanism to couple tubulin dynamics to chromosome motion. *Cell*, 135(2):322–333, October 2008.

[6] Adam G Hendricks, Jacob E Lazarus, Eran Perlson, Melissa K Gardner, David J Odde, Yale E Goldman, and Erika L F Holzbaur. Dynein Tethers and Stabilizes Dynamic Microtubule Plus Ends. *Current Biology*, 22(7):632–637, April 2012.

[7] Miho Katsuki, Douglas R Drummond, Michael Osei, and Robert A Cross. Mal3 masks catastrophe events in Schizosaccharomyces pombe microtubules by inhibiting shrinkage and promoting rescue. *Journal of Biological Chemistry*, 284(43):29246–29250, October 2009.

[8] L G Tilney, J Bryan, D J Bush, K Fujiwara, M S Mooseker, D B Murphy, and D H Snyder. Microtubules: evidence for 13 protofilaments. *Journal of Cell Biology*, 59(2 Pt 1):267–275, November 1973.

[9] E M Mandelkow. On the surface lattice of microtubules: helix starts, protofilament number, seam, and handedness. *The Journal of Cell Biology*, 102(3):1067–1073, March 1986.

[10] F Beuron and A Hoenger. Structural analysis of the microtubule-kinesin complex by cryo-electron microscopy. *Methods in molecular biology (Clifton, N.J.)*, 164(Chapter 20):235–254, 2001.

[11] A A Hyman. Structural changes accompanying GTP hydrolysis in microtubules: information from a slowly hydrolyzable analogue guanylyl-(alpha,beta)- methylene-diphosphonate. *The Journal of Cell Biology*, 128(1):117–125, January 1995.

[12] Isabelle Arnal and Richard H Wade. How does taxol stabilize microtubules? *Current Biology*, 5(8):900–908, August 1995.

[13] M C Choi, U Raviv, H P Miller, M R Gaylord, E Kiris, D Ventimiglia, D J Needleman, M W Kim, L Wilson, S C Feinstein, and C R Safinya. Human microtubule-associated-protein tau regulates the number of protofilaments in microtubules: a synchrotron x-ray scattering study. *Biophysical Journal*, 97(2):519–527, July 2009.

[14] Amédée des Georges, Miho Katsuki, Douglas R Drummond, Michael Osei, Robert A Cross, and Linda A Amos. Mal3, the Schizosaccharomyces pombe homolog of EB1, changes the microtubule lattice. *Nature Structural & Molecular Biology*, 15(10):1102–1108, September 2008.

[15] D Chrétien. Lattice defects in microtubules: protofilament numbers vary within individual microtubules. *The Journal of Cell Biology*, 117(5):1031–1040, June 1992.

[16] Eva Nogales, Michael Whittaker, Ronald A Milligan, and Kenneth H Downing. High-Resolution Model of the Microtubule. *Cell*, 96(1):79–88, January 1999.

[17] Denis Chrétien and Stephen D Fuller. Microtubules switch occasionally into unfavorable configurations during elongation. *Journal of Molecular Biology*, 298(4):663–676, May 2000.

[18] R H Wade, D Chrétien, and D Job. Characterization of microtubule protofilament numbers: How does the surface lattice accommodate? *Journal of Molecular Biology*, 212(4):775–786, April 1990.

[19] D Chrétien, S D Fuller, and E Karsenti. Structure of growing microtubule ends: two-dimensional sheets close into tubes at variable rates. *Journal of Cell Biology*, 129(5):1311–1328, June 1995.

[20] David Sept, Nathan A Baker, and J Andrew McCammon. The physical basis of microtubule structure and stability. *Protein Science*, 12(10):2257–2261, October 2003.

[21] Haixin Sui and Kenneth H Downing. Structural basis of interprotofilament interaction and lateral deformation of microtubules. *Structure*, 18(8):1022–1031, August 2010.

[22] Ahmed T Ayoub, Mariusz Klobukowski, and Jack A Tuszynski. Detailed Per-residue Energetic Analysis Explains the Driving Force for Microtubule Disassembly. *PLoS computational biology*, 11(6):e1004313, June 2015.

[23] Miho Katsuki, Douglas R Drummond, and Robert A Cross. Ectopic A-lattice seams destabilize microtubules. *Nature Communications*, 5:3094, January 2014.

[24] J R Simon and E D Salmon. The structure of microtubule ends during the elongation and shortening phases of dynamic instability examined by negative-stain electron microscopy. *Journal of Cell Science*, 96 (Pt 4):571–582, August 1990.

[25] J F Díaz and J M Andreu. Assembly of purified GDP-tubulin into microtubules induced by taxol and taxotere: reversibility, ligand stoichiometry, and competition. *Biochemistry*, 32(11):2747–2755, March 1993.

[26] M F Carlier and D Pantaloni. Kinetic analysis of cooperativity in tubulin polymerization in the presence of guanosine di- or triphosphate nucleotides. *Biochemistry*, 17(10):1908–1915, May 1978.

[27] J Löwe, H Li, K H Downing, and E Nogales. Refined Structure of $\alpha\beta$-Tubulin at 3.5 Å Resolution. *Journal of Molecular Biology*, 313:1045–1057, 2001.

[28] E Nogales, S G Wolf, and K H Downing. Structure of the alpha beta tubulin dimer by electron crystallography. *Nature*, 391(6663):199–203, January 1998.

[29] Henry T HT Schek, Melissa K MK Gardner, Jun J Cheng, David J DJ Odde, and Alan J AJ Hunt. Microtubule Assembly Dynamics at the Nanoscale. *Current Biology*, 17(17):11–11, September 2007.

[30] Julien Mozziconacci, Linda Sandblad, Malte Wachsmuth, Damian Brunner, and Eric Karsenti. Tubulin dimers oligomerize before their incorporation into microtubules. *PLoS ONE*, 3(11):e3821, 2008.

[31] Eva Nogales, Kenneth H Downing, Linda A Amos, and Jan L we. Tubulin and FtsZ form a distinct family of GTPases. *Nature Structural & Molecular Biology*, 5(6):451–458, June 1998.

[32] G Margolin, I V Gregoretti, T M Cickovski, C Li, W Shi, M S Alber, and H V Goodson. The mechanisms of microtubule catastrophe and rescue: implications from analysis of a dimer-scale computational model. *Molecular biology of the cell*, 23(4):642–656, February 2012.

[33] M W Kirschner, R C Williams, M Weingarten, and J C Gerhart. Microtubules from mammalian brain: some properties of their depolymerization products and a proposed mechanism of assembly and disassembly. *PNAS*, 71(4):1159–1163, April 1974.

[34] E M Mandelkow and E Mandelkow. Unstained microtubules studied by cryo-electron microscopy. Substructure, supertwist and disassembly. *Journal of Molecular Biology*, 181(1):123–135, January 1985.

[35] E M Mandelkow, E Mandelkow, and R A Milligan. Microtubule dynamics and microtubule caps: a time-resolved cryo-electron microscopy study. *Journal of Cell Biology*, 114(5):977–991, September 1991.

[36] Thomas Müller-Reichert, Denis Chrétien, Fedor Severin, and Anthony A Hyman. Structural changes at microtubule ends accompanying GTP hydrolysis: information from a slowly hydrolyzable analogue of GTP, guanylyl (alpha,beta)methylenediphosphonate. *PNAS*, 95(7):3661–3666, March 1998.

[37] T Horio and H Hotani. Visualization of the dynamic instability of individual microtubules by dark-field microscopy. *Nature*, 321(6070):605–607, June 1986.

[38] K W Farrell, M A Jordan, H P Miller, and L Wilson. Phase dynamics at microtubule ends: the coexistence of microtubule length changes and treadmilling. *The Journal of Cell Biology*, 104(4):1035–1046, April 1987.

[39] R A Walker, E T O'Brien, N K Pryer, M F Soboeiro, W A Voter, H P Erickson, and E D Salmon. Dynamic instability of individual microtubules analyzed by video

light microscopy: rate constants and transition frequencies. *Journal of Cell Biology*, 107(4):1437–1448, October 1988.

[40] H W Detrich, M A Jordan, L Wilson, and R C Williams. Mechanism of microtubule assembly. Changes in polymer structure and organization during assembly of sea urchin egg tubulin. *Journal of Biological Chemistry*, 260(16):9479–9490, August 1985.

[41] H P Erickson. Microtubule surface lattice and subunit structure and observations on reassembly. *Journal of Cell Biology*, 60(1):153–167, January 1974.

[42] Vincent VanBuren, Lynne Cassimeris, and David J Odde. Mechanochemical Model of Microtubule Structure and Self-Assembly Kinetics. *Biophysical journal*, 89(5):16–16, November 2005.

[43] Benjamin Vitre, Frédéric M Coquelle, Claire Heichette, Cyrille Garnier, Denis Chrétien, and Isabelle Arnal. EB1 regulates microtubule dynamics and tubulin sheet closure in vitro. *Nature Cell Biology*, 10(4):415–421, April 2008.

[44] Courtney E Coombes, Ami Yamamoto, Madeline R Kenzie, David J Odde, and Melissa K Gardner. Evolving Tip Structures Can Explain Age-Dependent Microtubule Catastrophe. *Current biology*, 23:1–7, July 2013.

[45] D N Drechsel and M W Kirschner. The minimum GTP cap required to stabilize microtubules. *Current Biology*, 4(12):1053–1061, December 1994.

[46] Dulal Panda, Herbert P Miller, and Leslie Wilson. Determination of the Size and Chemical Nature of the Stabilizing "Cap" at Microtubule Ends Using Modulators of Polymerization Dynamics. *Biochemistry*, 41:1609–1617, January 2002.

[47] M Caplow and J Shanks. Evidence that a single monolayer tubulin-GTP cap is both necessary and sufficient to stabilize microtubules. *Molecular biology of the cell*, 7(4):663–675, April 1996.

[48] R A Walker. Dilution of individual microtubules observed in real time in vitro: evidence that cap size is small and independent of elongation rate. *The Journal of Cell Biology*, 114(1):73–81, July 1991.

[49] A Dimitrov, M Quesnoit, S Moutel, I Cantaloube, C Poüs, and F Perez. Detection of GTP-tubulin conformation in vivo reveals a role for GTP remnants in microtubule rescues. *Science*, 322(5906):1353–1356, 2008.

[50] Dominique Seetapun, Brian T Castle, Alistair J McIntyre, Phong T Tran, and David J Odde. Estimating the microtubule GTP cap size in vivo. *Current biology*, 22(18):1681–1687, September 2012.

[51] Luke M Rice, Elizabeth A Montabana, and David A Agard. The lattice as allosteric effector: structural studies of alphabeta- and gamma-tubulin clarify the role of GTP in microtubule assembly. *Proceedings of the National Academy of Sciences of the United States of America*, 105(14):5378–5383, April 2008.

[52] Raimond B G Ravelli, Benoît Gigant, Patrick A Curmi, Isabelle Jourdain, Sylvie Lachkar, André Sobel, and Marcel Knossow. Insight into tubulin regulation from a complex with colchicine and a stathmin-like domain. *Nature*, 428(6979):198–202, March 2004.

[53] Agata Nawrotek, Marcel Knossow, and Benoît Gigant. The determinants that govern microtubule assembly from the atomic structure of GTP-tubulin. *Journal of Molecular Biology*, 412(1):35–42, September 2011.

[54] Gary J Brouhard and Luke M Rice. The contribution of $\alpha\beta$-tubulin curvature to microtubule dynamics. *The Journal of Cell Biology*, 207(3):323–334, November 2014.

[55] Andrea Grafmüller and Gregory A Voth. Intrinsic Bending of Microtubule Protofilaments. *Structure*, 19(3):409–417, March 2011.

[56] Eric Quiniou, Paul Guichard, David Perahia, Sergio Marco, and Liliane Mouawad. An Atomistic View of Microtubule Stabilization by GTP. *Structure*, 21(5):833–843, May 2013.

[57] Joseph R André, Marie-Jeanne Clément, Elisabeth Adjadj, Flavio Toma, Patrick A Curmi, and Philippe Manivet. The state of the guanosine nucleotide allosterically affects the interfaces of tubulin in protofilament. *Journal of computer-aided molecular design*, 26(4):397–407, April 2012.

[58] Andrea Grafmüller, Eva G Noya, and Gregory A Voth. Nucleotide-Dependent Lateral and Longitudinal Interactions in Microtubules. *Journal of Molecular Biology*, 425(12):2232–2246, June 2013.

[59] Odile Valiron, Isabelle Arnal, Nicolas Caudron, and Didier Job. GDP-tubulin incorporation into growing microtubules modulates polymer stability. *Journal of Biological Chemistry*, 285(23):17507–17513, June 2010.

[60] Melissa J Bennett, John K Chik, Gordon W Slysz, Tyler Luchko, Jack Tuszynski, Dan L Sackett, and David C Schriemer. Structural Mass Spectrometry of the $\alpha\beta$-Tubulin Dimer Supports a Revised Model of Microtubule Assembly. *Biochemistry*, 48(22):4858–4870, June 2009.

[61] Gregory M Alushin, Gabriel C Lander, Elizabeth H Kellogg, Rui Zhang, David Baker, and Eva Nogales. High-Resolution Microtubule Structures Reveal the Structural Transitions in $\alpha\beta$-Tubulin upon GTP Hydrolysis. *Cell*, 157(5):1117–1129, May 2014.

[62] Rui Zhang, Gregory M Alushin, Alan Brown, and Eva Nogales. Mechanistic Origin of Microtubule Dynamic Instability and Its Modulation by EB Proteins. *Cell*, 162:1–11, July 2015.

[63] Zhanghan Wu, Hong-Wei Wang, Weihua Mu, Zhongcan Ouyang, Eva Nogales, and Jianhua Xing. Simulations of Tubulin Sheet Polymers as Possible Structural Intermediates in Microtubule Assembly. *PLoS ONE*, 4(10):e7291, October 2009.

[64] Zhanghan Wu, Eva Nogales, and Jianhua Xing. Comparative Studies of Microtubule Mechanics with Two Competing Models Suggest Functional Roles of Alternative Tubulin Lateral Interactions. *Biophysical journal*, 102(12):2687–2696, June 2012.

[65] Hong-Wei Wang and Eva Nogales. Nucleotide-dependent bending flexibility of tubulin regulates microtubule assembly. *Nature*, 435(7044):911–915, June 2005.

[66] Iwan A T Schaap, Carolina Carrasco, Pedro J de Pablo, Frederick C MacKintosh, and Christoph F Schmidt. Elastic response, buckling, and instability of microtubules under radial indentation. *Biophysical journal*, 91(4):1521–1531, August 2006.

[67] Hiroaki Yajima, Toshihiko Ogura, Ryo Nitta, Yasushi Okada, Chikara Sato, and Nobutaka Hirokawa. Conformational changes in tubulin in GMPCPP and GDP-taxol microtubules observed by cryoelectron microscopy. *The Journal of Cell Biology*, 198(3):315–322, August 2012.

[68] Hugo Bowne-Anderson, Marija Zanic, Monika Kauer, and Jonathon Howard. Microtubule dynamic instability: A new model with coupled GTP hydrolysis and multistep catastrophe. *BioEssays*, 35(5):452–461, March 2013.

[69] H Flyvbjerg, TE Holy, and S Leibler. Stochastic dynamics of microtubules: A model for caps and catastrophes. *Physical review letters*, 73(17):2372–2375, October 1994.

[70] Henrik Flyvbjerg, Timothy Holy, and Stanislas Leibler. Microtubule dynamics: Caps, catastrophes, and coupled hydrolysis. *Physical Review E*, 54(5):5538–5560, November 1996.

[71] Vincent V VanBuren, David J DJ Odde, and Lynne L Cassimeris. Estimates of lateral and longitudinal bond energies within the microtubule lattice. *PNAS*, 99(9):6035–6040, April 2002.

[72] M Caplow, R L Ruhlen, and J Shanks. The free energy for hydrolysis of a microtubule-bound nucleotide triphosphate is near zero: all of the free energy for hydrolysis is stored in the microtubule lattice. *The Journal of Cell Biology*, 127(3):779–788, November 1994.

[73] Ekaterina L Grishchuk, Maxim I Molodtsov, Fazly I Ataullakhanov, and J Richard McIntosh. Force production by disassembling microtubules. *Nature*, 438(7066):384–388, November 2005.

[74] Hao Yuan Kueh and Timothy J Mitchison. Structural plasticity in actin and tubulin polymer dynamics. *Science*, 325(5943):960–963, August 2009.

[75] P T Tran, P Joshi, and E D Salmon. How Tubulin Subunits Are Lost from the Shortening Ends of Microtubules. *Journal of Structural Biology*, 118(2):12–12, March 1997.

[76] R A Walker, S Inoué, and E D Salmon. Asymmetric behavior of severed microtubule ends after ultraviolet-microbeam irradiation of individual microtubules in vitro. *Journal of Cell Biology*, 108(3):931–937, March 1989.

[77] D J Odde, L Cassimeris, and H M Buettner. Kinetics of microtubule catastrophe assessed by probabilistic analysis. *Biophysical Journal*, 69(3):796–802, September 1995.

[78] Melissa K Gardner, Marija Zanic, Christopher Gell, Volker Bormuth, and Jonathon Howard. Depolymerizing Kinesins Kip3 and MCAK Shape Cellular Microtubule Architecture by Differential Control of Catastrophe. *Cell*, 147(5):1092–1103, November 2011.

[79] L Cassimeris, N K Pryer, and E D Salmon. Real-time observations of microtubule dynamic instability in living cells. *Journal of Cell Biology*, 107(6 Pt 1):2223–2231, December 1988.

[80] A Desai and T J Mitchison. Microtubule polymerization dynamics. *Annual Review of Cell and Developmental Biology*, 13:83–117, 1997.

[81] Hugo Bowne-Anderson, Anneke Hibbel, and Jonathon Howard. Regulation of Microtubule Growth and Catastrophe: Unifying Theory and Experiment. *Trends in Cell Biology*, 25(12):769–779, October 2015.

[82] A Akhmanova and M O Steinmetz. Microtubule +TIPs at a glance. *Journal of Cell Science*, 123(20):3415–3419, October 2010.

[83] Anna Akhmanova and Michel O Steinmetz. Tracking the ends: a dynamic protein network controls the fate of microtubule tips. *Nature reviews*, 9(4):309–322, March 2008.

[84] Niels Galjart. Plus-End-Tracking Proteins and Their Interactions at Microtubule Ends. *Current Biology*, 20(12):R528–R537, June 2010.

[85] Anna Akhmanova and Casper C Hoogenraad. Microtubule minus-end-targeting proteins. *Current biology*, 25(4):R162–R171, February 2015.

[86] Peter Bieling, Liedewij Laan, Henry Schek, E Laura Munteanu, Linda Sandblad, Marileen Dogterom, Damian Brunner, and Thomas Surrey. Reconstitution of a microtubule plus-end tracking system in vitro. *Nature*, 450(7172):1100–1105, December 2007.

[87] Sebastian P Maurer, Franck J Fourniol, Gergő Bohner, Carolyn A Moores, and Thomas Surrey. EBs Recognize a Nucleotide-Dependent Structural Cap at Growing Microtubule Ends. 149(2):371–382, April 2012.

[88] Sebastian P Maurer, Peter Bieling, Julia Cope, Andreas Hoenger, and Thomas Surrey. GTPγS microtubules mimic the growing microtubule end structure recognized by end-binding proteins (EBs). *Proceedings of the National Academy of Sciences of the United States of America*, 108(10):3988–3993, March 2011.

[89] Marija Zanic, Jeffrey H Stear, Anthony A Hyman, and Jonathon Howard. EB1 recognizes the nucleotide state of tubulin in the microtubule lattice. *PLoS ONE*, 4(10):e7585, 2009.

[90] Marija Zanic, Per O Widlund, Anthony A Hyman, and Jonathon Howard. Synergy between XMAP215 and EB1 increases microtubule growth rates to physiological levels. *Nature Cell Biology*, 15(6):688–693, June 2013.

[91] Sebastian P Maurer, Nicholas I Cade, Gergő Bohner, Nils Gustafsson, Emmanuel Boutant, and Thomas Surrey. EB1 accelerates two conformational transitions important for microtubule maturation and dynamics. *Current biology*, 24(4):372–384, February 2014.

[92] Ashley D Grimaldi, Takahisa Maki, Benjamin P Fitton, Daniel Roth, Dmitry Yampolsky, Michael W Davidson, Tatyana Svitkina, Anne Straube, Ikuko Hayashi, and Irina Kaverina. CLASPs are required for proper microtubule localization of end-binding proteins. *Developmental cell*, 30(3):343–352, August 2014.

[93] David Gard and Marc W Kirschner. A Microtubule-associated Protein from Xenopus Eggs That Specifically Promotes Assembly at the Plus-End. *The Journal of Cell Biology*, 105:2203–2215, November 1987.

[94] Gary J Brouhard, Jeffrey H Stear, Tim L Noetzel, Jawdat Al-Bassam, Kazuhisa Kinoshita, Stephen C Harrison, Jonathon Howard, and Anthony A Hyman. XMAP215 is a processive microtubule polymerase. *Cell*, 132(1):79–88, January 2008.

[95] Iva Kronja, Anamarija Kruljac-Letunic, Maïwen Caudron-Herger, Peter Bieling, and Eric Karsenti. XMAP215-EB1 interaction is required for proper spindle assembly and chromosome segregation in Xenopus egg extract. *Molecular biology of the cell*, 20(11):2684–2696, June 2009.

[96] Michal Wieczorek, Sami Chaaban, and Gary J Brouhard. Macromolecular Crowding Pushes Catalyzed Microtubule Growth to Near the Theoretical Limit. *Cellular and Molecular Bioengineering*, 6(4):383–392, 2013.

[97] W A Voter and H P Erickson. The kinetics of microtubule assembly. Evidence for a two-stage nucleation mechanism. *Journal of Biological Chemistry*, 259(16):10430–10438, August 1984.

[98] Sabine Petry, Aaron C Groen, Keisuke Ishihara, Timothy J Mitchison, and Ronald D Vale. Branching microtubule nucleation in Xenopus egg extracts mediated by augmin and TPX2. *Cell*, 152(4):768–777, February 2013.

[99] Jacopo Scrofani, Teresa Sardon, Sylvain Meunier, and Isabelle Vernos. Microtubule nucleation in mitosis by a RanGTP-dependent protein complex. *Current biology*, 25(2):131–140, January 2015.

[100] Y Zheng, M L Wong, B Alberts, and T Mitchison. Nucleation of microtubule assembly by a gamma-tubulin-containing ring complex. *Nature*, 378(6557):578–583, December 1995.

[101] Justin M Kollman, Andreas Merdes, Lionel Mourey, and David A Agard. Microtubule nucleation by γ-tubulin complexes. *Nature Reviews Molecular Cell Biology*, 12(11):709–721, November 2011.

[102] Justin M Kollman, Charles H Greenberg, Sam Li, Michelle Moritz, Alex Zelter, Kimberly K Fong, Jose-Jesus Fernandez, Andrej Sali, John Kilmartin, Trisha N Davis, and David A Agard. Ring closure activates yeast γTuRC for species-specific microtubule nucleation. *Nature Structural & Molecular Biology*, 22(2):132–137, February 2015.

[103] Michal Wieczorek, Susanne Bechstedt, Sami Chaaban, and Gary J Brouhard. Microtubule-associated proteins control the kinetics of microtubule nucleation. *Nature Cell Biology*, 17(7):907–916, July 2015.

[104] Gary J Brouhard. Dynamic instability 30 years later: complexities in microtubule growth and catastrophe. *Molecular biology of the cell*, 26(7):1207–1210, April 2015.

[105] Jawdat Al-Bassam and Fred Chang. Regulation of microtubule dynamics by TOG-domain proteins XMAP215/Dis1 and CLASP. *Trends in Cell Biology*, 21(10):604–614, October 2011.

[106] Susanne Bechstedt, Kevan Lu, and Gary J Brouhard. Doublecortin recognizes the longitudinal curvature of the microtubule end and lattice. *Current biology*, 24(20):2366–2375, October 2014.

[107] Gregory M Alushin, Vincent H Ramey, Sebastiano Pasqualato, David A Ball, Nikolaus Grigorieff, Andrea Musacchio, and Eva Nogales. The Ndc80 kinetochore complex forms oligomeric arrays along microtubules. *Nature*, 467(7317):805–810, October 2010.

[108] Maria Alba Abad, Bethan Medina, Anna Santamaria, Juan Zou, Carla Plasberg-Hill, Arumugam Madhumalar, Uma Jayachandran, Patrick Marc Redli, Juri Rappsilber, Erich A Nigg, and A Arockia Jeyaprakash. Structural basis for microtubule recognition by the human kinetochore Ska complex. *Nature Communications*, 5:2964, 2014.

[109] Harukata Miki, Yasushi Okada, and Nobutaka Hirokawa. Analysis of the kinesin superfamily: insights into structure and function. *Trends in Cell Biology*, 15(9):467–476, September 2005.

[110] Robert A Cross and Andrew McAinsh. Prime movers: the mechanochemistry of mitotic kinesins. *Nature Reviews Molecular Cell Biology*, 15(4):257–271, April 2014.

[111] C J Lawrence. A standardized kinesin nomenclature. *The Journal of Cell Biology*, 167(1):19–22, October 2004.

[112] Toshihide Nariko Yuko Kimura Arimura Fukata, Hiroyasu Watanabe, Akihiro Iwamatsu, and Kozo Kaibuchi. Tubulin and CRMP-2 complex is transported via Kinesin-1. *Journal of Neurochemistry*, 93(6):1371–1382, June 2005.

[113] Vanessa Daire, Julien Giustiniani, Ingrid Leroy-Gori, Mélanie Quesnoit, Stéphanie Drevensek, Ariane Dimitrov, Franck Perez, and Christian Poüs. Kinesin-1 regulates microtubule dynamics via a c-Jun N-terminal kinase-dependent mechanism. *Journal of Biological Chemistry*, 284(46):31992–32001, November 2009.

[114] Claire T Friel and Jonathon Howard. The kinesin-13 MCAK has an unconventional ATPase cycle adapted for microtubule depolymerization. *The EMBO Journal*, 30(19):3928–3939, August 2011.

[115] Ana B Asenjo, Chandrima Chatterjee, Dongyan Tan, Vania DePaoli, William J Rice, Ruben Diaz-Avalos, Mariena Silvestry, and Hernando Sosa. Structural model for tubulin recognition and deformation by kinesin-13 microtubule depolymerases. *Cell reports*, 3(3):759–768, March 2013.

[116] Bill Wickstead, Keith Gull, and Thomas A Richards. Patterns of kinesin evolution reveal a complex ancestral eukaryote with a multifunctional cytoskeleton. *BMC evolutionary biology*, 10(1):110, 2010.

[117] F Kozielski, S Sack, A Marx, M Thormählen, E Schönbrunn, V Biou, A Thompson, E M Mandelkow, and E Mandelkow. The crystal structure of dimeric kinesin and implications for microtubule-dependent motility. *Cell*, 91(7):985–994, December 1997.

[118] Kristen J Verhey and Jennetta W Hammond. Traffic control: regulation of kinesin motors. *Nature Reviews Molecular Cell Biology*, 10(11):765–777, November 2009.

[119] Douglas R Drummond. Regulation of microtubule dynamics by kinesins. *Seminars in Cell and Developmental Biology*, 22(9):927–934, December 2011.

[120] Lukas C Kapitein, Erwin J G Peterman, Benjamin H Kwok, Jeffrey H Kim, Tarun M Kapoor, and Christoph F Schmidt. The bipolar mitotic kinesin Eg5 moves on both microtubules that it crosslinks. *Nature*, 435(7038):114–118, May 2005.

[121] Marvin E Tanenbaum, Libor Macurek, Babet van der Vaart, Matilde Galli, Anna Akhmanova, and René H Medema. A complex of Kif18b and MCAK promotes microtubule depolymerization and is negatively regulated by Aurora kinases. *Current biology*, 21(16):1356–1365, August 2011.

[122] Vladimír Varga, Cécile Leduc, Volker Bormuth, Stefan Diez, and Jonathon Howard. Kinesin-8 motors act cooperatively to mediate length-dependent microtubule depolymerization. *Cell*, 138(6):1174–1183, September 2009.

[123] Harjinder S Sardar, Vincent G Luczak, Maria M Lopez, Bradford C Lister, and Susan P Gilbert. Mitotic kinesin CENP-E promotes microtubule plus-end elongation. *Current biology*, 20(18):1648–1653, September 2010.

[124] Bipul R Acharya, Cedric Espenel, and Geri Kreitzer. Direct regulation of microtubule dynamics by KIF17 motor and tail domains. *Journal of Biological Chemistry*, 288(45):32302–32313, November 2013.

[125] Mark A Seeger and Sarah E Rice. Microtubule-associated protein-like binding of the kinesin-1 tail to microtubules. *Journal of Biological Chemistry*, 285(11):8155–8162, March 2010.

[126] Anneke Hibbel, Aliona Bogdanova, Mohammed Mahamdeh, Anita Jannasch, Marko Storch, Erik Schäffer, Dimitris Liakopoulos, Jonathon Howard, and Andrea Musacchio. Kinesin Kip2 enhances microtubule growth in vitro through length-dependent feedback on polymerization and catastrophe. *eLife*, 4:e10542, November 2015.

[127] Yalei Chen and William O Hancock. Kinesin-5 is a microtubule polymerase. *Nature Communications*, 6:8160, 2015.

[128] Robert A Cross. The kinetic mechanism of kinesin. *Trends in biochemical sciences*, 29(6):301–309, June 2004.

[129] S Ray, E Meyhöfer, R A Milligan, and J Howard. Kinesin follows the microtubule's protofilament axis. *Journal of Cell Biology*, 121(5):1083–1093, June 1993.

[130] Iwan A T Schaap, Carolina Carrasco, Pedro J de Pablo, and Christoph F Schmidt. Kinesin walks the line: single motors observed by atomic force microscopy. *Biophysical Journal*, 100(10):2450–2456, May 2011.

[131] Keitaro Shibata, Michi Miura, Yuta Watanabe, Kei Saito, Atsuko Nishimura, Ken'ya Furuta, and Yoko Y Toyoshima. A single protofilament is sufficient to support unidirectional walking of dynein and kinesin. *PLoS ONE*, 7(8):e42990, 2012.

[132] M J Schnitzer and S M Block. Kinesin hydrolyses one ATP per 8-nm step. *Nature*, 388(6640):386–390, July 1997.

[133] Steven M Block. Kinesin motor mechanics: binding, stepping, tracking, gating, and limping. *Biophysical journal*, 92(9):2986–2995, May 2007.

[134] M C Alonso, D R Drummond, S Kain, J Hoeng, L Amos, and R A Cross. An ATP Gate Controls Tubulin Binding by the Tethered Head of Kinesin-1. *Science*, 316(5821):120–123, April 2007.

[135] M Kikkawa, E P Sablin, Y Okada, H Yajima, R J Fletterick, and N Hirokawa. Switch-based mechanism of kinesin motors. *Nature*, 411(6836):439–445, May 2001.

[136] F J Kull, E P Sablin, R Lau, R J Fletterick, and R D Vale. Crystal structure of the kinesin motor domain reveals a structural similarity to myosin. *Nature*, 380(6574):550–555, April 1996.

[137] Masahide Kikkawa. The role of microtubules in processive kinesin movement. *Trends in Cell Biology*, 18(3):128–135, March 2008.

[138] Y Z Ma and E W Taylor. Kinetic mechanism of a monomeric kinesin construct. *Journal of Biological Chemistry*, 272(2):717–723, January 1997.

[139] Benoît Gigant, Weiyi Wang, Birgit Dreier, Qiyang Jiang, Ludovic Pecqueur, Andreas Plückthun, Chunguang Wang, and Marcel Knossow. Structure of a kinesin-tubulin complex and implications for kinesin motility. *Nature Structural & Molecular Biology*, 20(8):1001–1007, August 2013.

[140] Luyan Cao, Weiyi Wang, Qiyang Jiang, Chunguang Wang, Marcel Knossow, and Benoît Gigant. The structure of apo-kinesin bound to tubulin links the nucleotide cycle to movement. *Nature Communications*, 5:5364, 2014.

[141] Joseph Atherton, Irene Farabella, I-Mei Yu, Steven S Rosenfeld, Anne Houdusse, Maya Topf, and Carolyn A Moores. Conserved mechanisms of microtubule-stimulated ADP release, ATP binding, and force generation in transport kinesins. *eLife*, 3:e03680, 2014.

[142] Zhiguo Shang, Kaifeng Zhou, Chen Xu, Roseann Csencsits, Jared C Cochran, and Charles V Sindelar. High-resolution structures of kinesin on microtubules provide a basis for nucleotide-gated force generation. *eLife*, 3:e04686, November 2014.

[143] András Czövek, Gergely J Szöllosi, and Imre Derényi. Neck-linker docking coordinates the kinetics of kinesin's heads. *Biophysical Journal*, 100(7):1729–1736, April 2011.

[144] Olga Krylyshkina, Irina Kaverina, Wolfgang Kranewitter, Walter Steffen, Maria C Alonso, Robert A Cross, and J Victor Small. Modulation of substrate adhesion dynamics via microtubule targeting requires kinesin-1. *Journal of Cell Biology*, 156(2):349–359, January 2002.

[145] Richard J Kowalski and Robley C Williams. Unambiguous classification of microtubule-ends in vitro: Dynamic properties of the plus- and minus-ends. *Cell Motility and the Cytoskeleton*, 26(4):282–290, January 1993.

[146] Manatsu Morikawa, Hiroaki Yajima, Ryo Nitta, Shigeyuki Inoue, Toshihiko Ogura, Chikara Sato, and Nobutaka Hirokawa. X-ray and Cryo-EM structures reveal mutual conformational changes of Kinesin and GTP-state microtubules upon binding. *The EMBO Journal*, 34(9):1270–1286, March 2015.

[147] A Lockhart, I M Crevel, and R A Cross. Kinesin and ncd bind through a single head to microtubules and compete for a shared MT binding site. *Journal of Molecular Biology*, 249(4):763–771, June 1995.

[148] Anne Straube, editor. *Microtubule Dynamics: Methods and Protocols*, volume 777 of *Methods in Molecular Biology*. Humana Press, Totowa, NJ, 2011.

[149] Manuel Guizar-Sicairos, Samuel T Thurman, and James R Fienup. Efficient subpixel image registration algorithms. *Optics letters*, 33(2):156–158, January 2008.

[150] Honglian Guo, Chunhua Xu, Chunxiang Liu, E Qu, Ming Yuan, Zhaolin Li, Bingying Cheng, and Daozhong Zhang. Mechanism and Dynamics of Breakage of Fluorescent Microtubules. *Biophysical Journal*, 90(6):2093–2098, March 2006.

[151] Vladimir A Volkov, Anatoly V Zaytsev, and Ekaterina L Grishchuk. Preparation of segmented microtubules to study motions driven by the disassembling microtubule ends. *Journal of visualized experiments*, (85), 2014.

[152] Vivek Verma, William O Hancock, and Jeffrey M Catchmark. The role of casein in supporting the operation of surface bound kinesin. *Journal of biological engineering*, 2:14, 2008.

[153] Christopher Gell, Volker Bormuth, Gary J Brouhard, Daniel N Cohen, Stefan Diez, Claire T Friel, Jonne Helenius, Bert Nitzsche, Heike Petzold, Jan Ribbe, Erik Schäffer, Jeffrey H Stear, Anastasiya Trushko, Vladimir Varga, Per O Widlund, Marija Zanic, and Jonathon Howard. Microtubule dynamics reconstituted in vitro and imaged by single-molecule fluorescence microscopy. *Methods in cell biology*, 95:221–245, 2010.

[154] S B Andrews, P E Gallant, R D Leapman, B J Schnapp, and T S Reese. Single kinesin molecules crossbridge microtubules in vitro. *PNAS*, 90(14):6503–6507, July 1993.

[155] Emmanuel L P Dumont, Catherine Do, and Henry Hess. Molecular wear of microtubules propelled by surface-adhered kinesins. *Nature nanotechnology*, 10:166–169, January 2015.

[156] L J Harris, E Skaletsky, and A McPherson. Crystallographic structure of an intact IgG1 monoclonal antibody. *Journal of Molecular Biology*, 275(5):861–872, February 1998.

[157] A Lockhart and R A Cross. Kinetics and motility of the Eg5 microtubule motor. *Biochemistry*, 35(7):2365–2373, February 1996.

[158] I M Crevel, A Lockhart, and R A Cross. Weak and strong states of kinesin and ncd. *Journal of Molecular Biology*, 257(1):66–76, March 1996.

[159] Bo Zhang, Josiane Zerubia, and Jean-Christophe Olivo-Marin. Gaussian approximations of fluorescence microscope point-spread function models. *Applied optics*, 46(10):1819–1829, April 2007.

[160] Alexei O Demchouk, Melissa K Gardner, and David J Odde. Microtubule Tip Tracking and Tip Structures at the Nanometer Scale Using Digital Fluorescence Microscopy. *Cellular and Molecular Bioengineering*, 4(2):192–204, January 2011.

[161] Melissa K Gardner, Blake D Charlebois, Imre M Jánosi, Jonathon Howard, Alan J Hunt, and David J Odde. Rapid Microtubule Self-Assembly Kinetics. *Cell*, 146(4):582–592, August 2011.

[162] Laura Schaedel, Karin John, Jérémie Gaillard, Maxence V Nachury, Laurent Blanchoin, and Manuel Théry. Microtubules self-repair in response to mechanical stress. *Nature materials*, 14(11):1156–1163, September 2015.

[163] Jennifer C Waters. Accuracy and precision in quantitative fluorescence microscopy. *The Journal of Cell Biology*, 185(7):1135–1148, June 2009.

[164] Vivian A Lombillo, Russell J Stewart, and J Richard McIntosh. Minus-end-directed motion of kinesin-coated microspheres driven by microtubule depolymerization. *Nature*, 373(6510):161–164, January 1995.

[165] M I Molodtsov, E L Grishchuk, A K Efremov, J R McIntosh, and F I Ataullakhanov. Force production by depolymerizing microtubules: a theoretical study. *PNAS*, 102(12):4353–4358, March 2005.

[166] A Krebs, K N Goldie, and A Hoenger. Complex formation with kinesin motor domains affects the structure of microtubules. *Journal of Molecular Biology*, 335(1):139–153, January 2004.

[167] A Hoenger, M Thormählen, R Diaz-Avalos, M Doerhoefer, K N Goldie, J Müller, and E Mandelkow. A new look at the microtubule binding patterns of dimeric kinesins. *Journal of Molecular Biology*, 297(5):1087–1103, April 2000.

[168] Céline Elie-Caille, Fedor Severin, Jonne Helenius, Jonathon Howard, Daniel J Muller, and A A Hyman. Straight GDP-tubulin protofilaments form in the presence of taxol. *Current Biology*, 17(20):1765–1770, October 2007.

[169] Seiichi Uchimura, Yusuke Oguchi, You Hachikubo, Shin'ichi Ishiwata, and Etsuko Muto. Key residues on microtubule responsible for activation of kinesin ATPase. *The EMBO Journal*, 29(7):1167–1175, April 2010.

[170] T Nakata, S Niwa, Y Okada, F Perez, and N Hirokawa. Preferential binding of a kinesin-1 motor to GTP-tubulin-rich microtubules underlies polarized vesicle transport. *The Journal of Cell Biology*, 194(2):245–255, July 2011.

[171] D Chrétien, H Flyvbjerg, and S D Fuller. Limited flexibility of the inter-protofilament bonds in microtubules assembled from pure tubulin. *European Biophysics Journal*, 27(5):490–500, 1998.

[172] Lili X Peng, Monica T Hsu, Massimiliano Bonomi, David A Agard, and Matthew P Jacobson. The Free Energy Profile of Tubulin Straight-Bent Conformational Changes, with Implications for Microtubule Assembly and Drug Discovery. *PLoS computational biology*, 10(2):e1003464, February 2014.

[173] Hervé Mohrbach, Albert Johner, and Igor M Kulić. Cooperative lattice dynamics and anomalous fluctuations of microtubules. *European Biophysics Journal*, 41(2):217–239, December 2011.

[174] Arif Md Rashedul Kabir, Daisuke Inoue, Yoshimi Hamano, Hiroyuki Mayama, Kazuki Sada, and Akira Kakugo. Biomolecular Motor Modulates Mechanical Property of Microtubule. *Biomacromolecules*, 15(5):1797–1805, April 2014.

[175] Falko Ziebert, Hervé Mohrbach, and Igor M Kulić. Why microtubules run in circles: mechanical hysteresis of the tubulin lattice. *Physical review letters*, 114(14):148101, April 2015.

[176] A Vilfan, E Frey, F Schwabl, M Thormählen, Y H Song, and E Mandelkow. Dynamics and cooperativity of microtubule decoration by the motor protein kinesin. *Journal of Molecular Biology*, 312(5):1011–1026, October 2001.

[177] John S Allingham, Lisa R Sproul, Ivan Rayment, and Susan P Gilbert. Vik1 modulates microtubule-Kar3 interactions through a motor domain that lacks an active site. *Cell*, 128(6):1161–1172, March 2007.

[178] Wouter H Roos, Otger Campàs, Fabien Montel, Günther Woehlke, Joachim P Spatz, Patricia Bassereau, and Giovanni Cappello. Dynamic kinesin-1 clustering on microtubules due to mutually attractive interactions. *Physical Biology*, 5(4):046004, December 2008.

[179] Etsuko E Muto, Hiroyuki H Sakai, and Kuniyoshi K Kaseda. Long-range cooperative binding of kinesin to a microtubule in the presence of ATP. *Journal of Cell Biology*, 168(5):691–696, February 2005.

[180] Stuart Hameroff, Alex Nip, Mitchell Porter, and Jack Tuszynski. Conduction pathways in microtubules, biological quantum computation, and consciousness. *Biosystems*, 64(1-3):149–168, January 2002.

[181] Osman Kahraman, Hervé Mohrbach, Martin Michael Müller, and Igor M Kulić. Confotronic dynamics of tubular filaments. *Soft matter*, 10(16):2836–2847, April 2014.

[182] Daniel Demonte, Eric J Drake, Kok Hong Lim, Andrew M Gulick, and Sheldon Park. Structure-based engineering of streptavidin monomer with a reduced biotin dissociation rate. *Proteins*, 81(9):1621–1633, September 2013.

[183] C M Kacher, I M Weiss, R J Stewart, C F Schmidt, P K Hansma, M Radmacher, and M Fritz. Imaging microtubules and kinesin decorated microtubules using tapping mode atomic force microscopy in fluids. *European Biophysics Journal*, 28(8):611–620, 2000.

[184] Viktória Hunyadi and Imre M Jánosi. Metastability of microtubules induced by competing internal forces. *Biophysical journal*, 92(9):3092–3097, May 2007.

[185] I M Jánosi, D Chrétien, and H Flyvbjerg. Modeling elastic properties of microtubule tips and walls. *European Biophysics Journal*, 27(5):501–513, 1998.

[186] Imre M Jánosi, Denis Chrétien, and Henrik Flyvbjerg. Structural microtubule cap: stability, catastrophe, rescue, and third state. *Biophysical Journal*, 83(3):1317, September 2002.

[187] Viktória Hunyadi, Denis Chrétien, and Imre M Jánosi. Mechanical Stress Induced Mechanism of Microtubule Catastrophes. *Journal of Molecular Biology*, 348(4):927–938, May 2005.

[188] Sotaro Uemura, Kenji Kawaguchi, Junichiro Yajima, Masaki Edamatsu, Yoko Yano Toyoshima, and Shin'ichi Ishiwata. Kinesin-microtubule binding depends on both nucleotide state and loading direction. *PNAS*, 99(9):5977–5981, April 2002.

[189] Kritica Arora, Lama Talje, Ana B Asenjo, Parker Andersen, Kaleem Atchia, Monika Joshi, Hernando Sosa, John S Allingham, and Benjamin H Kwok. KIF14 binds tightly to microtubules and adopts a rigor-like conformation. *Journal of Molecular Biology*, 426(17):2997–3015, August 2014.

[190] Minhajuddin Sirajuddin, Luke M Rice, and Ronald D Vale. Regulation of microtubule motors by tubulin isotypes and post-translational modifications. *Nature Cell Biology*, 16(4):335–344, April 2014.

[191] R D Vale, C M Coppin, F Malik, F J Kull, and R A Milligan. Tubulin GTP hydrolysis influences the structure, mechanical properties, and kinesin-driven transport of microtubules. *Journal of Biological Chemistry*, 269(38):23769–23775, 1994.

[192] N J Carter and R A Cross. Mechanics of the kinesin step. *Nature*, 435(7040):308–312, May 2005.

[193] Benjamin H Blehm, Trina A Schroer, Kathleen M Trybus, Yann R Chemla, and Paul R Selvin. In vivo optical trapping indicates kinesin's stall force is reduced by dynein during

intracellular transport. *Proceedings of the National Academy of Sciences of the United States of America*, 110(9):3381–3386, February 2013.

[194] Nikita Gudimchuk, Benjamin Vitre, Yumi Kim, Anatoly Kiyatkin, Don W Cleveland, Fazly I Ataullakhanov, and Ekaterina L Grishchuk. Kinetochore kinesin CENP-E is a processive bi-directional tracker of dynamic microtubule tips. *Nature Cell Biology*, 15(9):1079–1088, September 2013.

[195] Cécile Leduc, Kathrin Padberg-Gehle, Vladimír Varga, Dirk Helbing, Stefan Diez, and Jonathon Howard. Molecular crowding creates traffic jams of kinesin motors on microtubules. *Proceedings of the National Academy of Sciences of the United States of America*, 109(16):6100–6105, April 2012.

[196] Hauke Drechsler, Toni McHugh, Martin R Singleton, Nicholas J Carter, and Andrew D McAinsh. The Kinesin-12 Kif15 is a processive track-switching tetramer. *eLife*, 3:e01724, 2014.

[197] Isabelle Crevel, Miklós Nyitrai, Maria C Alonso, Stefan Weiss, Michael A Geeves, and Robert A Cross. What kinesin does at roadblocks: the coordination mechanism for molecular walking. *The EMBO Journal*, 23(1):23–32, January 2004.

[198] René Schneider, Till Korten, Wilhelm J Walter, and Stefan Diez. Kinesin-1 motors can circumvent permanent roadblocks by side-shifting to neighboring protofilaments. *Biophysical Journal*, 108(9):2249–2257, May 2015.

[199] Ivo A Telley, Peter Bieling, and Thomas Surrey. Obstacles on the microtubule reduce the processivity of Kinesin-1 in a minimal in vitro system and in cell extract. *Biophysical Journal*, 96(8):3341–3353, April 2009.

[200] Christoph Herold, Cécile Leduc, Robert Stock, Stefan Diez, and Petra Schwille. Long-range transport of giant vesicles along microtubule networks. *ChemPhysChem*, 13(4):1001–1006, March 2012.

[201] Janina Beeg, Stefan Klumpp, Rumiana Dimova, Rubèn Serral Gracià, Eberhard Unger, and Reinhard Lipowsky. Transport of beads by several kinesin motors. *Biophysical Journal*, 94(2):532–541, January 2008.

[202] Carsten Peters, Katjuša Brejc, Lisa Belmont, Andrew J Bodey, Yan Lee, Ming Yu, Jun Guo, Roman Sakowicz, James Hartman, and Carolyn A Moores. Insight into

the molecular mechanism of the multitasking kinesin-8 motor. *The EMBO Journal*, 29(20):3437–3447, October 2010.

[203] Joshua S Weinger, Minhua Qiu, Ge Yang, and Tarun M Kapoor. A nonmotor microtubule binding site in kinesin-5 is required for filament crosslinking and sliding. *Current biology*, 21(2):154–160, January 2011.

[204] Vladimir Fridman, Adina Gerson-Gurwitz, Ofer Shapira, Natalia Movshovich, Stefan Lakämper, Christoph F Schmidt, and Larisa Gheber. Kinesin-5 Kip1 is a bi-directional motor that stabilizes microtubules and tracks their plus-ends in vivo. *Journal of Cell Science*, 126(18):4147–4159, September 2013.

[205] Guoxing Wang, Xiang Gao, Yun Huang, Zhan Yao, Qinghua Shi, and Mian Wu. Nucleophosmin/B23 inhibits Eg5-mediated microtubule depolymerization by inactivating its ATPase activity. *Journal of Biological Chemistry*, 285(25):19060–19067, June 2010.

[206] Johanna Roostalu, Christian Hentrich, Peter Bieling, Ivo A Telley, Elmar Schiebel, and Thomas Surrey. Directional switching of the kinesin Cin8 through motor coupling. *Science*, 332(6025):94–99, April 2011.

[207] T Nakata and N Hirokawa. Point mutation of adenosine triphosphate-binding motif generated rigor kinesin that selectively blocks anterograde lysosome membrane transport. *Journal of Cell Biology*, 131(4):1039–1053, November 1995.

[208] Christine Mieck, Maxim I Molodtsov, Katarzyna Drzewicka, Babet van der Vaart, Gabriele Litos, Gerald Schmauss, Alipasha Vaziri, and Stefan Westermann. Non-catalytic motor domains enable processive movement and functional diversification of the kinesin-14 Kar3. *eLife*, 4:e04489, 2015.

[209] Yanmin Chen and Zu-Hang Sheng. Kinesin-1-syntaphilin coupling mediates activity-dependent regulation of axonal mitochondrial transport. *The Journal of Cell Biology*, 202(2):351–364, July 2013.

[210] Naoko Mizuno, Shiori Toba, Masaki Edamatsu, Junko Watai-Nishii, Nobutaka Hirokawa, Yoko Y Toyoshima, and Masahide Kikkawa. Dynein and kinesin share an overlapping microtubule-binding site. *The EMBO Journal*, 23(13):2459–2467, July 2004.

[211] L'ubica Adamíková, Anne Straube, Irene Schulz, and Gero Steinberg. Calcium signaling is involved in dynein-dependent microtubule organization. *Molecular biology of the cell*, 15(4):1969–1980, April 2004.

[212] Liedewij Laan, Nenad Pavin, Julien Husson, Guillaume Romet-Lemonne, Martijn van Duijn, Magdalena Preciado López, Ronald D Vale, Frank Jülicher, Samara L Reck-Peterson, and Marileen Dogterom. Cortical dynein controls microtubule dynamics to generate pulling forces that position microtubule asters. *Cell*, 148(3):502–514, February 2012.

[213] Julie Huang, Anthony J Roberts, Andres E Leschziner, and Samara L Reck-Peterson. Lis1 Acts as a "Clutch" between the ATPase and Microtubule-Binding Domains of the Dynein Motor. *Cell*, 150(5):975–986, August 2012.

[214] Roop Mallik, Brian C Carter, Stephanie A Lex, Stephen J King, and Steven P Gross. Cytoplasmic dynein functions as a gear in response to load. *Nature*, 427(6975):649–652, February 2004.

[215] Sotaro Uemura and Shin'ichi Ishiwata. Loading direction regulates the affinity of ADP for kinesin. *Nature Structural & Molecular Biology*, 10(4):308–311, April 2003.

[216] Benjamin H Blehm and Paul R Selvin. Single-molecule fluorescence and in vivo optical traps: how multiple dyneins and kinesins interact. *Chemical reviews*, 114(6):3335–3352, March 2014.

[217] William O Hancock. Bidirectional cargo transport: moving beyond tug of war. *Nature reviews*, 15(9):615–628, September 2014.

[218] Nadine Zekert and Reinhard Fischer. The Aspergillus nidulans kinesin-3 UncA motor moves vesicles along a subpopulation of microtubules. *Molecular biology of the cell*, 20(2):673–684, January 2009.

[219] Dawen Cai, Dyke P McEwen, Jeffery R Martens, Edgar Meyhofer, and Kristen J Verhey. Single Molecule Imaging Reveals Differences in Microtubule Track Selection Between Kinesin Motors. *PLOS Biology*, 7(10):e1000216, October 2009.

[220] Christopher P Garnham and Antonina Roll-Mecak. The chemical complexity of cellular microtubules: tubulin post-translational modification enzymes and their roles in tuning microtubule functions. *Cytoskeleton*, 69(7):442–463, July 2012.

[221] Carolyn A Moores, Mylène Perderiset, Fiona Francis, Jamel Chelly, Anne Houdusse, and Ronald A Milligan. Mechanism of microtubule stabilization by doublecortin. *Molecular cell*, 14(6):833–839, June 2004.

[222] F Gittes, B Mickey, J Nettleton, and J Howard. Flexural rigidity of microtubules and actin filaments measured from thermal fluctuations in shape. *Journal of Cell Biology*, 120(4):923–934, February 1993.

[223] Benjamin J Lopez and Megan T Valentine. Mechanical effects of EB1 on microtubules depend on GTP hydrolysis state and presence of paclitaxel. *Cytoskeleton*, 71(9):530–541, September 2014.

[224] Mahito Kikumoto, Masashi Kurachi, Valer Tosa, and Hideo Tashiro. Flexural rigidity of individual microtubules measured by a buckling force with optical traps. *Biophysical journal*, 90(5):1687–1696, March 2006.